A HIGH PRESSURE THERMOBALANCE FOR PROCESS STUDIES

by

SAMUEL DOBNER

A dissertation submitted to the Graduate Faculty in Engineering in partial fulfillment of the requirements for the degree of Doctor of Philosophy, The City University of New York.

1976

This manuscript has been read and accepted for the Graduate Faculty in Engineering in satisfaction of the dissertation requirement for the degree of Doctor of Philosophy.

1/29/76
date

Arthur M. Squires
Chairman of Examining Committee

1/29/76
date

Jacques E. Beneviste
Executive Officer

Arthur M. Squires

Robert A. Graff

Amos Turk
Supervisory Committee

The City University of New York

Abstract

A duPont 950 Thermogravimetric Analyzer has been modified to permit operation at up to 30 atmospheres, 1100°C, with corrosive atmospheres, and steam partial pressures up to 15 atmospheres.

The major areas of instrument development included:

- modification of a TGA to accept corrosive gas atmospheres containing high partial pressures of steam
- design of a pressure balanced flow system for safe introduction of corrosive gas atmospheres
- design of a working steam generation system for low flows
- weight and temperature measurement at high pressures in a dynamic flow system

A preliminary series of experiments illustrating the utility of the high pressure thermobalance for process studies was carried out looking at the cyclic CO_2-acceptor reactions for half-calcined dolomite [$CaCO_3$+MgO].

$$[CaCO_3+MgO] \rightarrow [CaO+MgO] + CO_2 \quad (I)$$

$$[CaO+MgO] + CO_2 \rightarrow [CaCO_3+MgO] \quad (II)$$

In particular, the parameters surveyed include: calcination and regeneration temperatures, total pressure, and the partial pressures of carbon dioxide and steam during calcination and regeneration.

Acknowledgements

For their guidance and interest in this research, appreciation and thanks are due Professors Arthur M. Squires and Robert A. Graff of the Chemical Engineering Department.

I also thank John Bodnaruk and other members of the Chemical Engineering Shop for their invaluable assistance in making this instrument development possible.

I gratefully acknowledge the financial support provided by the National Science Foundation Graduate Trainee Program.

Grant number AP00945 from the Office of Air Programs of the Environmental Protection Agency supported a major part of this work.

Special thanks are due my wife, Judi, for her encouragement and continued patience.

Dedication

This thesis research is dedicated to the memory of Aaron Kestenbaum, a colleague and friend, who had so much to contribute but was not given the time.

Presentations

Portions of this research appear in both a paper presented at a meeting of the American Institute of Chemical Engineers and in papers submitted to journals for publication.

S. Dobner, G. Kan, R.A. Graff, A.M. Squires.
"Modification of a Thermobalance for High Pressure Process Studies," Paper 67d, 68th National Meeting of the American Institute of Chemical Engineers, November 16-20, 1975.

S. Dobner, G. Kan, R.A. Graff, A.M. Squires.
"A Thermobalance for High Pressure Process Studies," submitted for publication to Thermochimica Acta, (October 1975).

S. Dobner, L. Sterns, A.M. Squires, R.A. Graff.
"Recarbonation of Calcined Dolomite," submitted for publication to Industrial and Engineering Chemistry Process Design and Development, (December 1975).

Table of Contents

List of Figures

List of Tables

1.0 Introduction

With the advent of the recent energy crisis, new technologies are being developed to improve the utilization of our fossil fuel resources. The initial commercialization of these technologies will require huge sums of capital, most likely in the form of government supported financing. The costs of building pilot plants of reasonable size are, however, rapidly approaching the cost of demonstration plants themselves. We are also learning very quickly that the goals of process development hinge more strongly on questions of system operability than on any other factors, such as yields and throughput. Unfortunately, system operability can really only be demonstrated on a scale approaching commercial size. The expense of pilot plant programs and their long lead times to implementation demand a viable and more realistic bench scale program to provide some early fundamental answers. There is therefore a growing demand for development of bench scale instruments capable of operating at conditions which more closely simulate the particular processes.

Demands upon commercial thermobalances have in general not been too severe. For example, they have provided valuable service to the polymer industry, where questions of product stability, characterization and quality are of prime importance. Commercial thermobalances are designed to operate in vacuum to atmospheric pressures, cryogenic temperatures to near 800°C, using inert or mildly reactive gas atmospheres.

The need to develop an instrument capable of handling highly reactive and corrosive gas atmospheres at high pressures and temperatures arose from our efforts to study sulfur acceptor chemistries. A research team at The City College has over the past few years been investigating the feasibility of using calcined dolomite or other suitable acceptors for the removal of sulfur from high temperature fuel gases generated in the pressure gasification of "dirty" fossil fuels. The scope of the research effort includes the quantitative kinetic evaluation of the absorption and regeneration reactions, as well as the determination of optimum process conditions for maintaining high solid reactivities with repeated cycling. The experimental method adopted for investigating the various reactions is based on the use of thermobalances.

Some of the process steps, in particular the regeneration of sulfided dolomite via

$$[CaS + MgO] + CO_2 + H_2O = [CaCO_3 + MgO] + H_2S$$

can only be carried out effectively at pressure. A high pressure thermobalance was therefore required in order to explore this very important reaction step. This thermobalance must be able to operate at high pressure, high temperatures, and in gas environments containing corrosive sulfur species and sometimes high partial pressures of steam.

A program of research was therefore initiated to develop such an instrument. This thesis is a report of that development effort and its demonstrated application to the study of the cyclic recarbonation of calcined dolomite.

2.0 Object of the Research

The object of this research was to develop a high pressure thermobalance capable of process studies.

The first phase of the research included the design construction and testing of the unit. This was then followed by a demonstration phase where the ability of the unit to perform process studies was tested on the cognate cyclic acceptor reaction, the cyclic calcination and recarbonation of calcined dolomite. Ultimately, this development effort will yield an instrument capable of high pressure sulfur acceptor process studies.

3.0 Significance of the Research

This research will immediately contribute to the ongoing research program at The City College on sulfur acceptor chemistries by providing an instrument capable of high pressure investigations.

In addition, the information derived from this instrument development effort will prove valuable to other research groups seeking to develop instruments of similar capability. Bench scale instruments of this type will ultimately become an integral part of most major process development laboratories. This instrument should have broad application to studies of high temperature air separation, gas purification, metallurgical processing, fuel gasification, and to other important areas of noncatalytic gas-solids processing.

4.0 Experimental Development of High Pressure Thermobalances

4.01 Previous Developments

The development of high pressure thermobalances has been a continuing effort over the past two decades. Table 1 summarizes the chronology of these developments as described in the open literature. As yet, no high pressure thermobalances are available commercially.

The earlier units, in general, did not have a dynamic flow system for sweeping the reaction products away from the sample. The first high pressure thermobalance capable of process studies was described by McKewan (4). This unit and many subsequent units provided for the vertical suspension of the sample in a heated zone from an isolated balance housing which contained a transducer, quartz spring, or torsion assembly. Reaction gas continuously flowed vertically over the sample while a purge gas flowed through the balance housing to protect the balance assembly.

In an effort to reduce the size of the pressure assembly and to minimize the need for custom built components, several investigators have developed high pressure apparatus based on the duPont 950 TGA (8,10,11,12,13,16). Figure 1 shows a schematic of the apparatus as provided by duPont. Close coupling of the furnace and furnace tube to the balance housing is made possible by suspending the sample directly from the balance beam. The horizontal orientation of the furnace tube and gas flows help to reduce convection effects observed in apparatus having a vertical orientation.

TABLE 1: PRESSURIZED THERMOBALANCES

	Balance Mechanism	Orientation	Max. Pres., atm.	Max. Temp., °C	Flow System	Gases
Rabatin & Card, 1959 (1)	torsion	vertical	40	1200	static	CO_2, N_2, CO (O_2, NH_3, H_2S)
Baker, 1962 (2)	quartz spring	vertical	300	1300	static	CO_2
Biermann & Hienrichs, 1962 (3)	transducer	vertical	70	1000	static	O_2, N_2
McKewan, 1962 (4)	quartz spring	vertical	40	1000	dynamic	H_2
Boehlen et al., 1964 (5)		vertical	20	500	static	N_2, CO_2, CH_4, C_2H_6
Feldkirchner & Johnson, 1968 (6)	transducer	vertical	100	925	dynamic	N_2, H_2, CO, CO_2, CH_4, H_2O
Sasaki et al., 1969 (7)		vertical	100	1000	static	
Brown et al., 1971 (8)	duPont	horizontal	20	350	static	N_2
Ho Bae, 1972 (9)	transducer	vertical	70	600	dynamic	N_2, air
Williams et al., 1972 (10), 1973 (11)	duPont	horizontal	500	500	static	N_2, CO_2
Dobner, 1972	duPont	horizontal	30	1100	dynamic	N_2, CO_2, O_2, CO, H_2, H_2S, SO_2, H_2O
Keairns, 1972 (12), 1973 (13)	duPont	horizontal	40	1100	dynamic	N_2, CO_2, O_2, CO, H_2, H_2S, SO_2, H_2O
Gardner et al., 1974 (14)	transducer	vertical			dynamic	H_2, H_2O
Chauhan et al., 1975 (15)	transducer	vertical	100	1200	dynamic	H_2, H_2O, He
Tomita et al., 1975 (16)	duPont	horizontal	35	1000	dynamic	H_2

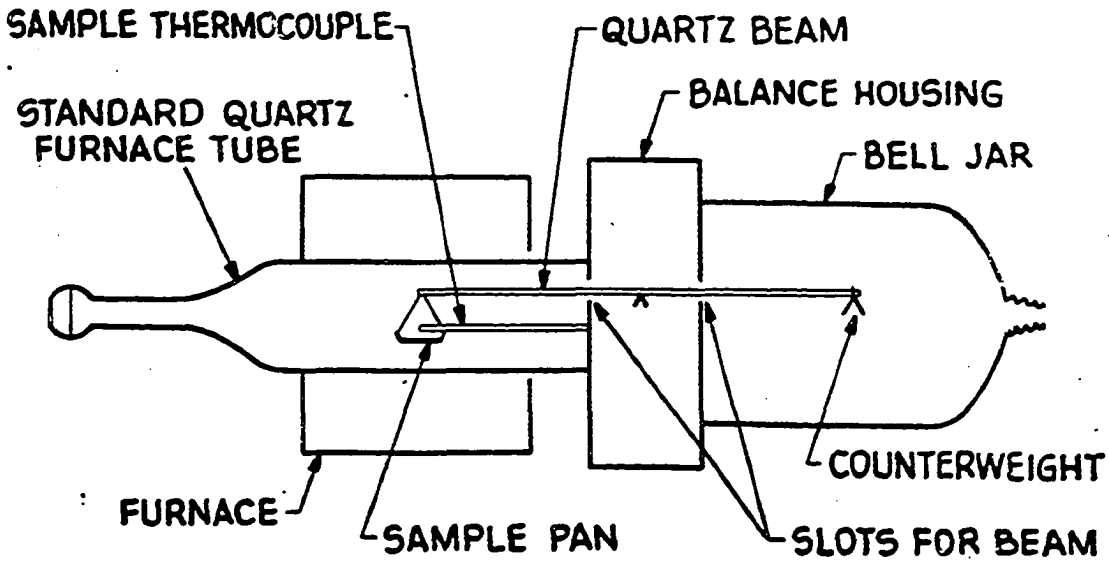

Figure 1. The duPont 950 Thermogravimetric Analyzer (TGA)

While the feasibility of pressurizing the duPont TGA was demonstrated by Brown et al. (8) and Williams et al. (10,11), operation in dynamic atmospheres and at temperatures above 500°C had as yet not been established. Our instrument development objectives called for further modification of the duPont TGA to permit operation at temperatures to 1100°C, pressures to 30 atmospheres and corrosive gas environments containing H_2S, SO_2, CO, and high partial pressures of steam. Other research groups have since followed our development and have constructed units having similar capabilities (12,13,16).

4.02 duPont Thermogravimetric Analyzer

The instrument consists of two separate units: the duPont 900 Thermal Analyzer, which includes the temperature programmer-controller and X-Y recorder, and the duPont 950 Thermogravimetric Analyzer, which contains an electrobalance and furnace.

The balance capacity is effectively 150 mg and the weight sensitivity is variable from 0.20 mg/inch to 20 mg/inch in seven steps. This means that at the maximum sensitivity attainable, a weight change of 0.02 mg should be easily seen. For a typical sample size of 20 mg, weight changes corresponding to as little as 0.2% conversion of [CaO+MgO] to [$CaCO_3$+MgO], for example, can be recorded.

The instrument can be used in the isothermal mode to 1000°C, in which case the recorder produces a graph of sample weight versus time, or the temperature can be raised linearly to 1200°C at rates up to 30°C/min. In this case, a graph of sample weight versus sample temperature is produced.

4.03 Modification of duPont TGA for Atmospheric Studies

The TGA, as provided by duPont, accepts the reaction gas through an opening in the balance housing which then passes over the sample and exits at the rear of the quartz furnace tube. In this form the duPont TGA is not equipped to handle corrosive gases or steam since either would ruin the balance. Early objectives of the acceptor research program called for atmospheric kinetic studies of the reactions of H_2S with calcined dolomites. The TGA, was, therefore, modified by Ruth as shown in Figure 2 (17,18). This required redesign of the quartz furnace tube and a baffle to separate the balance and reaction zones. The purpose is twofold: to keep corrosive H_2S from the balance mechanism, and to keep purge nitrogen away from the sample, so that composition of gas in the reaction zone is not affected.

In this modification, purge gas enters the end of the balance bell jar and flows through the slot in the balance housing containing the beam. Reaction gas enters the inner tube of the concentric furnace tube depicted in Figure 2, and passes over the sample. The reaction gas leaves the inner tube through slots in the circular platinum baffle held in place at the end of the inner tube by means of a sidearm (not shown in Figure 2) attached to the balance housing. The slots in the baffle are provided for passage of the balance beam and the thermocouple. Reaction gas and nitrogen purge pass together through the annular space between inner and outer tubes and are discharged together through an opening near the end of the outer tube.

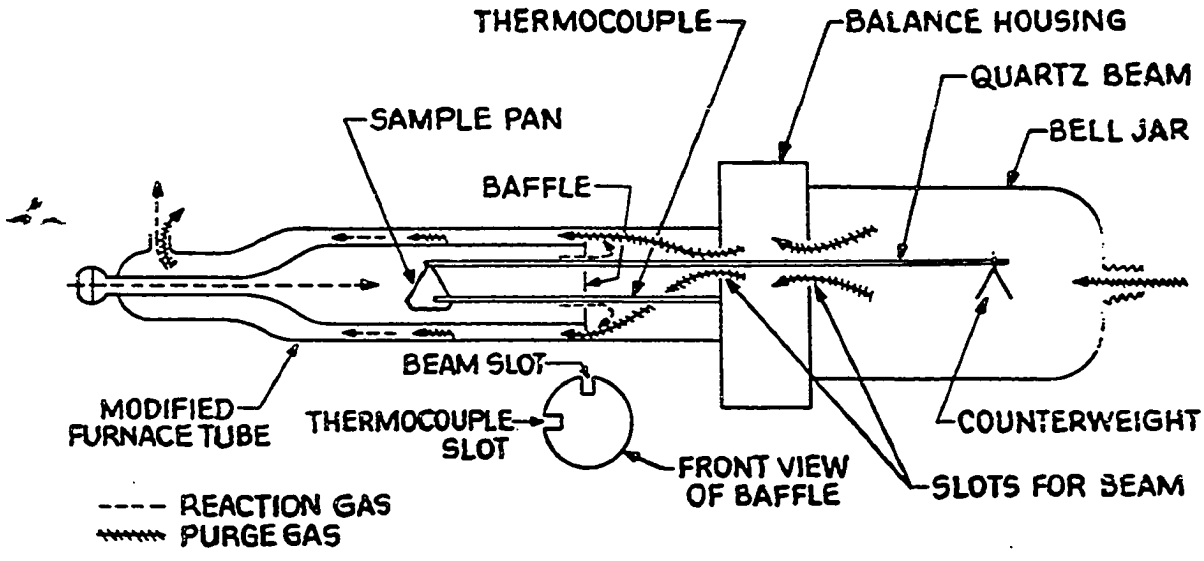

Figure 2. duPont 950 TGA with Modifications for Coorsive Gases (L. Ruth)

A purge gas flow rate of 800 cm^3/min was found adequate to prevent any damage to the balance assembly by the H_2S. This was confirmed by the unchanging appearance of a shiny copper wire located within the balance housing. On the basis of penetration tests a minimum reaction gas flow rate of 75 cm^3/min was found necessary to prevent purge gas penetration into the reaction zone. The penetration tests were carried out using oxygen as the purge gas, nitrogen as the reaction gas, and a finely divided copper powder sample maintained at 600°C as an oxygen detector.

Sample temperature in the duPont TGA is determined by a bare Chromel-Alumel thermocouple located one millimeter above the center of the sample. This was subsequently substituted by a sheathed chromel-alumel thermocouple fabricated of 304 stainless steel in order to be more resistent to corrosive atmospheres.

4.04 Modification of duPont TGA for High Pressure Studies

Pressurization was achieved by enclosing the balance and furnace module inside a pressure vessel, as shown in Figure 3. Designed for 450 psig by Autoclave Engineers, the pressure vessel measures approximately 3 feet long and 10 inches in inside diameter. The unit consists of a horizontal pressure shell on rails to permit easy access to the TGA and a fixed bulkhead through which all instrument and flow connections are made. The TGA itself rests on a beam extending from the fixed end. Heat generated by the TGA is removed by a cooling water jacket surrounding the pressure shell. Safety

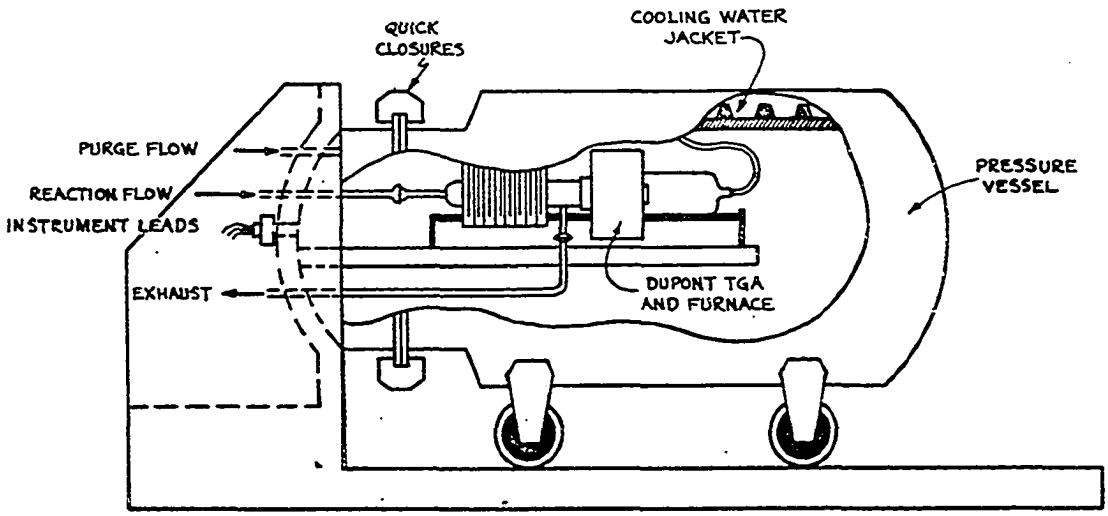

Figure 3. Pressurized duPont 950 TGA

precautions include a ½" rupture disc located in the bulkhead and a 5/8" plywood pressure shield for operating personnel protection. The pressure shield facing the bulkhead end of the vessel is of 1¼" plywood.

At the outset, we hoped the modified TGA shown in Figure 2 would also be capable of high pressure operation. However, serious problems were quickly encountered when using this configuration in the high pressure unit.

During early shakedown runs of the unit it was observed that at high pressure (300 psig) the characteristic calcination temperatures of dolomite in one atmosphere of CO_2 appeared to be shifted to higher temperatures by 60 to 100°C. This shift could not be simply explained on any chemical basis. Errors in temperature measurement were therefore suspected, and this was subsequently confirmed by temperature calibrations of the instrument at high pressures using the melting point of aluminum (660°C) and silver (966°C) as standards. This calibration procedure required the construction of aluminum and silver sample pans having the same geometry as the platinum pans used in the experiments. These pans were suspended from the balance beam by tungsten wires. During temperature programming a sharp weight loss would be registered at the melting point of these materials. At atmospheric pressure this calibration procedure showed the sample thermocouple to be satisfactorily accurate to within 10°C. However, at 300 psig the indicated melting points were consistently 60 to 80°C higher than their true values.

The source of these difficulties was quickly identified. In the duPont TGA the sample thermocouple is not in direct contact with the sample but is situated a few millimeters above it (see Figure 1) and consequently only "sees" the sample temperature. The geometry of the furnace is such that reaction gases entering the furnace tube never approach anything near the furnace wall temperature. The convection effects resulting from the "cold" flowing gases can play havoc with temperature measurement, especially at high pressures, where convection cooling becomes very effective. The fact that the indicated sample temperature was consistently higher than the actual sample temperature at high pressures may simply reflect a more effective cooling of the sample pan in comparison to the sample thermocouple, the difference owing to their very different geometries.

The "cooling" effect at high pressure was confirmed by simultaneous measurement of furnace wall (control thermocouple) and sample thermocouple temperatures. At atmospheric pressure (100 cm^3/min each of reaction gas and purge gas) the maximum difference between the two temperatures remained within 10 to 20°C and increased with increasing flowrates. At 300 psig maximum differences of almost 180°C were noted (at 600°C).

A remedy to the troubling convection effects would be to remove the source of temperature inhomogeneities by preheating the incoming reaction gas to sample temperature. This was simply achieved by packing the furnace tube ahead of the sample with a suitable packing material. The packing

should be sufficiently transparent to permit radiative heat to penetrate to the center of the packing but should also be sufficiently opaque for absorption of radiation. Materials tested were: stainless steel mesh, crushed quartz (20 mesh), crushed silicon carbide (20 mesh), and 1/8" Vycor cylinders (cut from 1/8" Vycor rod). The results are shown in Figure 4 in terms of measured sample thermocouple temperature versus furnace wall (control thermocouple) temperatures. The vycor packing gave the best results, but still yielded temperature differences between furnace wall (furnace thermocouple) and sample thermocouple of 100°C. Increasing the heated length of packing by lengthening the furnace tube and adding a preheat furnace ahead of the reaction zone reduced the temperature difference to only 25°C. This approach, however, required excessive preheat temperatures, which effectively limited operation of the thermobalance to below 650°C. These difficulties were puzzling at first since heat transfer calculations predicted that little heat transfer surface would be needed to preheat the gas. Subsequently, the source of these difficulties were identified. At the low reaction gas flows employed, a convection cell was formed between hot gas inside the heated zone and cooler gases downstream of the reaction zone, adjacent to the balance housing.

Eventually, the configuration shown in Figure 5 was adopted. The open space containing the sample pan was reduced to 0.5 inches by completely filling the downstream section of the furnace tube with a ceramic block, thus preventing the formation of a convection cell. With refractory

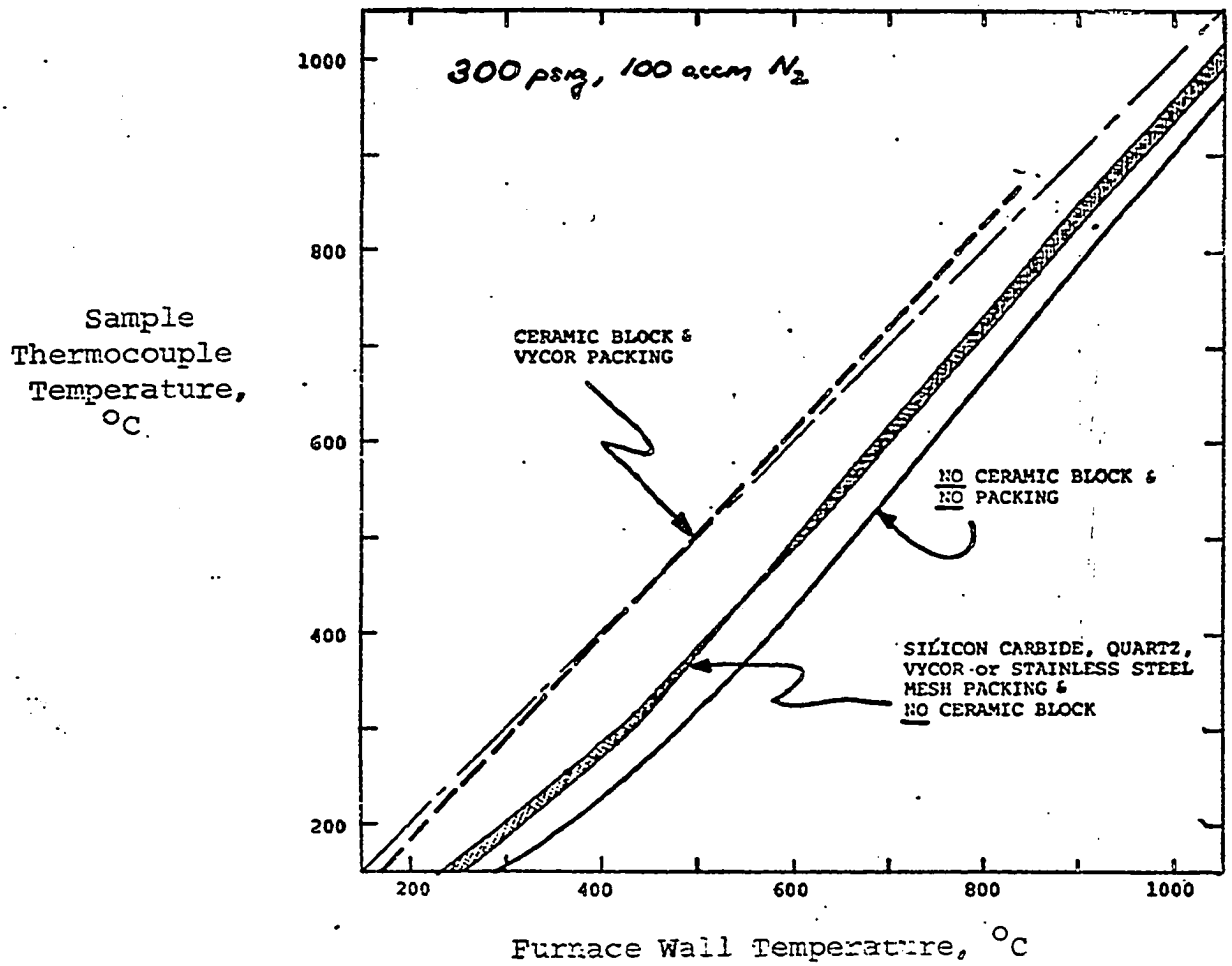

Figure 4. Sample Thermocouple and Furnace Wall Temperatures in Pressurized Thermobalance

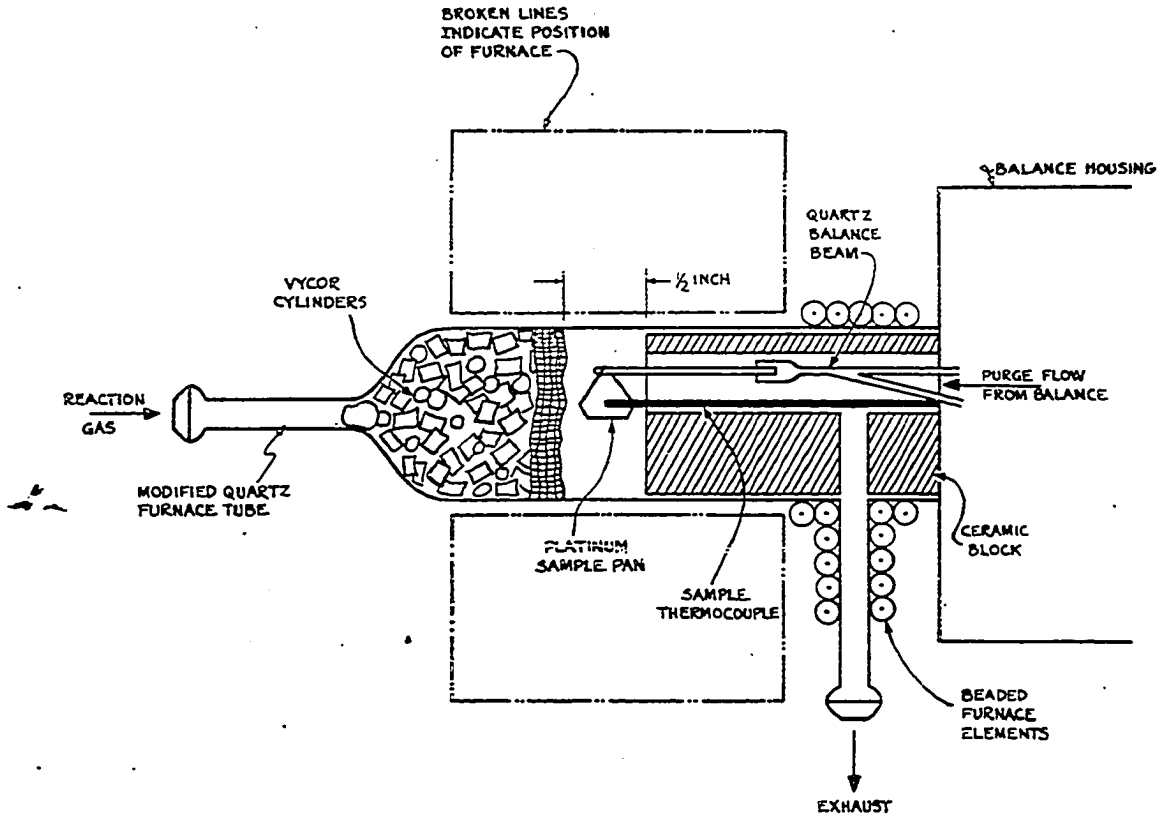

Figure 5. duPont TGA Modified for High Pressure Process Studies

surfaces surrounding the sample from all directions and with uniform gas and surface temperatures, both the sample and sample thermocouple are now able to "see" the same temperature. This was confirmed by uniform readings of furnace wall and sample thermocouple temperatures as shown in Figure 4 and by satisfactory calibration of the melting point standards at all pressures.

The present modifications of the TGA also solved another serious problem which was encountered with the earlier configuration (Figure 2). When running with steam-containing atmospheres at high pressure, significant condensation took place on the quartz balance beam or in the narrow slot between the beam and the aluminum balance housing. This was not entirely unanticipated since mixing of the cold purge gas with the steam-laden reaction gases must take place in the cooler regions of the furnace tube adjacent to the balance housing. Simply providing external heating to the exposed sections of the furnace tube did not alleviate the problem. Apparently, the formation of a convection cell, which had earlier interfered with the measurement of temperature, was also responsible for mist formation and condensation.

Several attempts were made to solve the condensation problem by modifying the furnace tube to permit the introduction of "hot" purge gas to the mixing zone, as shown in Figure 6. Only a small flow of "cold" nitrogen would then be used to purge the balance housing itself. The first two attempts (Figure 6a and 6b) required an external purge gas

Figure 6. Attempted Modifications of Furnace Tube for Introduction of Hot Purge Gas to Mixing Zone

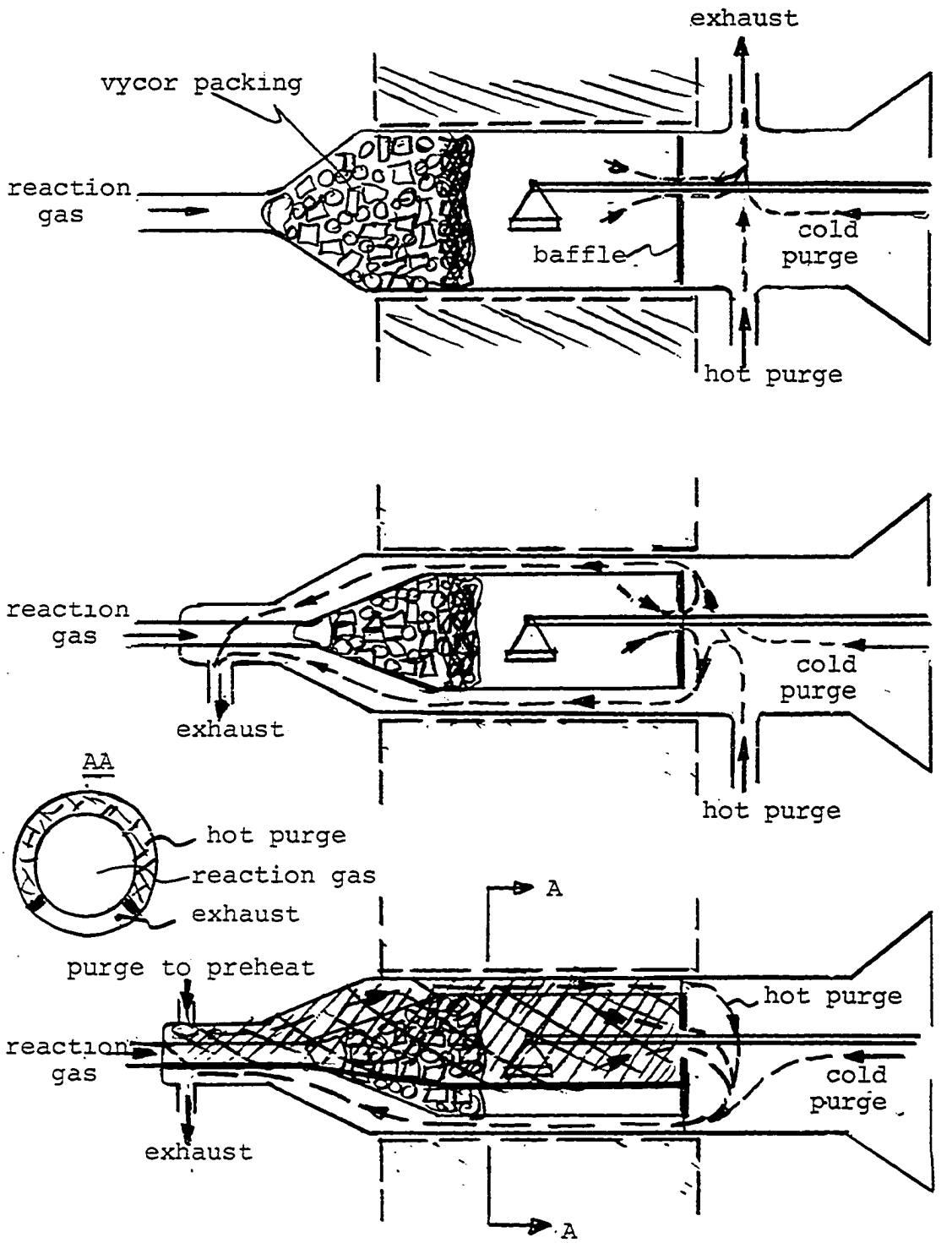

preheater to be closely coupled to the furnace tube. These efforts failed due to excessive heat leak. A furnace tube having a split annulus was then tried (Figure 6c). In this arrangement purge gas would be heated directly in the TGA furnace while flowing over crushed quartz in the larger of the two annulus channels. Exhaust gases exit the TGA via the remaining annulus channel. This attempt likewise failed.

The ceramic block design was able to solve the condensation problem by preventing the formation of convection cells. Reaction gases leaving the sample area now mix with the purge gas in a narrow passage in the hot ceramic block, which also houses the balance beam. A separate passage in the ceramic block houses the sample thermocouple; this passage is not shown in Figure 5. The combined gas flow is then vented out of the hot ceramic block through a narrow transverse passage which leads to a sidearm in the quartz furnace tube. With this configuration steam partial pressures up to 15 atmospheres have thus far been used without difficulty.

Similar designs utilizing aluminum or stainless steel blocks failed due to rapid conduction of heat away from the block to the cold balance housing, resulting in condensation on the block surfaces and balance beam.

The ceramic block also provides for effective separation of the reaction and purge gases. Penetration tests,

again using the copper/oxygen/nitrogen technique, showed that little, if any, penetration occurs at 300 psig with typical flows of 100 cm^3/min (actual) of purge gas and 100 cm^3/min (actual) of reaction gas.

4.05 Flow System for the Pressure Thermobalance

The principle difficulty in designing a high pressure dynamic flow system for the thermobalance with corrosive gas atmospheres is the absolute necessity for maintaining stable flow of gases while providing continuous balancing of pressure inside the thermobalance with its surrounding atmosphere. Unsteady flows to the pressure thermobalance can result in the inadvertent introduction of corrosive gases into the balance housing.

Figure 7 is a schematic of the flow system for the pressurized thermobalance. Inlet pressures of the various gases are controlled using standard cylinder regulators. Lo-flow regulated rotameters are used for flow measurement and control of the individual gases. System pressure is maintained by a lo-flow back pressure regulator (hand-loading, piston type) through which all gases are vented.

Pressure is equalized in the balance and pressure vessel by a common upstream tee connection on the nitrogen purge line. This connection also serves as a bypass to direct nitrogen flow into the pressure vessel during pressurization and as purge to the balance during run conditions. This arrangement permits rapid pressurization to take place without adversely affecting the balance. The initial reser-

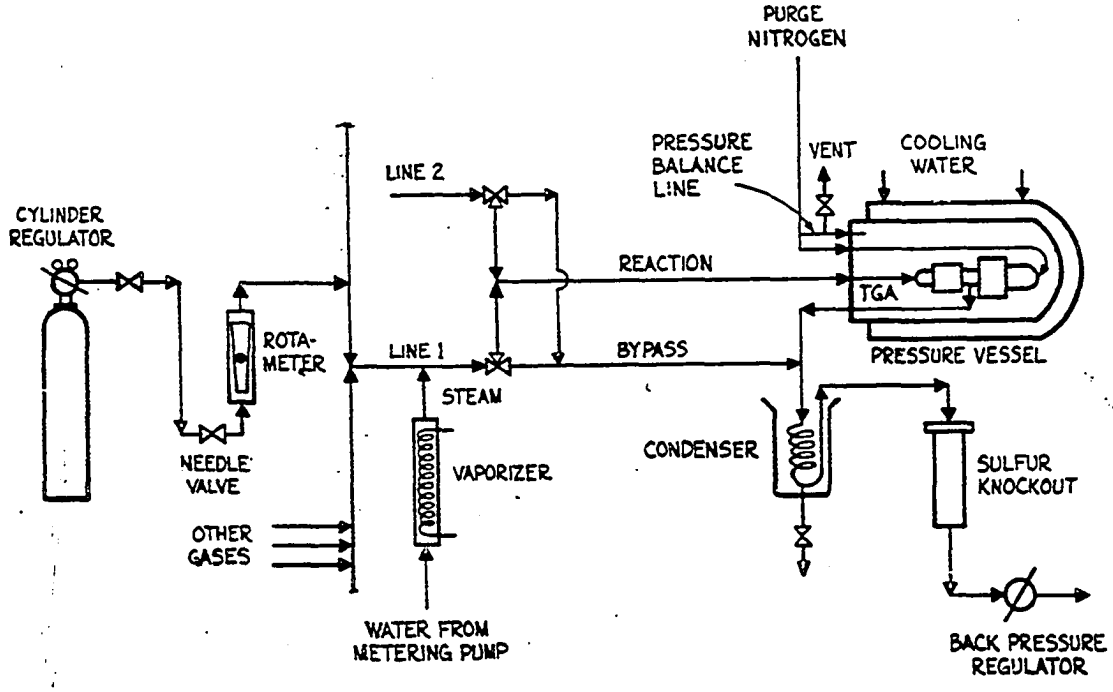

Figure 7. Schematic of Flow System for High Pressure Thermobalance

voir of nitrogen remains in the vessel throughout a run until depressurization. Rapid depressurization is achieved by throttling from the pressure balancing line directly (not shown in Figure 7).

Studies were made to determine the maximum purge flow rate possible at various pressures. It was found that at atmospheric pressure, turbulence, as detected on the chart recorder, became severe at a purge flow of 2500 cm^3/min (actual). At 300 psig, turbulence was well established at the very low purge flow of 300 cm^3/min (actual). This suggests that a "safe" purge flow of 100 cm^3/min (actual) be used during runs at higher pressures.

The reaction gas flow system is designed with duplicate sets of feed lines. This permits one reaction gas mixture to flow into the thermobalance while another gas mixture is either being prepared or awaiting the next phase of a reaction cycle. A system of three-way solenoid valves, (Laurence Cat. #330817S) situated close to the pressure vessel, instantaneously switches one reaction gas stream to the thermobalance while diverting the other reaction gas stream to the condenser for venting, thus bypassing the thermobalance. This design also anticipates future needs for studying short residence time kinetics.

At the present, steam is only available to one of the feed lines so that only one reaction gas mixture in a reaction cycle can contain steam.

Corrosive gases, e.g. hydrogen sulfide, sulfur dioxide, have their own feed line (not shown in Figure 7) to the

pressurized thermobalance. A three-way solenoid must be activated in order to direct these gases to the thermobalance, thus providing additional protection for the balance. Mixing of the corrosive gases with the remaining reaction gases takes place close to the pressure vessel in order to minimize the need for corrosion resistant fittings and valves in the flow system.

All valves and fittings are manufactured by Hoke, and have thus far performed reliably. The three-way ball valves do leak occasionally as a result of deformation and creep of the teflon seat at pressure and must therefore be checked regularly.

The low flow back pressure regulator is of Circle Seal manufacture (BPR-7). Performance of this unit is not entirely satisfactory. At pressures near 300 psig and typical flows of 400 cm^3/min (actual) the unit will cycle ± 5 psig every few minutes or so. Leakage of the piston seals is a nuisance.

In order to prevent damage to the back pressure regulator, gases leaving the high pressure thermobalance are first dried in a condenser at $0^{\circ}C$ and then desulfurized in a zinc oxide bed. These precautions were reported by others (13) to be necessary in order to prevent sulfur deposition in the back pressure regulator when operating with H_2S-laden gases.

Because of the large range of concentrations of the various gases to be used in the research, it was found necessary to prepare our own gas mixtures.

One would like to use capillary flowmeters to meter the individual gases; they are extremely accurate and give very nearly linear calibrations. In fact, capillary flowmeters were used by Pell (19,20) and Ruth (17,18) in their researches. Unfortunately, as one goes to higher pressures, typical Reynolds numbers in the capillaries begin to straddle the transition region, thus precluding any hope for reproducible calibrations.

Schutte and Koerting Lo-Flo rotameters are presently used in the experimental setup. They have a 10-to-1 range for a tube-float combination and can withstand pressures up to 400 psig. Their tested calibrated accuracy is about 2 percent of full scale. The minimum measurable flow with the above stated accuracy is about 2 cm^3/min (actual). At high pressure (300 psig) and a total reaction gas flow of 100 cm^3/min (actual) this translates to a minimum measurable gas composition of 2 percent. Below this minimum, purchased gas mixtures are used.

Calibration of the flowmeters were made using either a Brooks Calibrator, a wet test meter, or a bubble meter. For H_2S, only the latter method proved feasible.

All lines leading to and from the thermobalance are heated to above 300°C to prevent condensation of steam. Various methods were tried for connecting the gas lines to the TGA furnace tube. Silicone rubber tubing was found to be permeable to hydrogen sulfide and could not be used even on a disposable basis. Eventually, glass to metal ball joints,

lubricated by high temperature grease, were fitted and have performed without difficulties.

With a little experience, the workings of the flow system were mastered. A maximum drift in pressure of 2% was noted at the back pressure regulator. A similar drift of 5% was observed for the flow rates. This confirms the workability of the flow system.

4.06 Steam Generation for the High Pressure Thermobalance

Three methods were considered for generating controlled amounts of steam:

- hydrogen-oxygen burner
- gas saturator
- vaporizer using metered flow of liquid water

The first scheme has been used successfully by Pell (19,20) and Ruth (18) in their researches at atmospheric pressure. It avoids the difficulties associated with vaporizing liquids and is easily calibrated. However, at high pressures this technique was considered risky due to expected high heat release concentrations and the fine degree of control needed for its operation.

Saturation always involves a certain degree of uncertainty, especially for small gas flows.

The last technique was finally adopted for its simplicity and safety. A sketch of the vaporizer is shown in Figure 8. A water-cooled stainless steel hypodermic needle (22 gauge) feeds vertically into a 5/16" OD packed bed of oxidized copper beads (20 mesh). The packed bed is heated externally

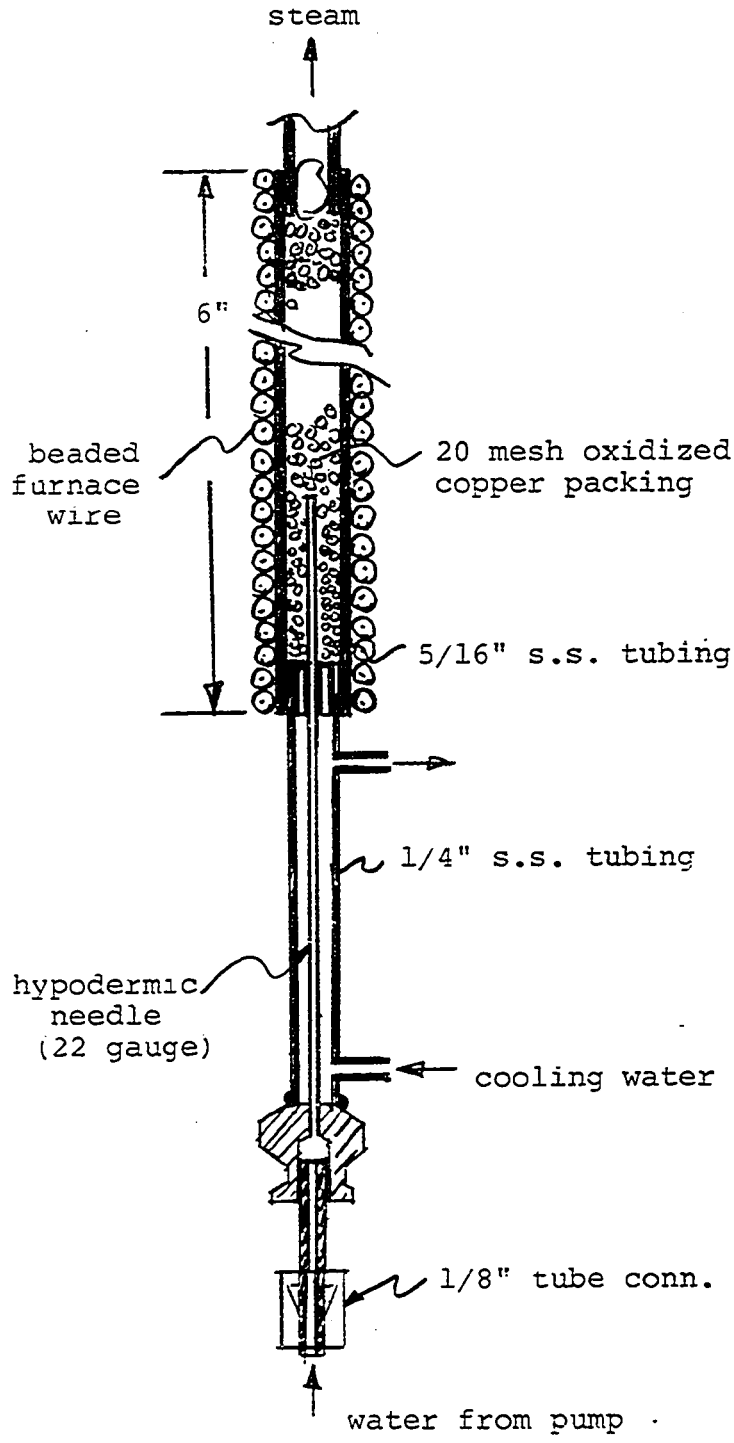

Figure 8. Vaporizer for Steam Generation in High Pressure Thermobalance

to 600°C by beaded furnace wire. The other reaction gases are heated to above saturation temperature in a packed bed preheater (1.5 mm borosilicate glass bead packing in 2 feet of ¼" tubing) before being mixed with the steam. All sections of tubing leaving the vaporizer leading to the thermobalance and from there to the condenser are wrapped with heating tape maintained at above the saturation temperature of the reaction gas mixture.

Two pumps are available for metering fluids at the low flow rates called for by the experiments. The Millroyal D pump is a positive displacement pump capable of generating a head of 1000 psig and a variable flow of 1 to 10 ml/min by adjusting the piston stroke with a micrometer type dial. Calibration of the pump delivery rate showed it to be independent of pressure for pressures greater than 30 psig.

The other pump used is a Harvard Apparatus 975 syringe injection pump capable of flows starting at 0.0048 ml/min and going up to 77 ml/min in 30 logarithmic increments for a total syringe capacity of 100 ml. It was thought that use of a high pressure syringe alone would permit use of the pump at pressures of 300 psig. However, this turned out not to be the case. A successful modification was finally found whereby two syringes are placed back to back, both under system pressure, so that the driving pressure was relieved from the motor drive and transferred to the piston of the other pressurized syringe. Calibration of the pump was found to be pressure independent. At the highest flows envisioned for the syringe pump a maximum continuous

run time of 100 minutes is possible. The syringe pump was used for lower flows and pressures and the metering pump for the higher flows and pressures.

Operation of the syringe pump at high pressure was not entirely satisfactory. At very low displacement rates (less than 0.1 ml/min liquid) the O-ring seals on the barrel of the syringes began to bind. Substitution of the manufacturer's seals with silicone rubber O-rings improved its high pressure performance considerably. The accuracy of the flow rate of steam with this technique is better than 3%. In all runs, approximately 95% of the steam fed was directly recovered in the condenser.

Subsequent to completion of this research (see Section 11.0) a high pressure LC single stroke pump was purchased to replace the existing pumps.

Difficulties with feeding high concentrations of steam at pressure were experienced with the above system. Condensation occurred inside the balance housing; no amount of purge flow or auxiliary heating of the ceramic block was able to prevent its occurrence. The source of the problem was identified to be the very nature of the vaporization process itself. Vaporization is not a steady state process, but takes place explosively as each droplet is converted to vapor. The dynamics of the flow system for the high pressure thermobalance are such that any pulses generated during vaporization could be propagated as far as the balance housing. Dynamic analysis of the system (see Section 9.0) confirmed that unsteady state penetration of steam into the balance was indeed possible and

also indicated the solution. Pulseless flow of steam was finally achieved by placing a surge volume (2 liters) and an orifice (C_v=.002) in the steam line to the thermobalance. These modifications have resulted in demonstrated operation of the instrument at 300 psig (21.4 atm) with 15 atmospheres of steam.

4.07 Continuous Weight Measurement with the High Pressure Thermobalance

The design modifications incorporated into the duPont TGA did change some of its operating characteristics. For example, at atmospheric pressure the baseline weight was found to continuously increase with temperature (~0.07mg/100°C) and total gas flow rate (~0.08mg/100 cm^3/min @ 25°C and ~0.19mg/100 cm^3/min @ 925°C). These effects, normally not observed with the original duPont instrument, are attributable to aerodynamic drag forces exerted by gases flowing over the quartz balance beam as they exit out of the ceramic block (see Figure 5).

On the other hand, weight changes observed in going to pressure are entirely attributable to buoyancy effects caused by design features of the duPont balance. In particular, the small difference in volumes of the balance arms in the duPont TGA will result in a linear decrease in baseline weight with increasing pressure, as shown in Figure 9. This linear dependency is also predicted by the relation (11):

$$\Delta R_P = (V_\ell - V_r)\Delta P_g \propto (V_\ell - V_r)\Delta P \qquad (1)$$

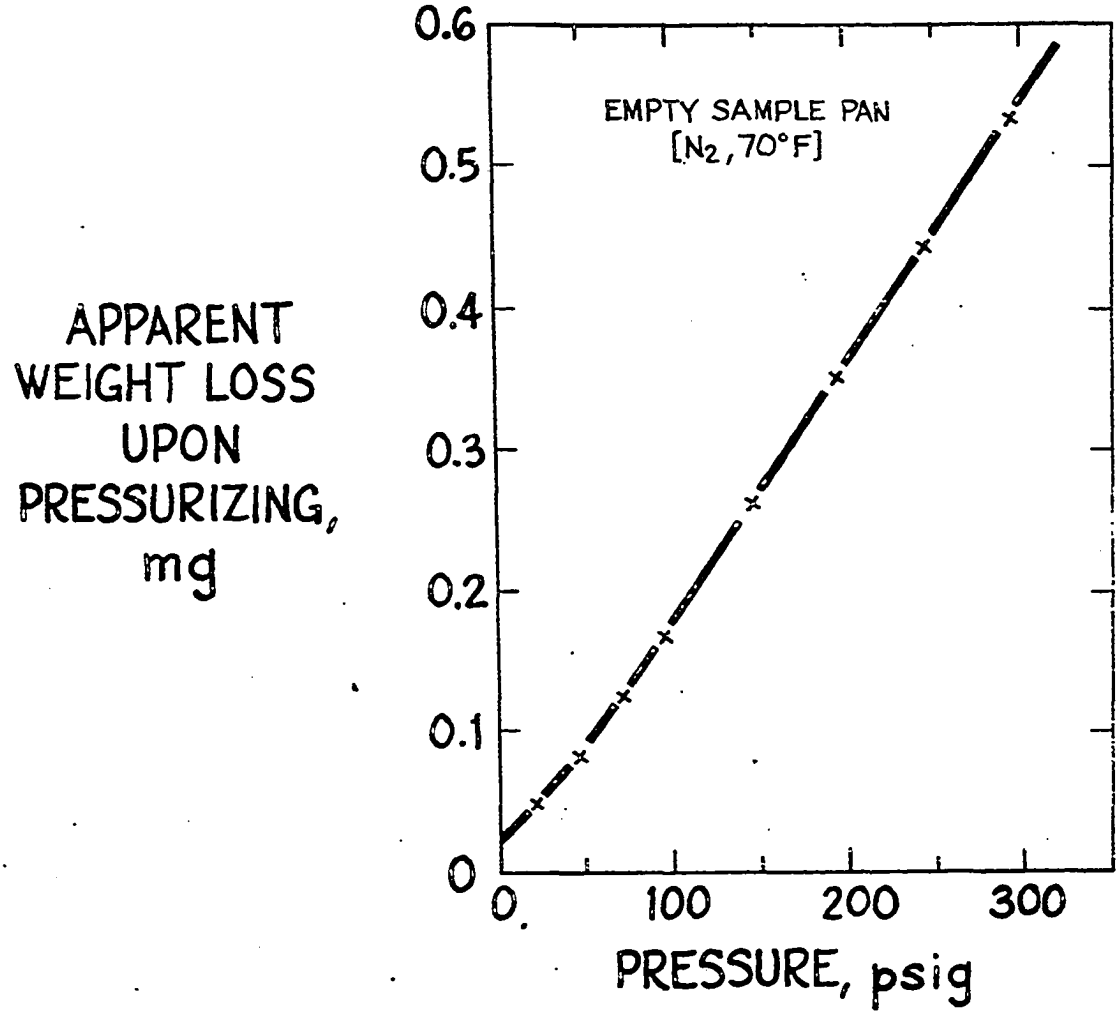

Figure 9. Effect of Increasing Pressure on Baseline Weight

where ΔR_p - shift in baseline weight with increasing pressure

$\Delta\rho_g$ - change in gas density due to increasing pressure, ΔP

V_r, V_ℓ - effective volume of right and left balance arms, respectively

A value for $(V_\ell - V_r)$ of 0.023 cm^3 can be calculated from the slope of the plot in Figure 9.

Figure 10 shows an increase in baseline weight obtained at 300 psig with increasing temperature. The sharp initial rise is attributed to the reduction in gas density in the hot reaction zone, while the slower linear rise at the higher temperatures simply reflects the aerodynamic effects discussed earlier. Employing the same principles used in developing Equation 1, we obtain the relation (11):

$$\Delta R_t = V_h \Delta\rho_g \propto V_h \left[\frac{1}{T_c} - \frac{1}{T_h}\right] \qquad (2)$$

where ΔR_t - shift in baseline weight at pressure with increasing temperature

V_h - effective volume of left balance arm in hot zone

$\Delta\rho_g$ - change in gas density in hot zone due to increasing temperature

T_c, T_h - ambient and hot zone temperatures, respectively

The above equation predicts a linear relationship for the shift in baseline weight with the inverse absolute temperature in the hot zone; i.e., the sample temperature. After correction for aerodynamic effects (0.07mg/100°C), Figure 10 was accordingly replotted in Figure 11, from which a value of V_h of 0.0412 cm^3 was calculated from the slope.

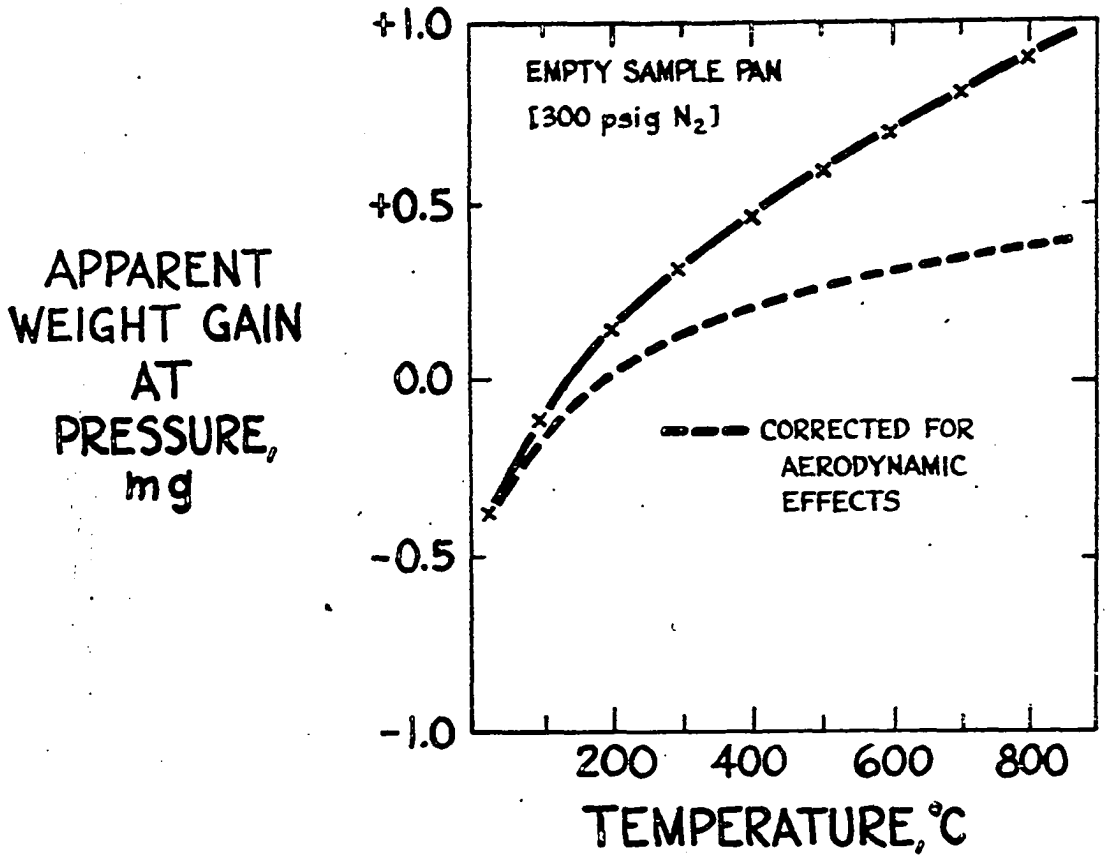

Figure 10. Effect of Increasing Temperature at 300 psig on Baseline Weight

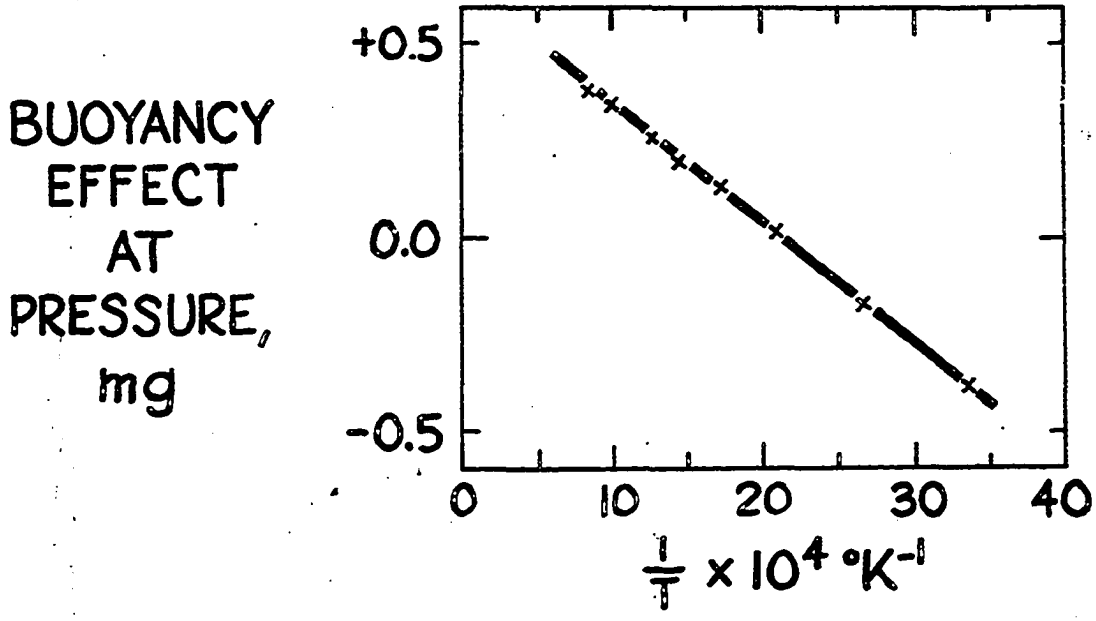

Figure 11. Buoyancy Correlation for Effect of Increasing Temperature at 300 psig on Baseline Weight

The above discussions serve to illustrate that not only are these shifts in baseline weights explainable but they are also easily amenable to calibration. Similar calibrations have, in fact, been used by many investigators to correct TGA temperature scans in order to extract the "true" scans (5,8,11). There is even one report of a high pressure instrument with built-in circuits for automatic compensation of buoyancy effects (7).

When operating in the isothermal mode, the above calibration procedure becomes unnecessary since all calculations will then be made relative to the apparent starting weight just prior to the run. However, a buoyancy correction to the apparent weight change for a sample undergoing reaction is still required in order to relate it to a "true" weight change. This correction factor is given by the relation:

$$\Delta w = \left[\frac{\rho_g}{\rho_p} + 1\right] \Delta w' \qquad (3)$$

where $\Delta w'$, Δw - apparent and real weight change at isothermal conditions, respectively

ρ_g - gas density

ρ_p - mean particle density of starting and final solid

In most cases the above correction is usually very small and can be neglected. For half-calcined dolomite at 300 psig and 800°C this correction corresponds to only 0.3% of the sample weight, or 0.5% conversion in the reaction of calcined dolomite with carbon dioxide.

5.0 Recarbonation of Calcined Dolomite - Technical Background

5.01 Introduction and Objectives

Solid acceptors for carbon dioxide, used cyclically at high temperatures, have found applications in gas separation and purification and as a source for process heat. The solid acceptors are most often in the form of metal oxides prepared from naturally occurring minerals.

Minerals which have received considerable attention are limestones and dolomites. Calcium oxide has been proposed as an acceptor for several reactions, including desulfurization, lignite gasification and carbonization, shift conversion, steam reforming of hydrocarbons, catalytic cracking of hydrocarbon oils, and the reduction of metallic ores. In some of these reactions the solid may serve to catalyze the reaction as well.

In dolomitic acceptors only the calcium species are reactive. The magnesium species, aside from their possible catalytic properties, are chemically inert and serve only to support the microstructure by finely dispersing the small crystallites of the active calcium species. Often, the resulting superior durability or reactivity of dolomitic acceptors will lead to their selection in a process in spite of their lower theoretical capacity in comparison to limestones.

The principal reaction in many of the applications of limestone and dolomitic acceptors is the cyclic calcination and recarbonation of the CaO via

$$CaO + CO_2 = CaCO_3 \quad \Delta H_{298^\circ K} = -42.33 \text{ kcal/mole}$$

The recarbonation reaction usually serves two functions: to provide a source of high temperature process heat to endothermic reactions and to selectively remove diluent carbon dioxide generated by these reactions. This is best illustrated by the CO_2-Acceptor Process for gasifying lignite (21), where heat for endothermic gasification reactions with steam is provided by the in situ recarbonation of fully-calcined dolomite. Removal of carbon dioxide generated during gasification also considerably upgrades the heating value of the make gas. Regeneration of the acceptor is carried out in a separate calciner where heat for calcination is provided by in situ combustion of a portion of ungasified char with air.

Recarbonation of calcium oxide prepared from a range of materials has been investigated extensively over the past four decades (21-40). There have also been studies reported for the recarbonation of fully-calcined dolomite as well (21,24-27,40-43), although here the information is much more sparse. In general, it has been found that fully-calcined dolomite will recarbonate to a greater extent than any form of calcium oxide (21,25-27,40). This has been attributed to the microcrystallinity of the calcium species in dolomitic materials and to the microporous supporting structure provided by the magnesium oxide.

The only sizeable body of data on the cyclic recarbonation of fully-calcined dolomite is that provided by Consol Coal for their CO_2-Acceptor process (21,40,43) and by the Gesellschaft für Kohlentechnik for their CO-Shift process (22).

A series of exploratory experiments on the cyclic calcination and recarbonation of calcined dolomite were undertaken to provide early demonstration of the utility of the high pressure thermobalance and at the same time to expand the existing body of knowledge relevant to the above processes. In particular, the effects of calcination conditions, total pressure, and partial pressures of carbon dioxide and steam during recarbonation were explored.

In retrospect, the results from the study of the cyclic recarbonation reactions also provide valuable conceptual information for research into other acceptor chemistries, in particular, of calcined dolomite. The importance of the temperature-environment history of a reacting solid is a lesson relevant to almost any cyclic acceptor reaction. The role played by the reaction topochemistries is well illustrated by this reaction and may find similar analogies in other gas-solid reactions.

A brief review of the dolomite literature through 1964 can be found in reference 44.

5.02 Cyclic Calcination and Recarbonation of Calcined Dolomite: Previous Work

In the Gesellschaft für Kohlentechnik's CO-Shift process (22), water gas is shifted and stripped of carbon dioxide via the reaction

$$[CaO + MgO] + CO + H_2O = [CaCO_3 + MgO] + H_2$$

The CaO species acts as a carbon dioxide acceptor while the MgO species catalyze the water gas shift reaction and also serve to support the CaO acceptor.

In the commercial process calcination is usually carried out at 800 to 850°C in a large excess of air. The shift reaction is carried out at about 500°C.

Gluud et al., of the Gesellschaft für Kohlentechnik (22), studied the recarbonation at about 550 to 580°C of the product of calcination of a wide variety of dolomitic rocks. In all cases, the initial reaction of [CaO + MgO] with carbon dioxide was extremely rapid. The course of the latter stages of the reaction was found to depend upon the Ca/Mg ratio of the starting material. For lime only 75 percent of the CaO reacts. Gluud et al. preferred dolomites having Ca/Mg atomic ratios as close to unity as possible. Working with dolomites having ratios below about 1.2, Gluud et al. were able to achieve 90 percent recarbonation of the CaO at good rates, provided the dolomite had not been exposed to a temperature above 1050°C. At calcination temperatures above 1150°C dolomite becomes dead-burned, and its reactivity is drastically reduced. Ideally, calcination temperatures should be kept below 1000°C. Cyclic recarbonation tests showed no loss in activity even after 8 cycles, for dolomites calcined in steam at 800°C.

In the Consol Coal CO_2-Acceptor process (45) lignite is gasified with steam at about 11 atmospheres pressure and 830°C. Heat for the reaction is provided by in situ recarbonation of calcined dolomite. The calcined dolomite also

serves as a sulfur and carbon dioxide acceptor to upgrade and clean the product fuel gas. Regeneration of the dolomite acceptor is carried out in a fluid bed calciner operating at about 1010°C. Heat for calcination is provided by combustion of the ungasified char with air. The Consol Coal CO_2-Acceptor process has recently been demonstrated for lignite in a pilot plant in Rapid City, South Dakota (45) at a throughput of 40 tons per day.

Support data for their process was obtained in an atmospheric thermobalance (modified Chevenard balance), in a batch fluid bed autoclave, and in a 10 lb/hr continuous bench scale unit.

Curran et al. (21,40) report results obtained in their thermobalance for the isothermal calcination and recarbonation of a Greenfield dolomite (16x20 mesh). Complete recarbonation of calcined dolomite is obtained in 2 to 10 minutes at cycle temperatures of 813 to 887°C for a CO_2 partial pressure driving force in the range of 0.08 to 0.4 atmospheres. No simple kinetic model was found to correlate the data. Curran et al. (43) also present thermobalance data for recarbonation of calcined dolomite in 1 atmosphere carbon dioxide at 830°C. Calcination for these runs were carried out in nitrogen at 1038°C with varying hold times in nitrogen. At all calcination conditions tested the recarbonation reaction ceased after about 2 to 5 minutes. If the calcinate is held in nitrogen for 16 hours at 1038°C only 80 percent of the calcium oxide could be recarbonated.

In the batch fluid bed autoclave tests (43), recarbona-

tion was carried out at 900°C in 1.5 atmospheres carbon dioxide plus 7.0 atmospheres of steam. Calcination temperatures were varied from 1038 to 1094°C, corresponding to CO_2 partial pressures of 5 to 8 atmospheres.. Twenty cycles of calcination and recarbonation were achieved with little loss in acceptor activity.

Acceptor life studies (21,40) were carried out in Consol's continuous bench scale unit. Table 2 lists the experimental conditions for calcination and recarbonation investigated.

Acceptor activities were followed during the course of cycling, which sometimes extended to more than 90 cycles. In contrast to results obtained in the earlier batch fluid bed studies (43), there is a continuous decline in activity with cycling. Greenfield dolomite retains only 25 to 35 percent of its original activity after about 70 cycles. Limestone, in comparison, retains less than 15 percent of its original activity after the same number of cycles. Correlation of all the data indicated that the activity is reduced with increasing calcination and recarbonation temperatures and with increasing acceptor residence times in the cycle. The lowest activity for any of the dolomite runs was obtained for recarbonation in the absence of any steam (40).

Physical inspections of solids removed from the continuous bench scale unit (40) showed that the activity of the acceptor decreases linearly with loss of pore volume. This process reveals itself as an increase in particle density with continued cycling.

Table 2: Experimental Conditions for CO_2-Acceptor Life Studies in Consol Coal's Continuous Bench Scale Unit (40)

Pressure, atm	11-20
Calcination	
Temperature, °C	1000-1060
P_{CO_2}, atm	2.3-6.1
Recarbonation	
Temperature, °C	815-871
P_{CO_2}, atm	0.3-1.7
P_{H_2O}, atm	2.8-6.6

Consol Coal has also carried out a number of studies on the physical chemistries of the $CaO-CaCO_3-Ca(OH)_2-CO_2-H_2O$ system (21,40). Several low temperature eutectics were identified in the course of these studies.

Results obtained from trials in their pilot plant (45) confirmed earlier estimates of acceptor makeup rates (2 to 3 percent) needed to maintain a reasonable level of activity (20 to 35 percent) of the solid.

5.03 Review of Previous Related Work at The City College

The calcination and recarbonation of fully-calcined dolomite are most easily studied by following weight changes taking place during the reaction. Two series of experiments undertaken earlier at The City College are described below.

In both experiments the same sample of Greenfield dolomite (sample A) was used. The assay and particle sizes for this sample is given in Table 3. This sample was used earlier by Pell (19,20,46) in his investigation of the reaction of hydrogen sulfide with fully calcined dolomite.

The first series of experiments was carried out in 1970 by Gary Weil, a senior in Chemical Engineering at The City College, in a duPont 950 TGA. The purpose of these experiments was to determine the effects of calcination conditions on the recarbonation rates in 1 atmosphere of carbon dioxide. In these tests calcination was carried out nonisothermally at $10^{\circ}C$/min to a preselected temperature in the desired gas

Table 3: Assays and Particle Sizes of Greenfield Dolomite Samples

	Sample A (19)	Sample B (18)
Particle Size	-80+350 mesh	-250+250 mesh
Atomic Ratio, Ca/Mg	1.09	1.01
Assay, weight percent		
Magnesium	12.32	13.48
Calcium	22.04	22.43
Iron	0.37	0.18
Silicon	0.X	0.X
Aluminum	0.X	0.X
Others	0.X or less	0.0X or less

atmosphere, and then held at the maximum temperature for a given period of time, again in some preselected gas atmosphere. The sample was then cooled in nitrogen to near room temperature, whereupon recarbonation was carried out non-isothermally at 10°C/min in 1 atmosphere of carbon dioxide. At all conditions tested complete recarbonation was achieved below 900°C. The effects of calcination atmosphere, hold atmosphere, hold temperature, and hold time were explored in this series of experiments.

Figure 12 illustrates results obtained for two runs made in these experiments. A complete summary of results is contained in Table 4. The relative reaction rates for non-isothermal recarbonation may be expressed in terms of the temperature, $T_{\frac{1}{2}}$, at 50 percent recarbonation. The lower this temperature, the more reactive the material.

Between 925 and 975°C there appears to be only a small effect of increasing hold temperature on reactivity. Increasing the hold time from 1 to 4 hours increased the value for $T_{\frac{1}{2}}$ by 50°C at 925°C and by only 20°C at 975°C. The most reactive material is formed when calcination is carried out in nitrogen to 800°C, with no hold period. This material is approximately 30 to 40 times more reactive than that produced by calcining in carbon dioxide. Addition of a hold period at 975°C in nitrogen increases $T_{\frac{1}{2}}$ by only 40°C. In contrast, the addition of a hold period in carbon dioxide increases $T_{\frac{1}{2}}$ by more than 150°C, bringing $T_{\frac{1}{2}}$ within 35°C of that obtained by calcining in carbon dioxide. It

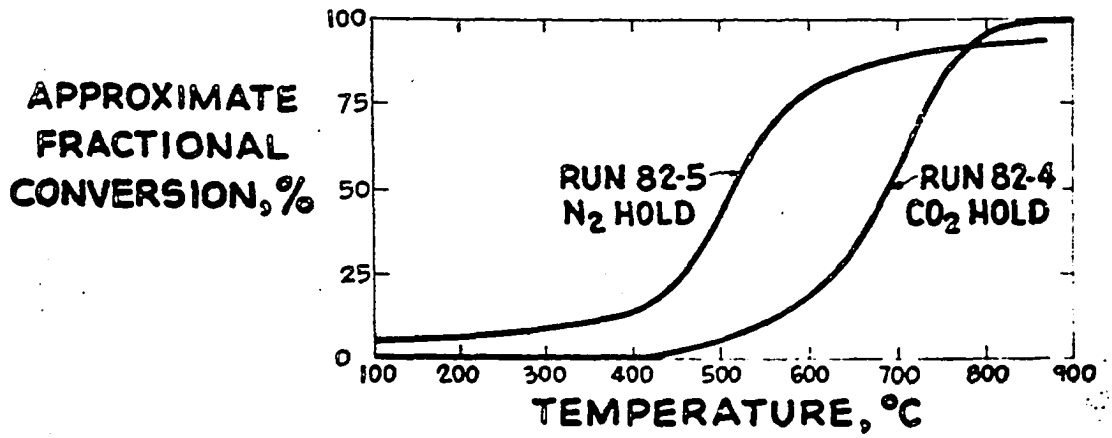

Figure 12. Nonisothermal Recarbonation of Calcined Dolomite in 1 Atmosphere of CO_2 (G. Weil)

Table 4: Nonisothermal Recarbonation of Calcined Dolomite

conditions: 1 atm. CO_2, 10°C/min
(G. Weil)

Run No.	Calcination Atm.	Hold Atm.	Hold Temp, °C	Hold Time, Hrs.	Temp @ 50% Conversion, C
82-6	CO_2	CO_2	925	1	668
82-1	CO_2	CO_2	950	1	643
82-2	CO_2	CO_2	940-970	1	651
82-4	CO_2	CO_2	975	1	691
82-8	CO_2	CO_2	925	4	707
82-7	CO_2	CO_2	975	4	710
82-3	N_2	N_2	800 max	5 mins	475
82-5	N_2	N_2	975	1	515
82-9	N_2	CO_2	975	1	629

therefore appears that the factors most strongly affecting the reactivity of the calcinate are hold atmosphere and calcination atmosphere (and hence calcination temperature).

A second series of experiments was carried out in 1971 by Lauris Sterns, also a senior in Chemical Engineering at The City College, using an Ainsworth automatic recording balance. The experimental arrangement is described in reference 19. Calcination of the raw stone was carried out non-isothermally at 10 to 15°C/min to 925°C in 1 atmosphere of carbon dioxide. The sample was then held at 925°C in nitrogen for an additional 15 to 30 minutes before being cooled to the desired recarbonation temperature. Unlike the first series of experiments, recarbonation was carried out isothermally. Conditions for subsequent calcinations varied from run to run. In this second series of experiments the cyclability of calcined dolomite was explored at three temperature levels and in various gas atmospheres containing carbon dioxide, nitrogen and steam. Table 5 lists the experimental conditions for the more salient runs.

Figures 13 and 14 show results for cycling carried out at 550°C in carbon dioxide and in 50/50 CO_2/N_2, respectively. The observed loss in reactivity with cycling is characteristic of the results obtained with this material.

The catalytic effect of steam on the recarbonation reaction is illustrated in Figure 15. The substitution of half the carbon dioxide by steam accelerates the recarbonation rate by a factor of 30 to 100 times. Cycling experi-

Table 5: Experimental Conditions for Cyclic Calcination and Recarbonation of Greenfield Dolomite at Atmospheric Pressure (Lauris Sterns)

I. Effects of Temperature and Gas Composition

Temp. °C	Composition $CO_2/N_2/H_2O$	Sample Numbers	Number of Cycles	Remarks
475	50/50/0	10	2	Calcination in CO_2
		11	1	" " "
550	10/90/0	1	2	" " "
	50/50/0	4	5	" " "
	100/0/0	3	9	" " "
		2	3	" " "
	50/0/50	8	3	" " "
		5,6,7	1	" " "
	50/0/50	12	23	Calcination in 50/0/50
700	50/0/50	9	5	Calcination in CO_2
	50/0/50	13	31	Calcination in 50/0/50

II. Special Runs

Sample Number	Temp °C	Composition $CO_2/N_2/H_2O$	Cycle Number	Remarks
1		10/90/0	1-2	550°C
			3-8	700°C
2	550°C	100/0/0	1-3	Calcination in CO_2
			4	Calcination in N_2
9	700°C		12	50/50/0 0-185 mins 50/0/50 185-250 mins 50/50/0>250 mins

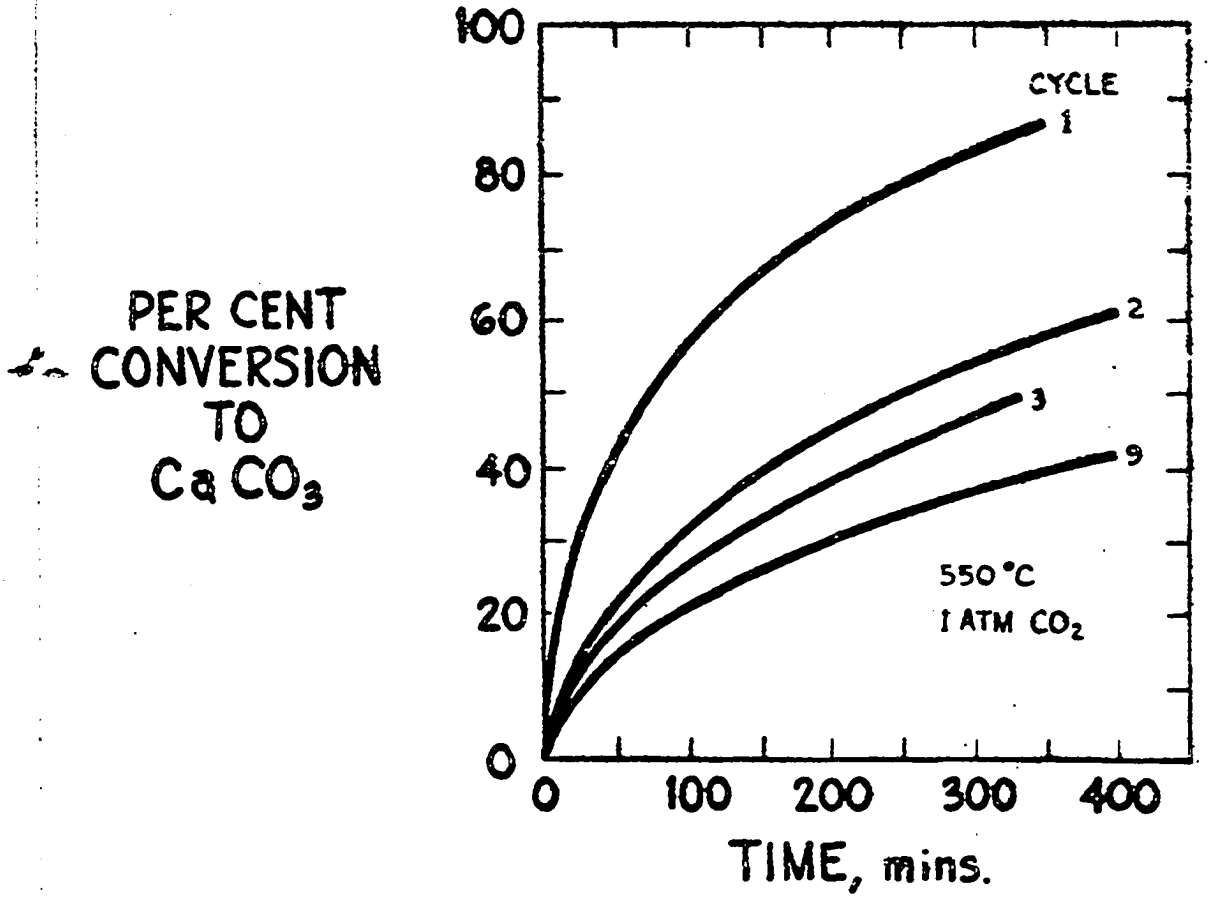

Figure 13. Cyclic Recarbonation of Calcined Dolomite at 550°C in 1 atm. CO_2 (L. Sterns)

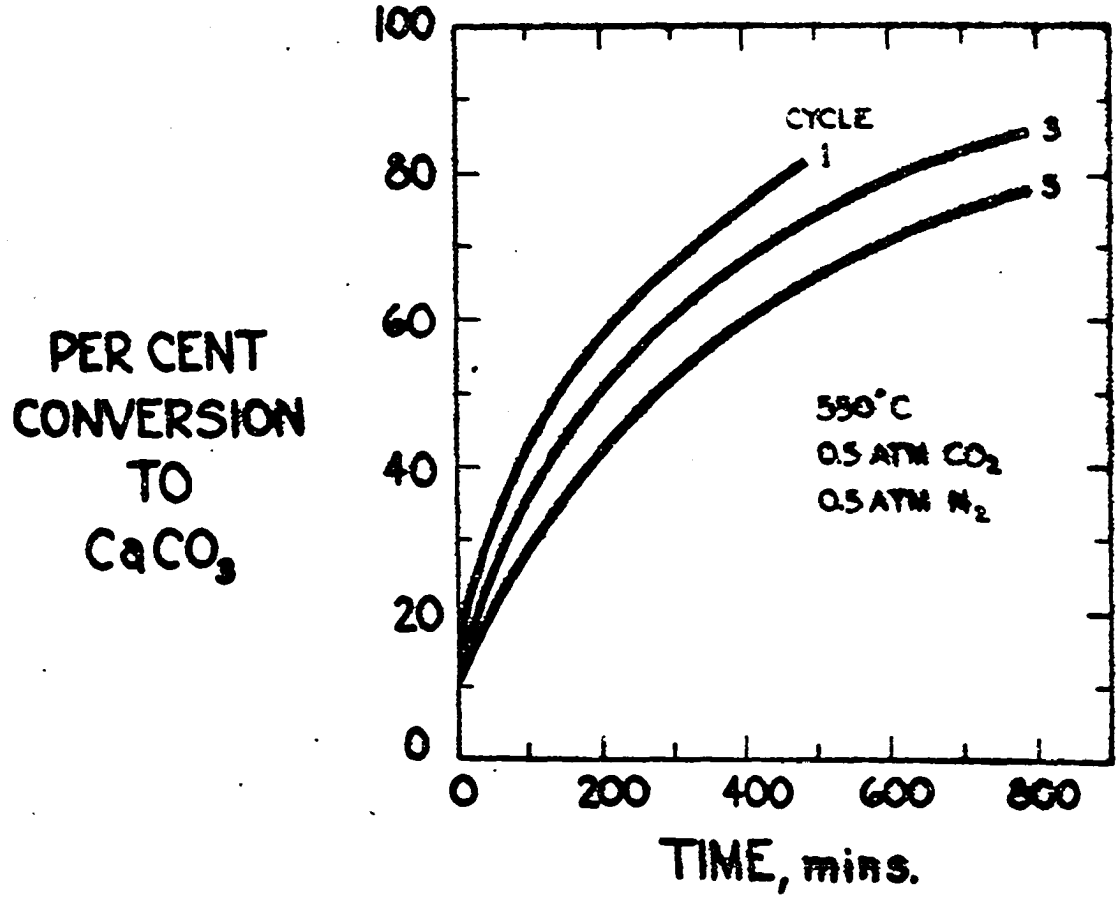

Figure 14. Cyclic Recarbonation of Calcined Dolomite at 550°C and Atmospheric Pressure in 50/50 CO_2/N_2 (L. Sterns)

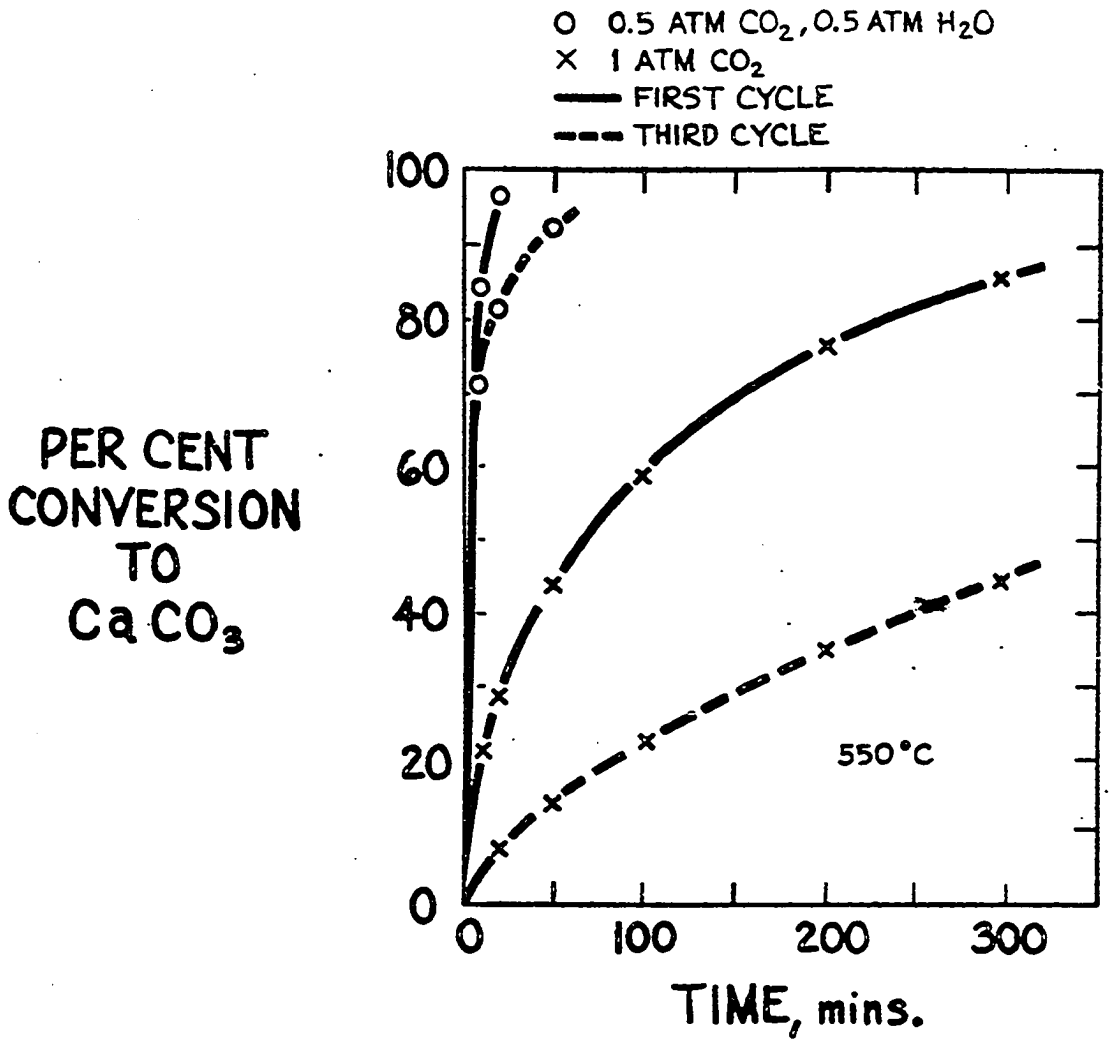

Figure 15. Recarbonationcof Calcined Dolomite at 550°C and Atmospheric Pressure in 100% CO_2 and in 50/50 CO_2H_2O (L. Sterns)

ments were therefore carried out in order to assess the extent of deactivation at these more favorable reaction conditions. Two runs of 23 and 31 cycles were completed at 550° and 700°C respectively. The results are shown in Figures 16 and 17 respectively. Calcinations in both these runs were conducted in the recarbonation gas atmosphere to 870°C. The initial reaction rates do not appear to suffer with continued cycling. Deactivation at these conditions occurs primarily by formation of inactive or "deadburnt" calcium oxide species in the solid.

The effect of partial pressure of carbon dioxide on the recarbonation rate at 550°C is shown in Figure 18 for dolomite freshly calcined in carbon dioxide. The recarbonation reaction appears to be first order in carbon dioxide partial pressure above 0.5 atmospheres CO_2 and approaches zero order at lower partial pressures. A similar comparison of rates for cycled materials is made difficult by the important influence of recarbonation history on reaction rate.

A complete study of the effect of recarbonation temperature was not made. Figure 19 illustrates the increase in recarbonation rate in 50/50 CO_2/N_2 obtained in going from 475 to 550°C. Again, comparison of rates for cycled materials is not easily interpreted due to the influence of recarbonation history.

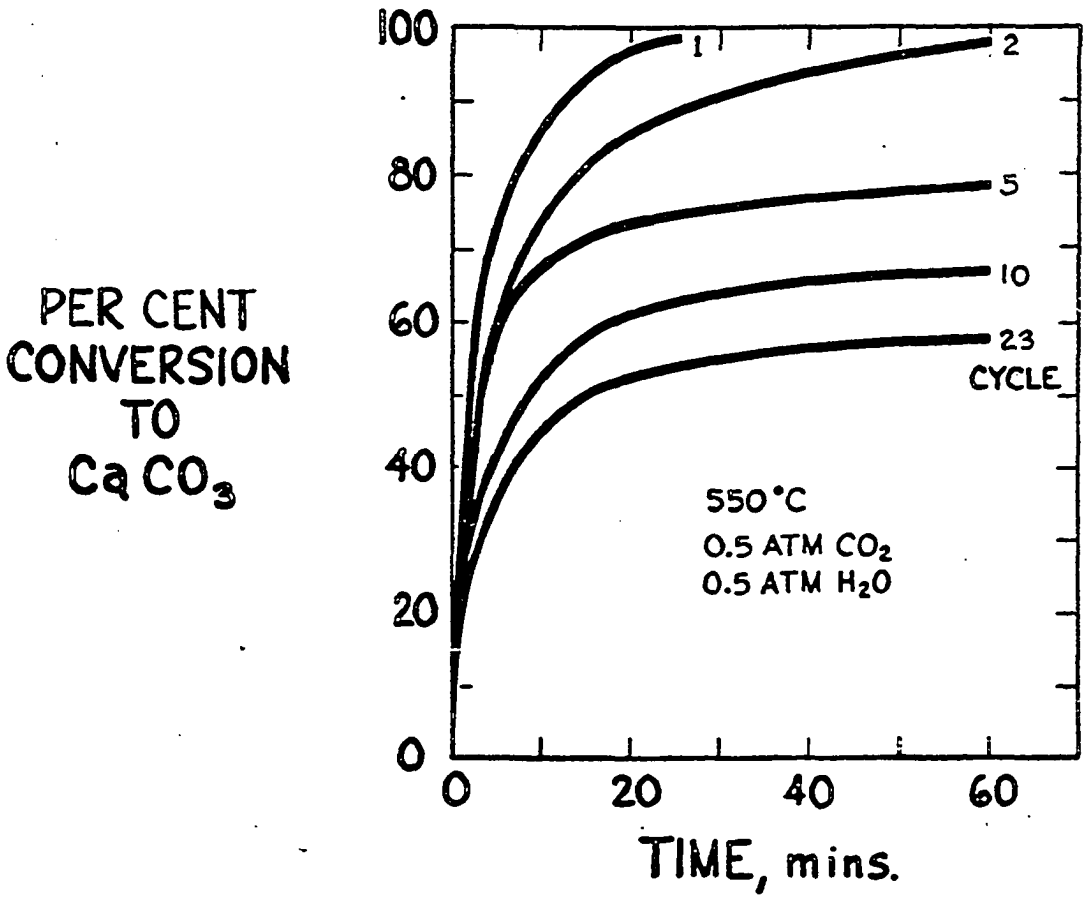

Figure 16. Cyclic Recarbonation of Calcined Dolomite at 550°C and Atmospheric Pressure in 50/50 CO_2/H_2O (L. Sterns)

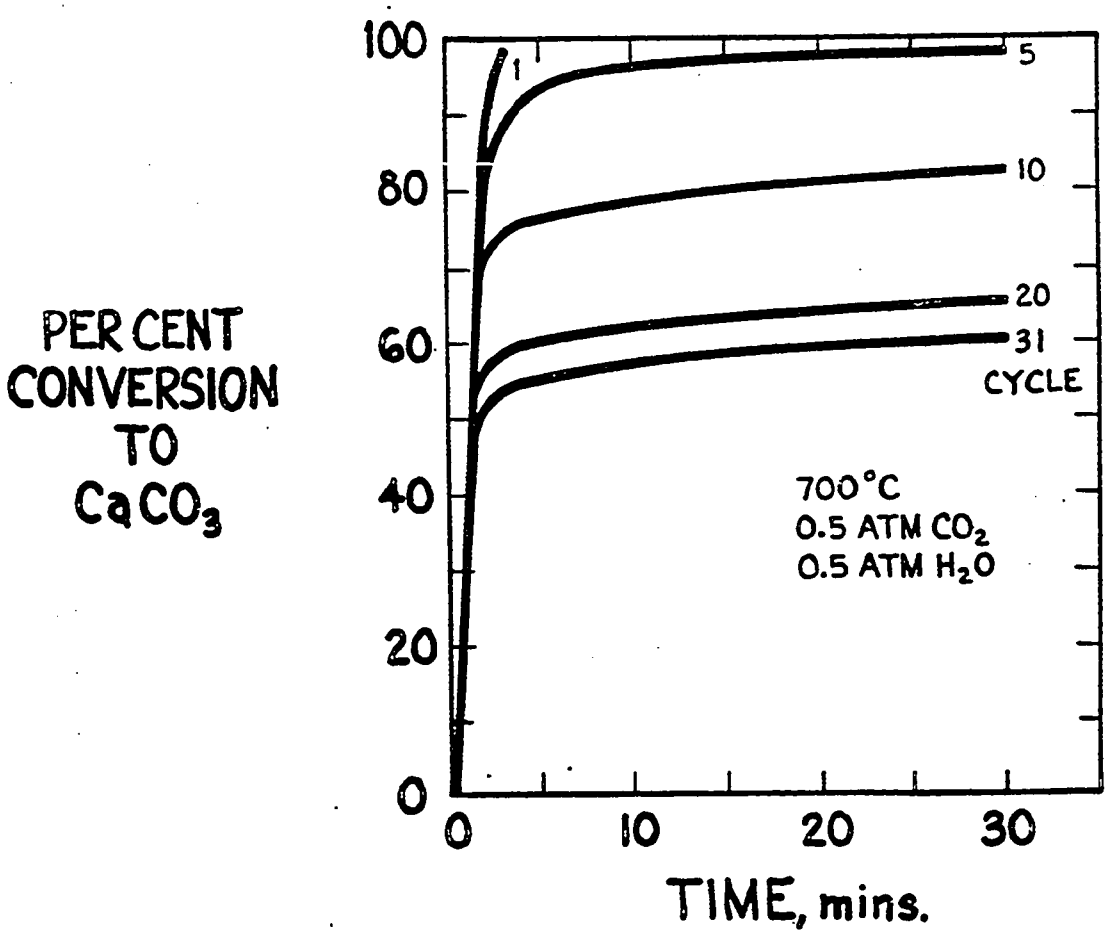

Figure 17. Cyclic Recarbonation of Calcined Dolomite at 700°C and Atmospheric Pressure in 50/50 CO_2H_2O (L. Sterns)

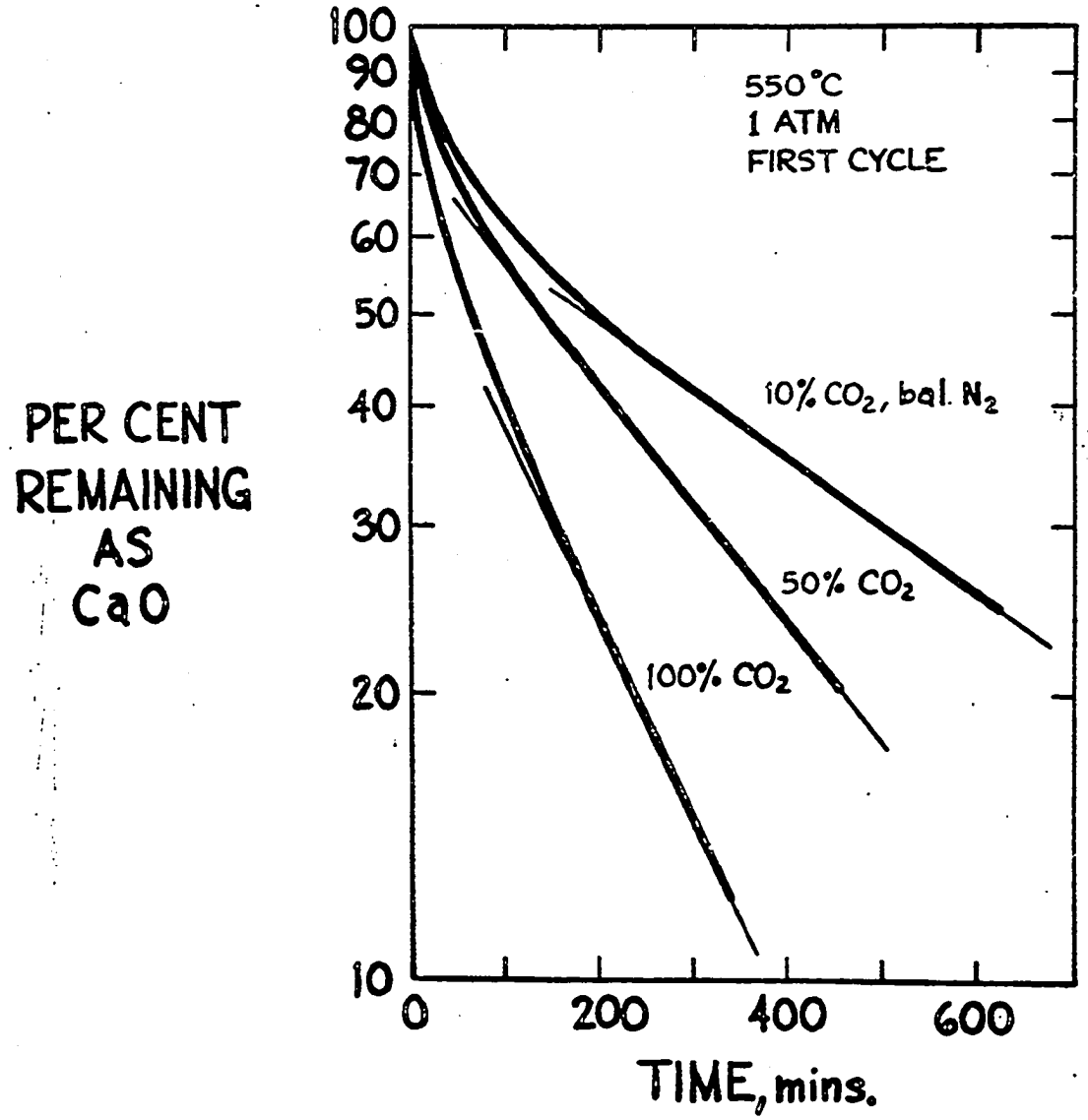

Figure 18. Recarbonation of Calcined Dolomite at 550°C and Atmospheric Pressure in Various Partial Pressures of CO_2 (L. Sterns)

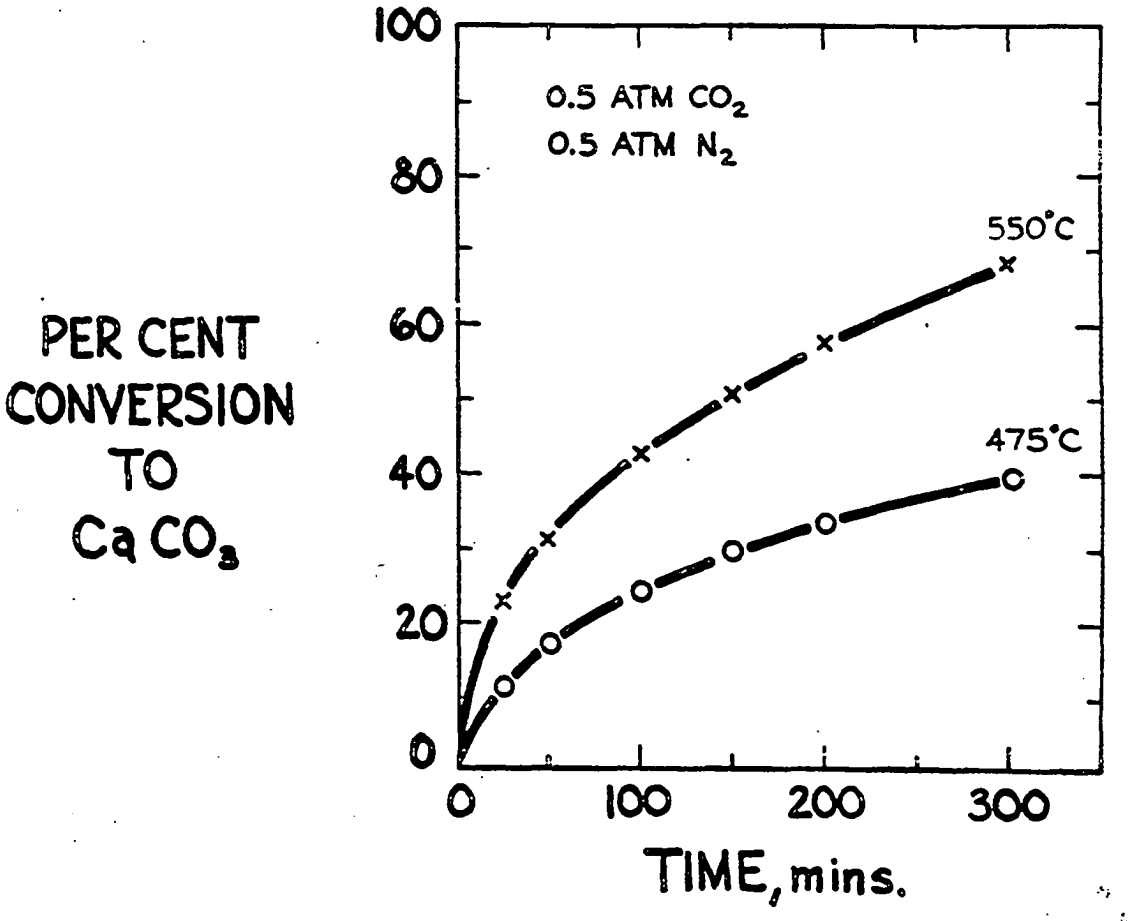

Figure 19. Recarbonation of Calcined Dolomite at Atmospheric Pressure in 50/50 CO_2N_2 at 475°C and 550°C (L. Sterns)

6.0 Cyclic Recarbonation of Calcined Dolomite in High Pressure Thermobalance

6.01 Experimental

Shakedown of the high pressure thermobalance was performed by studying the cyclic calcination and recarbonation of calcined dolomite at high pressures.

For these runs a second sample of Greenfield dolomite (Sample B) was used. The assay and particle size for this sample is given in Table 3. This sample was used earlier by Ruth in his investigation of the reaction of hydrogen sulfide with half-calcined dolomite (17,18).

Calcination was carried out nonisothermally at 20°C/min to the maximum temperature selected and held there for an additional 10 minutes in nitrogen. The sample was then cooled in nitrogen to the selected recarbonation temperature. In this series of experiments the effects of calcination conditions and the partial pressures of carbon dioxide and steam during recarbonation were explored at a pressure of 300 psig. Table 6 lists the experimental conditions for the various runs.

6.02 Experimental Results

Figure 20 shows results for 7 cycles carried out at 650°C and 300 psig with 4 atmospheres of carbon dioxide. A maximum temperature of 1030°C is needed to affect calcination at these conditions. Again, we obtain the characteristic deactivation behavior seen earlier by Lauris Sterns.

Table 6: Experimental Conditions for Cyclic Calcination and Recarbonation of Greenfield Dolomite in a High Pressure Thermobalance

I. Effects of temperature, pressure, gas composition and calcination conditions

Run Number	Number of Cycles	Pressure, psig	Calcination			Recarbonation		
			Temp, °C	partial pressure, atm CO_2	H_2O	Temp, °C	partial pressures, atm CO_2	H_2O
20	3	0	930	1	-	700	1	-
11	5	0	930	1	-	700	1	-
12	5	0	930	1	-	700	0.5	0.5
15,16,17	3	300	930	1	-	700	1	-
14	4	300	930	1	-	700	4	-
7	7	300	1030	4	-	650	4	-
21	3	300	1030	4	-	700	4	-
10	3	300	1030	4	4	700	4	4

II. Special Runs

Run Number	Cycle Number	Calcination			Recarbonation		
		Temp. °C	Pressure Total, psig	CO_2, atm.	Temp. °C	Pressure Total, psig	CO_2, atm.
18	1	930	0	1	700	300	1
	2	930	300	1	700	300	1

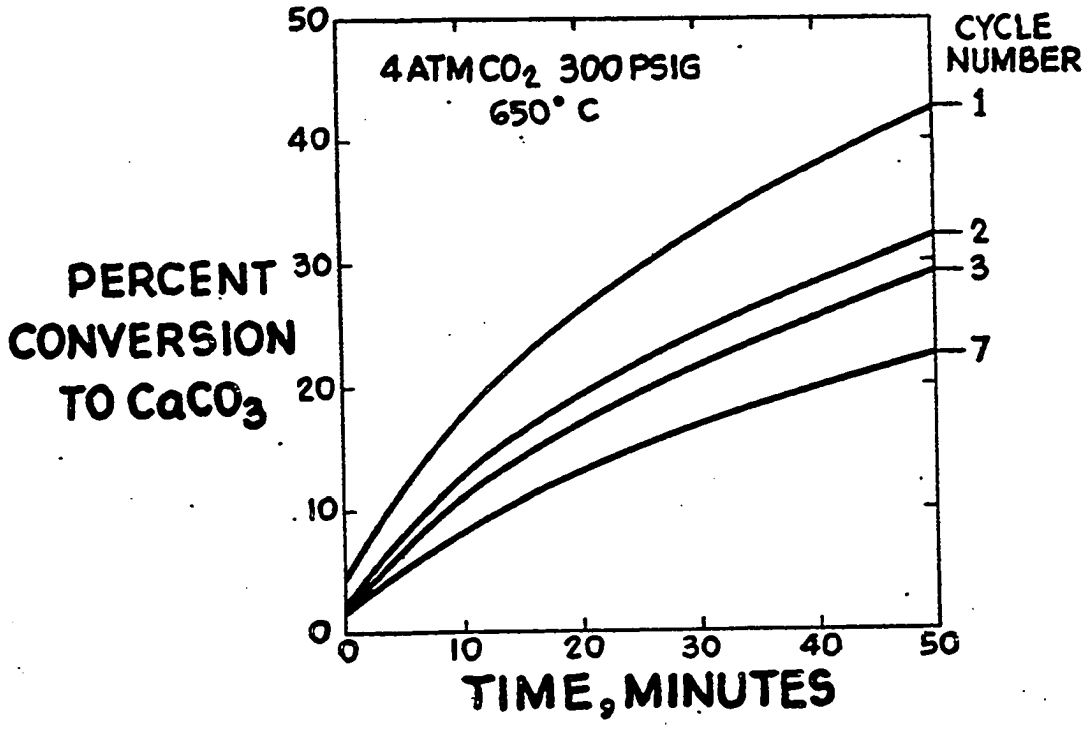

Figure 20. Cyclic Recarbonation of Calcined Dolomite at 650°, 300 psig in 4 atm. CO_2

The effect of partial pressure of carbon dioxide on the recarbonation rate was explored. Results shown in Figure 21 for recarbonation at 700°C and a total pressure of 300 psig indicate that the reaction is approximately first order in carbon dioxide over the range of 1 to 4 atmospheres CO_2. Calcinations for these runs were carried out to 930°C, at pressure, in 1 atmosphere of carbon dioxide. These results agree with the reaction orders for carbon dioxide obtained earlier by Sterns at atmospheric pressure.

Total pressure was found to significantly affect the recarbonation rate as shown in Figure 22. The recarbonation rate is nearly halved in going from atmospheric pressure to 300 psig. In both runs calcination was at atmospheric pressure in carbon dioxide and the recarbonation was at 700°C in 1 atmosphere carbon dioxide partial pressure. This suggests that mass transfer may become important at higher pressures.

The catalytic effect of steam on the recarbonation reaction at higher pressure was also explored. The addition of 4 atmospheres of steam at 700°C, 300 psig and 4 atmospheres carbon dioxide is shown in Figure 23 to result in a 15 to 50 fold improvement in the recarbonation rate. This agrees in magnitude with the catalytic effect obtained by Sterns at atmospheric pressure.

In agreement with the earlier nonisothermal recarbonation experiments it was found that the calcination temperature strongly affects the reactivity of the calcined dolomite.

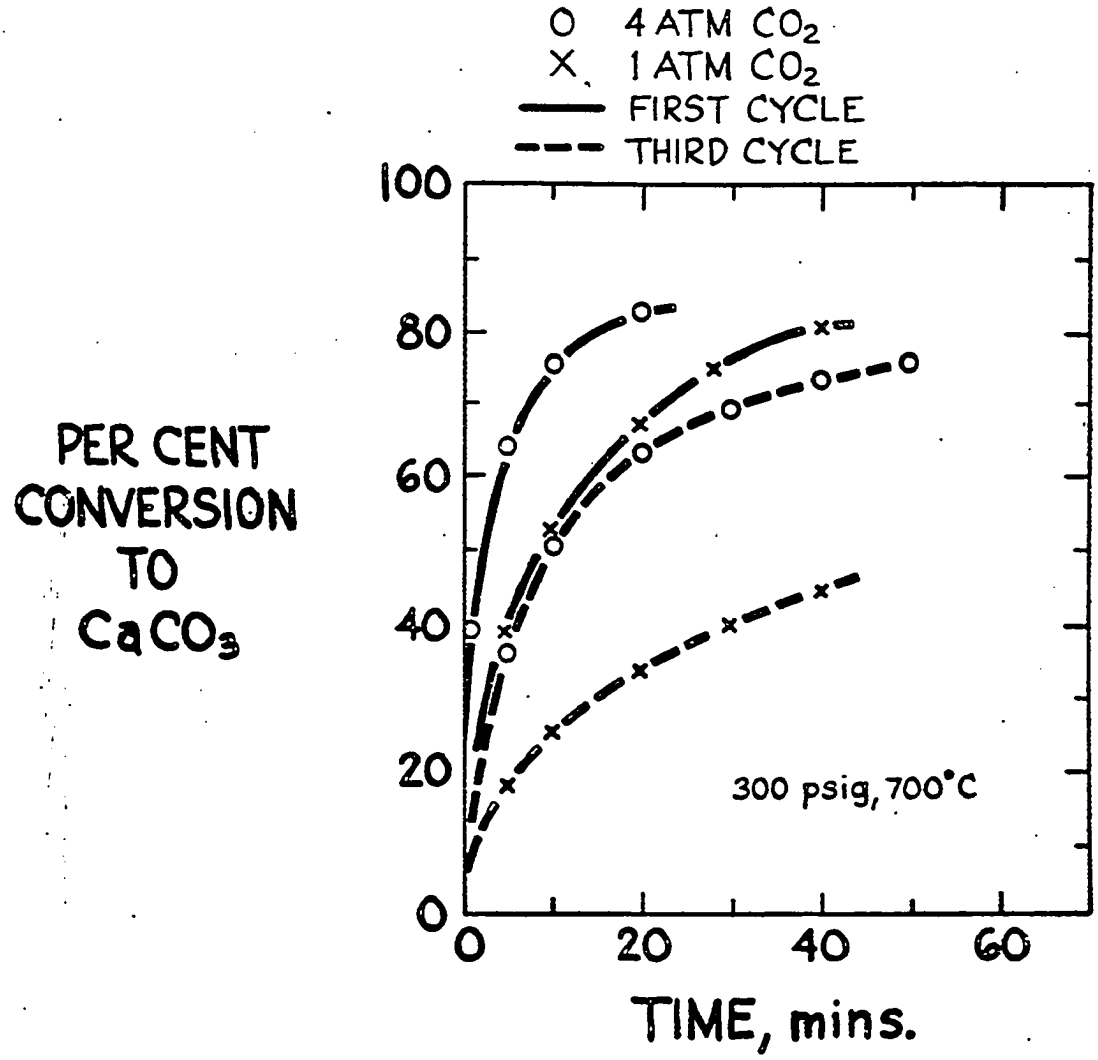

Figure 21. Recarbonation of Calcined Dolomite at 700°C, 300 psig in 1 and 4 atm. CO_2

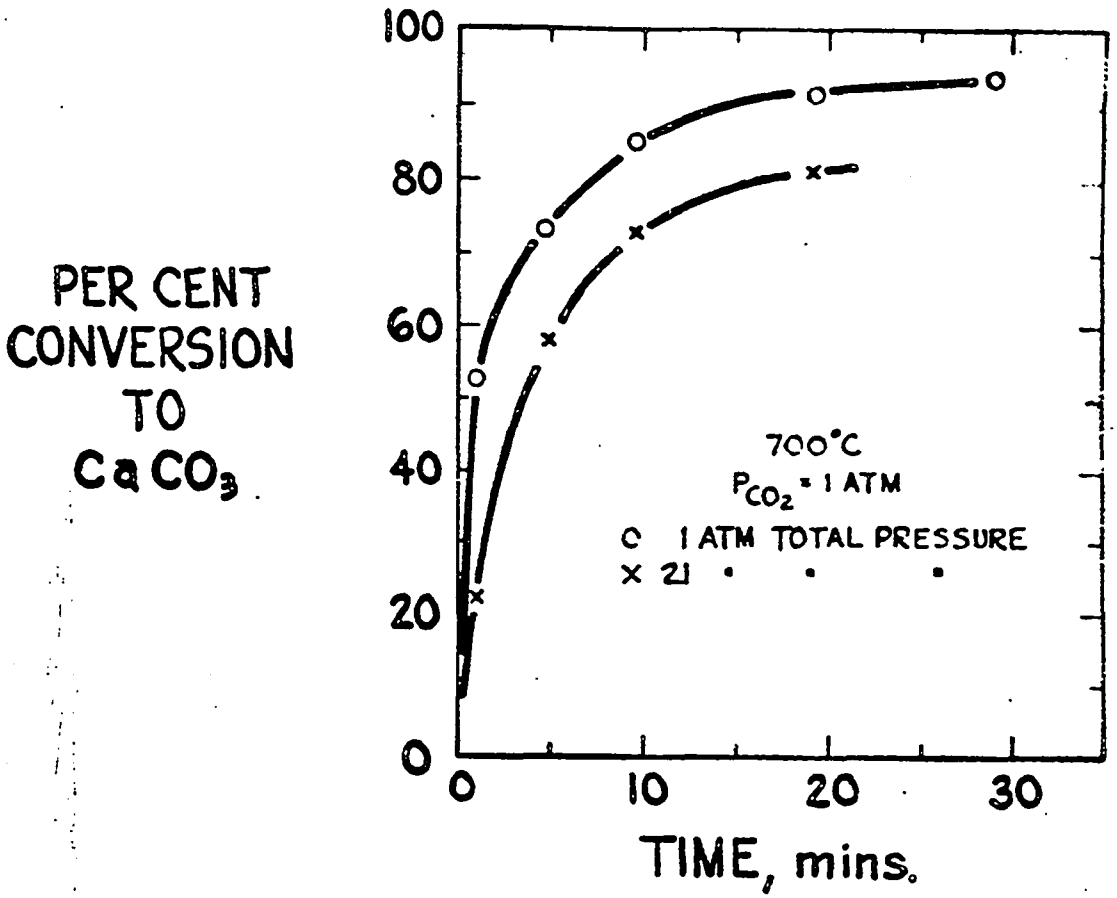

Figure 22. Recarbonation of Calcined Dolomite at 700°C in 1 atm. CO_2 Partial Pressure at Atmospheric and 300 psig Total Pressure

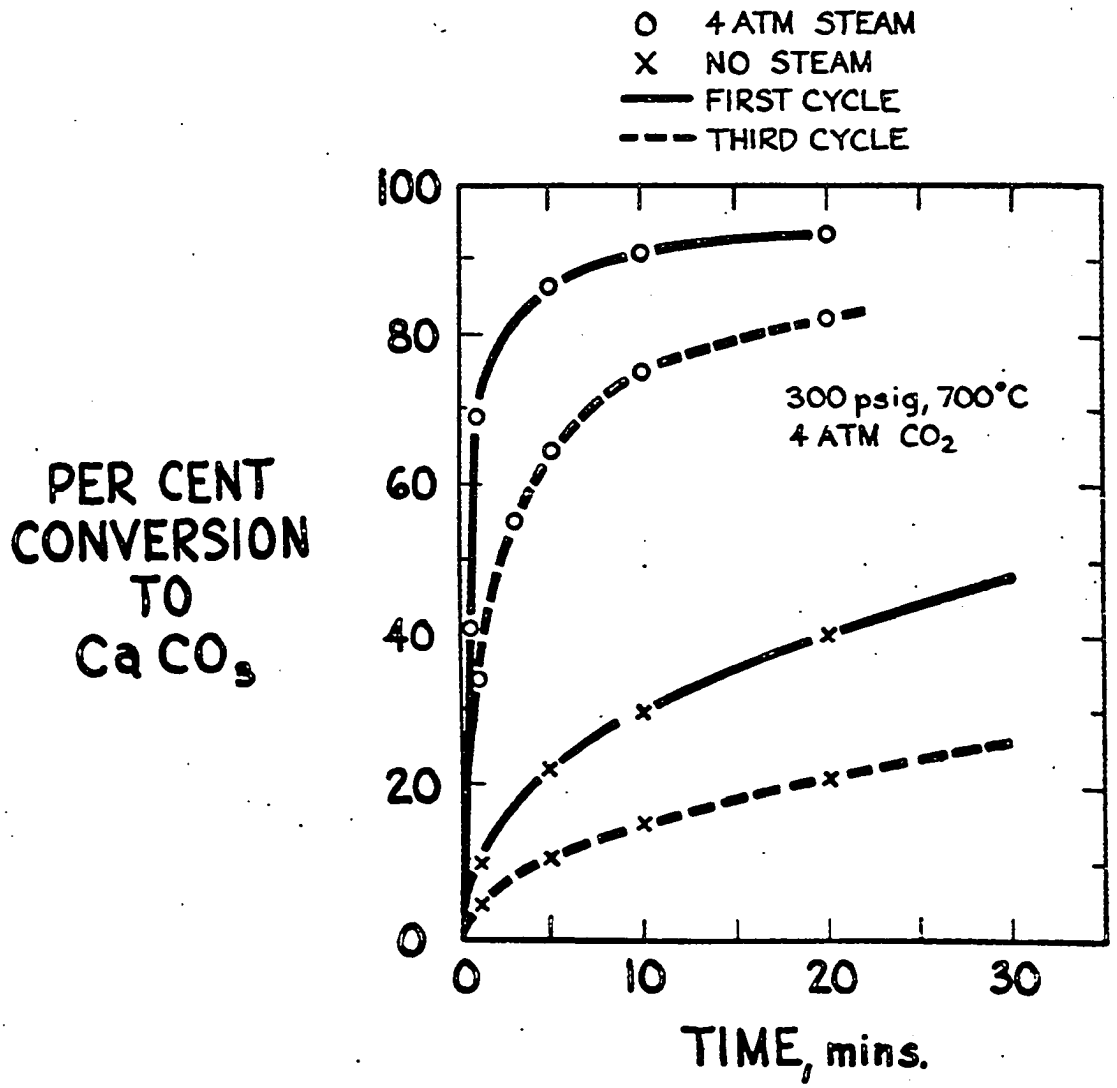

Figure 23. Recarbonation of Calcined Dolomite at 700°C, 300 psig, in 4 atm. CO_2, with and without Steam Addition

This is illustrated in Figure 24 where the recarbonation reaction of a stone calcined at 1030°C in 4 atmospheres CO_2 was found to be significantly slower than for a stone that had been calcined at 930°C in 1 atmosphere CO_2.

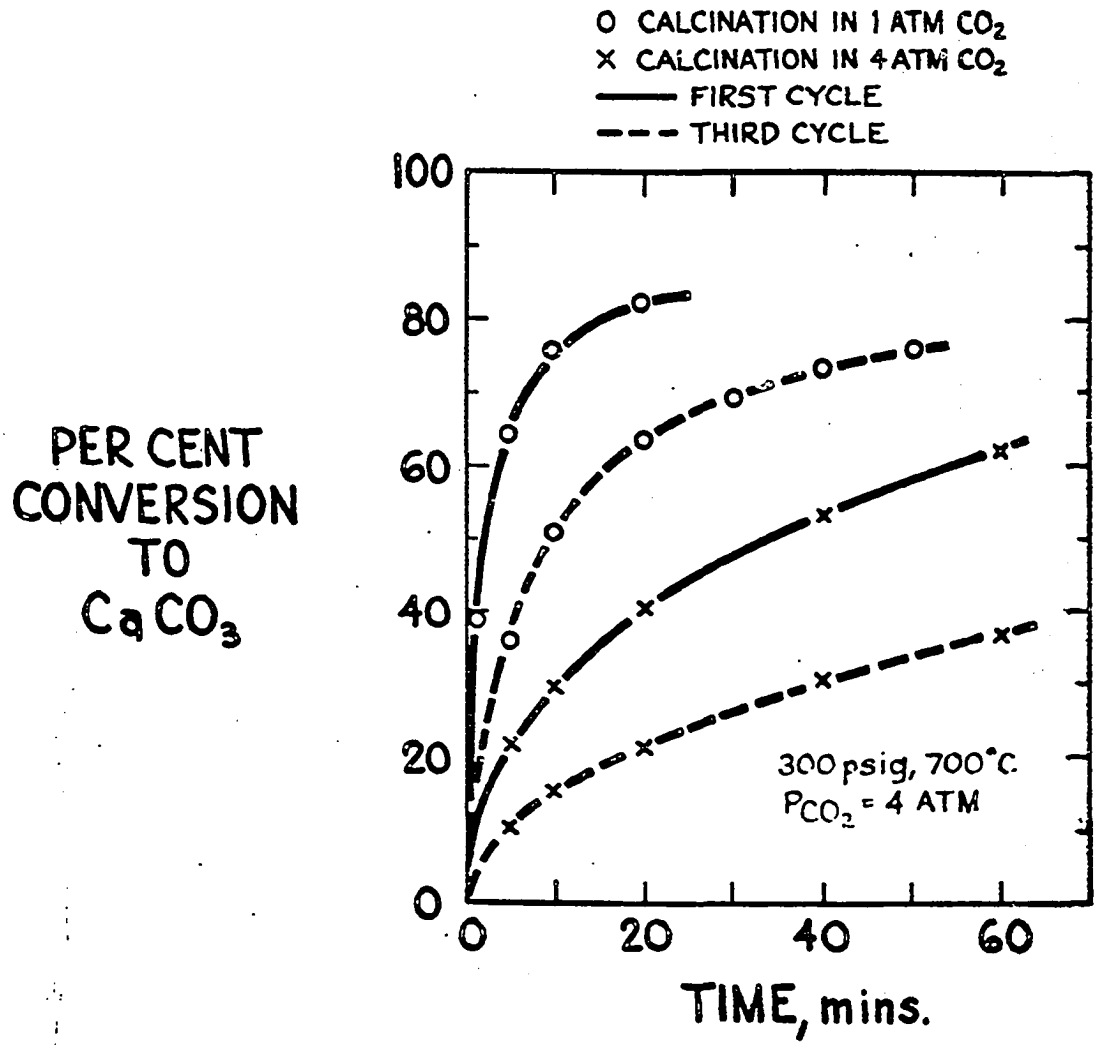

Figure 24. Recarbonation of Calcined Dolomite at 700°C, 300 psig, in 4 atm. CO_2, for Calcination at Pressure in 1 atm. CO_2 (930°C max.) and 4 atm. CO_2 (1030°C max.)

7.0 Cyclic Recarbonation of Calcined Dolomite: Discussion of Results

The discussion of this Section 7.0 is based upon the data obtained during shakedown experiments with the modified TGA (see Section 6.0) as well as upon the earlier City College data obtained by Weil and Sterns (Section 5.03). Because of the exploratory character of the work, the present discussion emphasizes the leads given by the data for further research.

The complexities of the kinetics can be attributed to the important role played by topochemistry in association and dissociation reactions, an area very often overlooked in discussions of gas-solid kinetics. Where possible, the experimental results will be interpreted in terms of our knowledge of the topochemistries of the reaction.

7.01 Effect of Partial Pressure of Carbon Dioxide and Total Pressure on Recarbonation Reaction

The recarbonation reaction appears to be first order in carbon dioxide over the range of 0.5 to 4 atmospheres carbon dioxide at temperatures 550 to 700°C. Reaction orders of zero (38) and unity (23,37) have been reported in the literature for the recarbonation of calcium oxide. Reaction orders in carbon dioxide approaching zero were obtained by Sterns at low partial pressures.

Zero order kinetics is consistent with a reaction model proposed by Hyatt et al. (30) and later by Nitsch (37), if the formation of active calcium oxide, CaO*, is assumed to be rate-determining in their reaction sequence.

$$CaO \rightleftarrows CaO^*$$

$$CaO^* + CO_2 \rightleftarrows CaCO_3$$

A variable reaction order which increases from zero to unity with increasing partial pressure can also be explained by the not too unreasonable assumption that the rate constant for CaO* formation, k*, is itself dependent on the partial pressure of carbon dioxide (23,37,47).

The first order (in solid) rate constants derived from the slope of the later portions of the curves shown in Figure 18 are well correlated by the expression

$$k^* = \alpha + \beta P_{CO_2}$$

with $\beta/\alpha = 3.1$.

The effect of total pressure may be interpreted assuming a series resistance model for first order reactions (48),

$$\text{rate} = \frac{1}{\frac{1}{k_d} + \frac{1}{k_r}} P_{CO_2}$$

where k_d and k_r are the mass transfer coefficient and reaction rate constant, respectively. The mass transfer coefficient is inversely proportional to total pressure. Based on the results shown earlier in Figure 22 we find that the reaction rate at 700°C and 1 atmosphere CO_2 is chemical reaction controlled at atmospheric pressure, and about equally controlled by mass transfer and chemical reaction at high pressure.

7.02 Extent of Reaction and Reaction Rate

The rate of reaction, r, in gas-solid reactions is sometimes given by

$$r = f(\alpha)g(P_i, T)$$

where α is the fractional conversion of solid, and $f(\alpha)$ is assumed to be invariant with temperature, time, and gas environment. This simplification finds great utility in the analysis of nonisothermal scans (thermograms) (49). In fact, this simplification turns out seldom to be valid, except maybe over a small range of experimental conditions.

The results of this research as well as that of Sterns were analyzed in order to develop correlating rate expressions. Classical forms of rate equations for gas-solid reactions did not give good correlation of the recarbonation data. Reasonable fit was obtained with the double exponential relation,

$$\alpha = 1 - \alpha_o e^{-r't} - (1 - \alpha_o) e^{-r''t} \qquad r' > r''$$

representative of dual reactivity solids, and the logarithmic relation

$$\alpha = \alpha_o t^n$$

representative of diffusion controlled reactions.

Figure 18 shown earlier illustrates the use of the double exponential equation for correlating rate data. Similarly, Figures 25 and 26 indicate the good fit obtained with the logarithmic rate expression. Where applicable, the

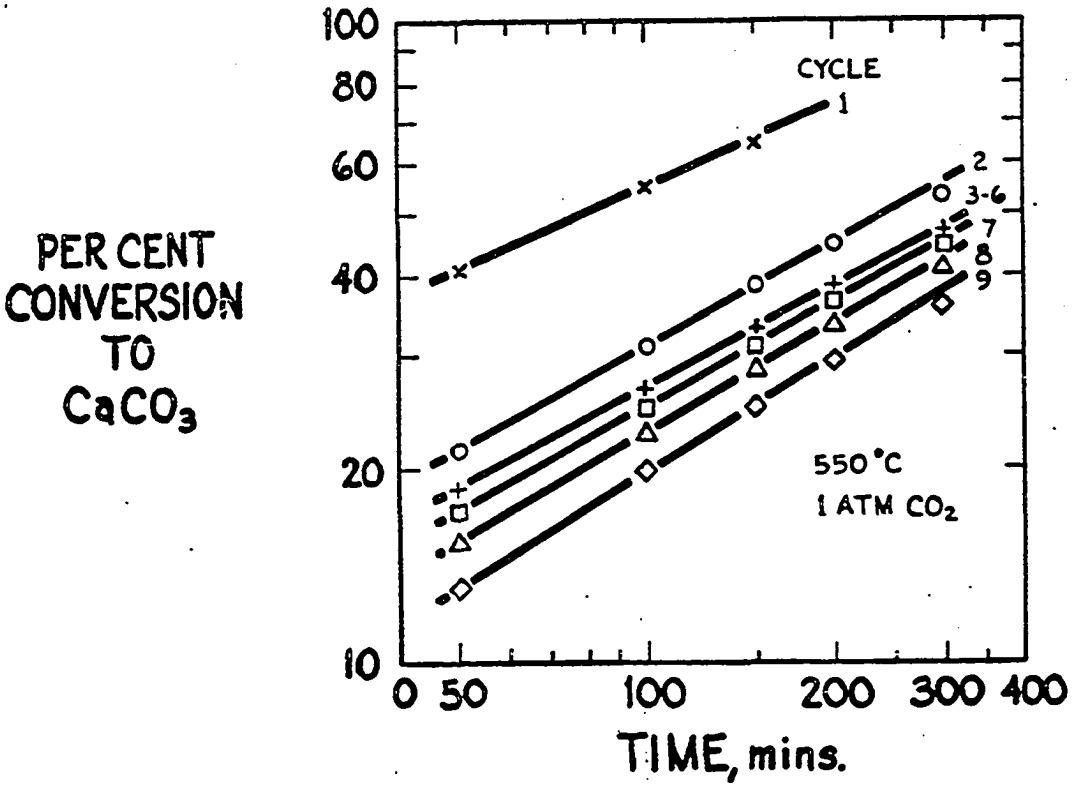

Figure 25. Cyclic Recarbonation of Calcined Dolomite at 550°C in 1 atm. CO_2 (L. Sterns)

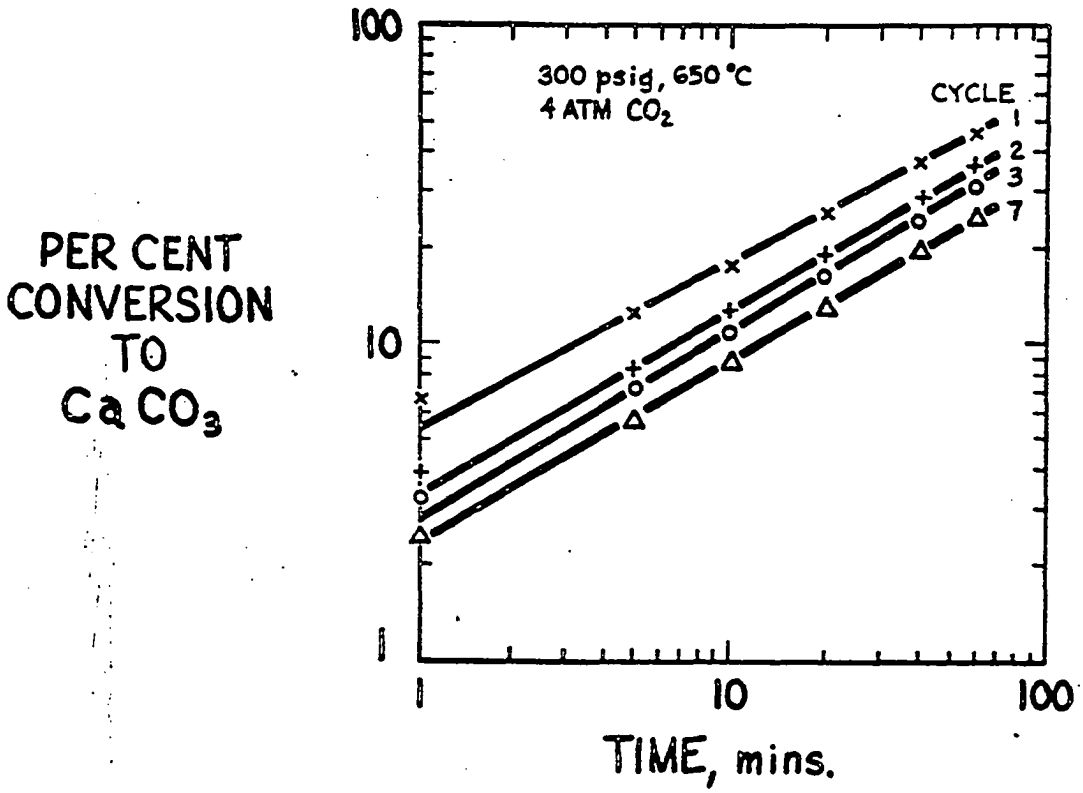

Figure 26. Cyclic Recarbonation of Calcined Dolomite at 650°C, 300 psig in 4 atm. CO_2

logarithmic rate expression yielded values of n in the range of 0.5 to 0.6. The effect of cycling was to reduce the value for α_o. In contrast, the value for n remained relatively constant with cycling.

No single rate expression was found capable of correlating all the rate data. The kinetic constants are very often complicated functions of temperature, gas environment and cycle number. The pattern of reaction behavior is also very different depending on whether steam is present or not. This becomes readily apparent when trying to relate the behavior in Figure 14 to that of Figure 16.

These difficulties are characteristic of true topochemical reactions where the progress of the reaction interface is governed not only by the local gas environment and temperature but also by the nature and temperature-environment history of the underlying solid reactant substrate and the developing solid product phase (50-53).

7.03 The Effect of Temperature on Reaction Rate

No thorough investigation of the effect of temperature was undertaken in this research.

Weil's nonisothermal recarbonation data may be analyzed using standard techniques for thermogravimetric analysis (49). An activation energy of 20 kcal/mole was obtained, assuming the reaction to be first order in both carbon dioxide and unreacted solid. This value also agrees well with estimates determined from Sterns' atmospheric data at 475 to 550°C and from results of this research at high

pressure at 650 to 700°C.

No activation energies were obtained for recarbonation in steam-containing atmospheres.

An interesting effect was observed by Sterns (Figure 27) when increasing the temperature of recarbonation from 550 to 700°C after 2 calcination/recarbonation cycles in a run of 8 cycles at atmospheric pressure in 10 percent carbon dioxide. As expected, the recarbonation at 700°C (cycle 3) was significantly faster than the previous recarbonation (cycle 2) at 550°C. It was, however, surprising to observe an additional increase in reactivity during the 4th cycle, also at 700°C. From cycle 4 onward the reactivity decreased from cycle to cycle in the expected manner. Only in cycle 8 did the reactivity return to that of cycle 3.

This phenomenon suggests that the recarbonation reaction possesses "memory". That is, the reactivity of the solid is both a function of reaction conditions as well as the reactivity of the solid during previous recarbonations. In cycle 3 the solid, while being at 700°C, retains "memory" of its lower reactive state during cycle 2 at 550°C. In contrast, the solid in cycle 4, also at 700°C, retains "memory" of a higher reactive state in cycle 3 at 700°C. From cycle 5 onwards the usual deactivation phenomenon governs the solid's reactivity.

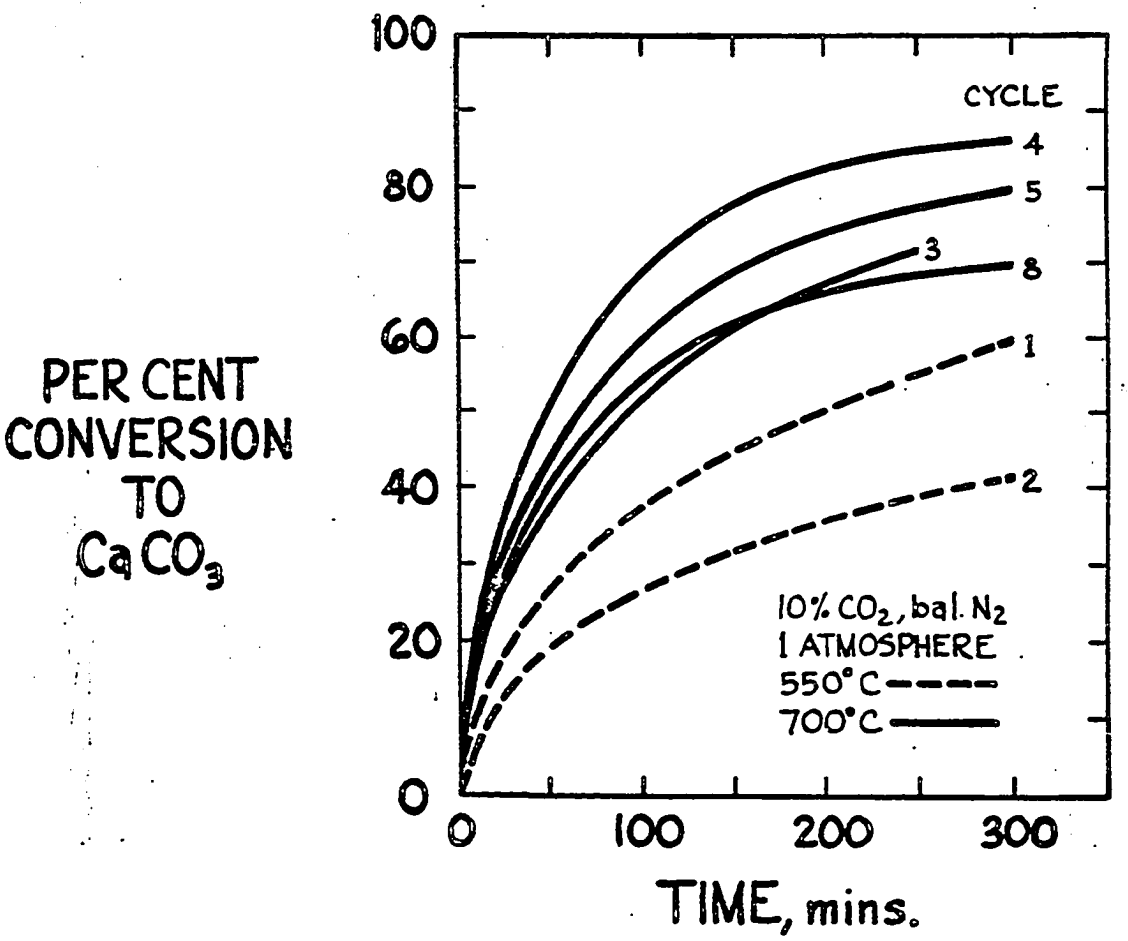

Figure 27. Cyclic Recarbonation of Calcined Dolomite at Atmospheric Pressure in 10/90 CO_2/N_2 with 2 Cycles at 550°C Followed by 6 Cycles at 700°C (L. Sterns)

7.04 Steam Catalysis of Recarbonation Reaction

Steam may be termed an "ideal catalyst" (54) as a result of its ability to strongly catalyze both the decomposition of $CaCO_3$ and its formation from CaO (55). Bischoff, in particular, has demonstrated that steam catalyzes the calcination of half-calcined dolomite (56). The catalytic recarbonation of lime in steam is only briefly mentioned in the literature (24,36,37). Curran et al. (40) suggested that steam also catalyzes the recarbonation of calcined dolomite but gave little data. Our results confirm the strong catalytic influence of steam on the recarbonation reaction. At 550°C the replacement of half the carbon dioxide by steam was found to increase the recarbonation rate by a factor of 30 to 100.

We originally believed that steam plays a very important role in the topochemistry of the reaction. Other investigators (50,51) have reported the ability of steam to promote fissurization of the product layer. The catalytic effect of steam was therefore thought to be the result of forming of cracks that open up the reaction interface to the reactive gas atmosphere. Figure 28 shows the result of a test of this hypothesis. In this run, at 700°C, steam was introduced after the solid had reached a steady level of conversion. As expected the rate increased considerably with steam addition. After about 70 minutes the original gas atmosphere was returned. Fissurization of the product

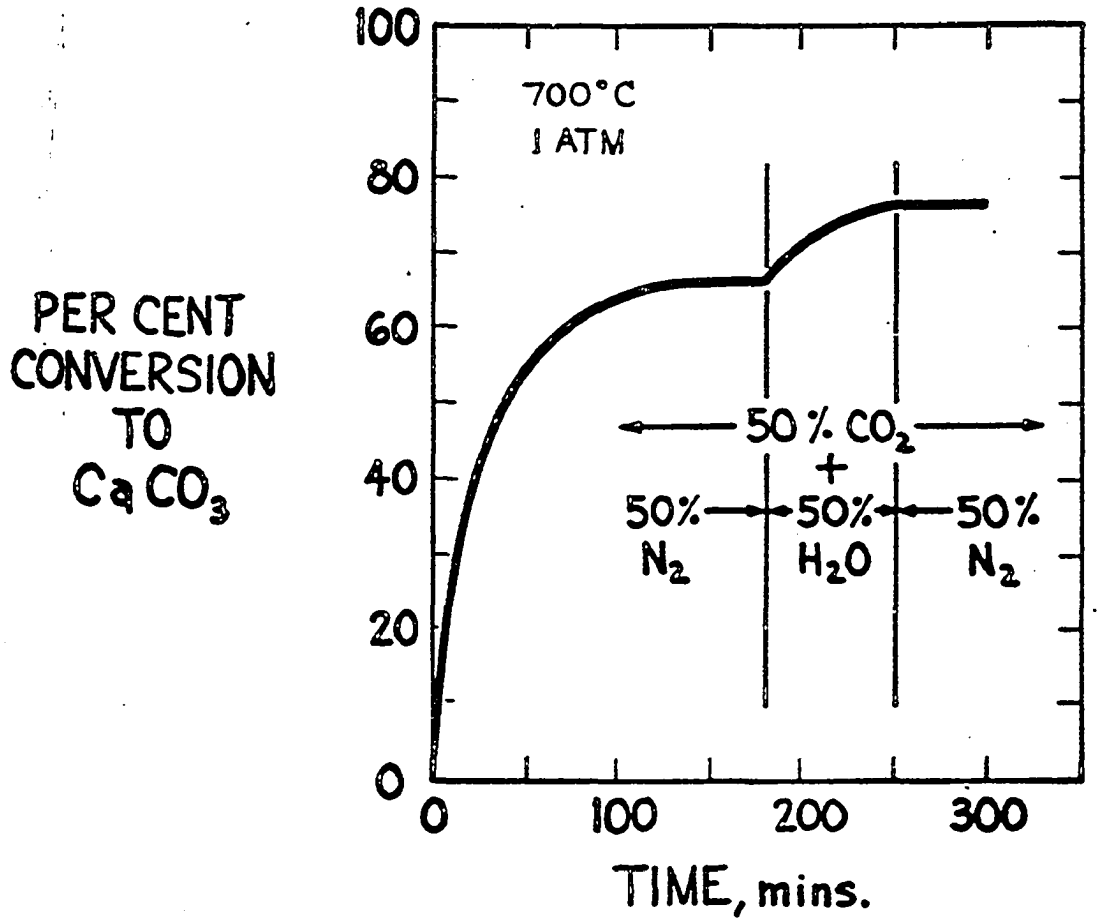

Figure 28. Substitution of 50/50 CO_2/H_2O During Recarbonation of Calcined Dolomite (Tenth Cycle) at 700°C and Atmospheric Pressure in 50/50 CO_2/N_2 (L. Sterns)

layer by steam should have reactivated the solid considerably, yet the solid remained just as inactive as prior to steam addition. Apparently, the catalytic effect of steam has no "memory". We may speculate that its catalytic nature derives rather from an ability to promote nucleation of the "active CaO", which is proposed to be rate-limiting.

Infrared studies by Low (57) revealed the presence of hydroxyl groups on the surface of calcium oxide at above the decomposition temperature for calcium hydroxide. It is possible that the interaction of steam during the recarbonation reaction is related to the presence of these hydroxyl groups.

In steam containing atmospheres the initial recarbonation rates are extremely high (Figures 16,17,23). Temperature and cycle number have little influence on the initial rates but strongly affect the final asymptotic level of conversion. This invariance of initial rate is indicative of possible mass transfer effects which become important at high reaction rates.

7.05 Recarbonation of Calcined Dolomite Relative to Other Forms of Calcium Oxide

There are two factors of importance in discussing acceptor utilization: reaction rate and capacity. The reaction rate is governed by the size and lattice strain of the crystallites of solid reactant as well as the macropore structure of the material. The capacity of the acceptor,

on the other hand, is governed by the microporosity of the product layer formed behind the reaction interface. For CaO reacting to $CaCO_3$ the product layer will have a much larger specific molar volume than the substrate so that closing off of pores to the reaction interface will be a limiting factor to achieving high capacities (27,29,34).

Single crystals of calcite, for example, when calcined in nitrogen at 700°C will recarbonate only to 50 percent in 645mm Hg of carbon dioxide at 700°C and will require more than 10 hours to achieve 40 percent conversion (30). The low surface area of the calcia accounts for the low reaction rates, and the very compact growth of the recarbonated calcite phase prevents carbon dioxide from diffusing to the reaction interface. Precipitated $CaCO_3$ will produce finer crystallites of CaO, but here again the reaction falls short of completion and requires nearly 5 hours to achieve 40 percent conversion (30). Lime reacts fairly rapidly under the same conditions requiring less than an hour to achieve the same levels of conversion (28,33). Impedance by the product layer is still a problem and maximum conversion is limited to about 70 to 80 percent (25-7,29,31,34,37). Calcined dolomite (prepared in carbon dioxide), on the other hand, reacts completely at 700°C, requiring only 30 minutes to achieve essentially complete conversion. Its high reaction rate relative to lime is attributed to the microcrystallinity of its CaO species. The size of the CaO crystals in calcined dolomite (first cycle) are only 400Å (40,58) compared

to 2000-3000Å for limes (59). The MgO in calcined dolomite, while being inert towards CO_2 at these conditions, is capable by virtue of its ultrafine dispersion in the solid of forming a microporous structure which facilitates the exchange of carbon dioxide to and from the particle, therefore resulting in high capacities for this material (27).

7.06 Reactivity and Calcination Conditions

The effect of calcination temperature on the reactivity of calcined dolomite toward recarbonation is illustrated by the results shown in Table 4 and Figure 24 described earlier. In general, the higher the calcination temperature and hence partial pressure of carbon dioxide the less reactive the resulting oxide. Soaking of the calcined solid in carbon dioxide at temperatures above 925°C will also result in a severe loss of reactivity. These observations confirm similar findings reported by other investigators (27-9,40,48,60).

Another effect of increased calcination temperatures is the deactivation of the solid with repeated cycling. The data in Figures 16, 17 and 20 are replotted in Figures 29a, 29b and 30 as a function of cycle number, N, at constant reaction times, t. The data are well correlated by

$$\alpha_t = aN^b$$

The slope, b, in the log-log plots may be looked upon as a form of deactivation rate constant. The larger this value the greater will be the falloff in conversion with repeated

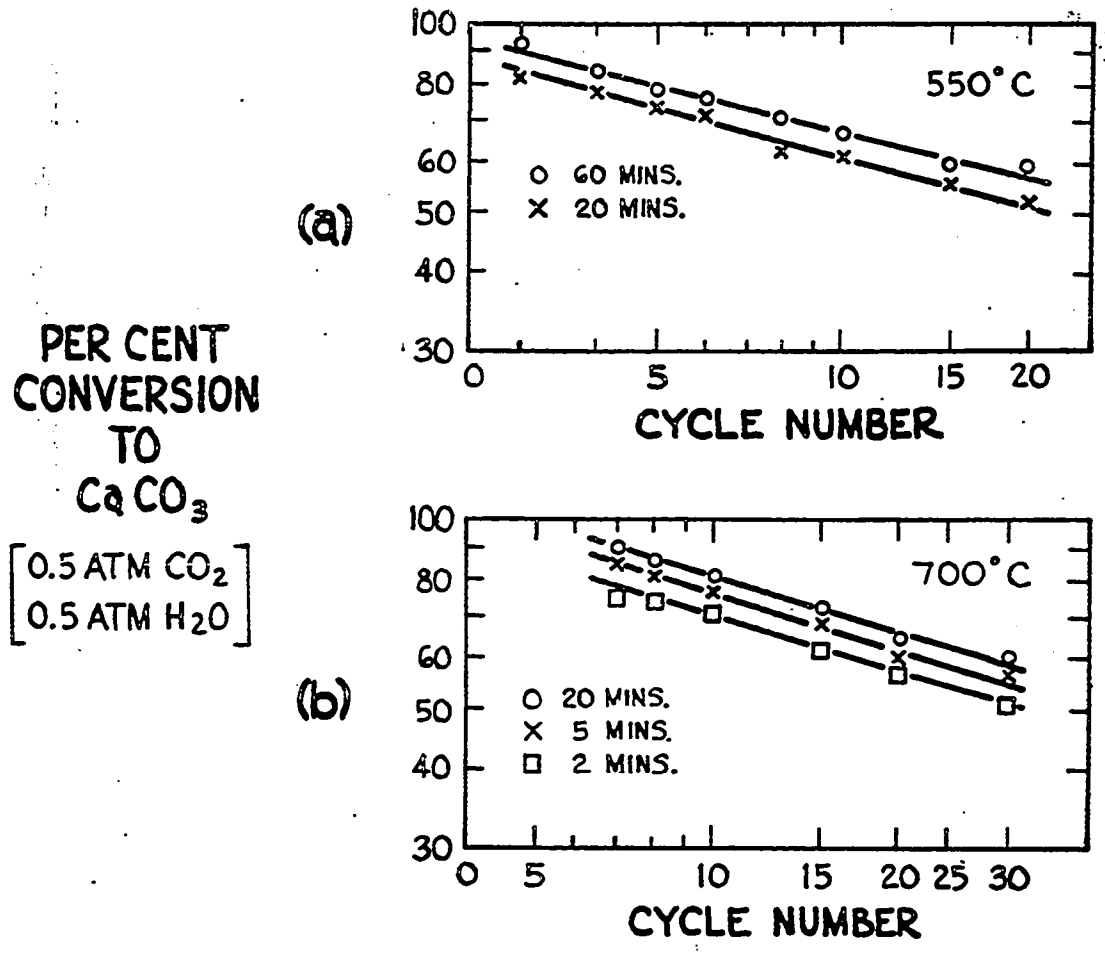

Figure 29. Cyclic Recarbonation of Calcined Dolomite at Atmospheric Pressure in 50/50 CO_2/H_2O at (a) 550°C and (b) 700°C (L. Sterns).

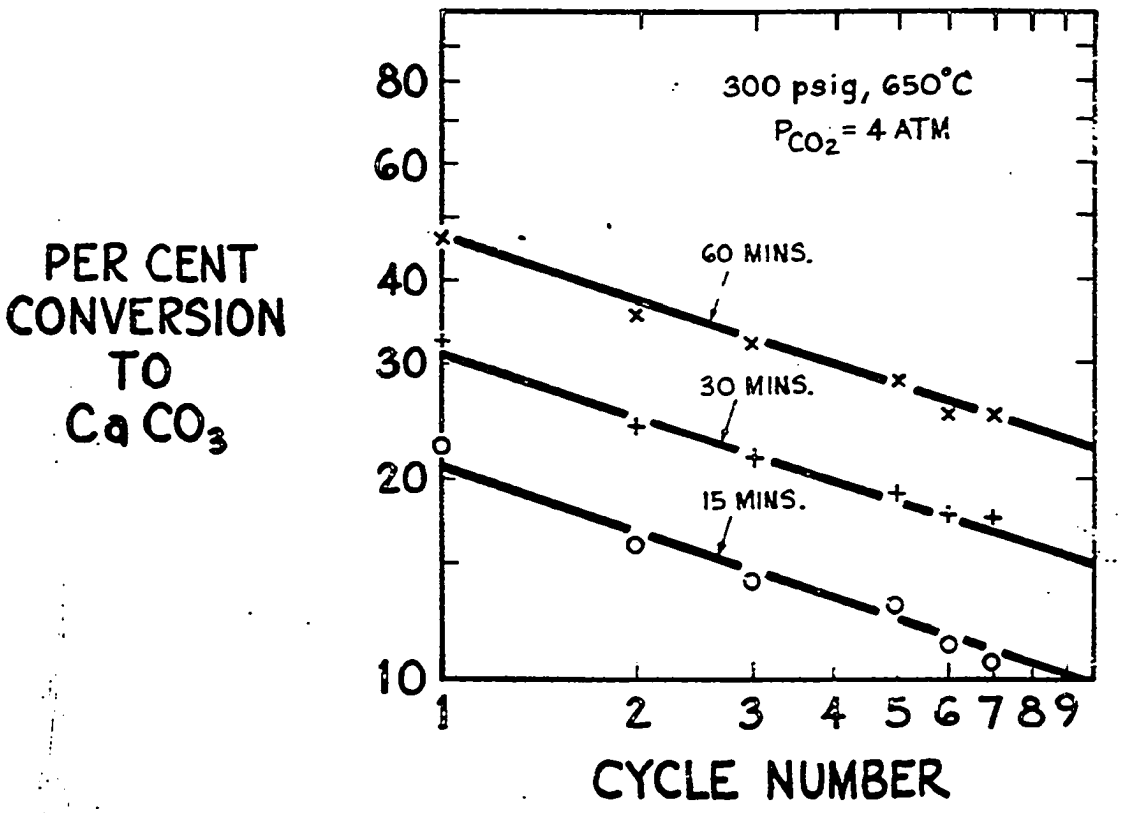

Figure 30. Cyclic Recarbonation of Calcined Dolomite at 650°C, 300 psig in 4 atm. CO_2

cycling. Figure 31 is a plot for data reported by Curran et al. (21,40) for calcined dolomite cycled in a continuous reactor. Table 7 lists the values for b and their corresponding experimental conditions. The increasing value for b with increasing calcination temperature reflects a higher degree of deactivation of the solid at the higher temperatures.

The effects of calcination conditions on reactivity may be understood in terms of the topochemistries taking place (27,28,59,61-64). When the $CaCO_3$ species in half-calcined dolomite decomposes there first occurs the epitaxial growth of CaO at points of high lattice strain, such as dislocations, holes and grain boundaries. This metastable crystal structure results in the formation of a dense and amorphous-like product layer at the reaction interface. Recrystallization of the CaO to its normal habit soon follows but usually lags behind CO_2 evolution. Depending on the temperature and gas environment the resulting CaO crystallites will begin to sinter. Sintering may be defined simply as a bulk migration of ions in the crystal lattice. The effect of sintering is twofold: an increase in crystallite size and the annealing of lattice imperfections, such as dislocations and holes. The former reduces the specific surface area of the solid formed, while the latter reduces the concentration of potential nucleation sites for subsequent reaction.

The rate of sintering of CaO in various gas atmospheres is reported to increase in the same order as its affinity

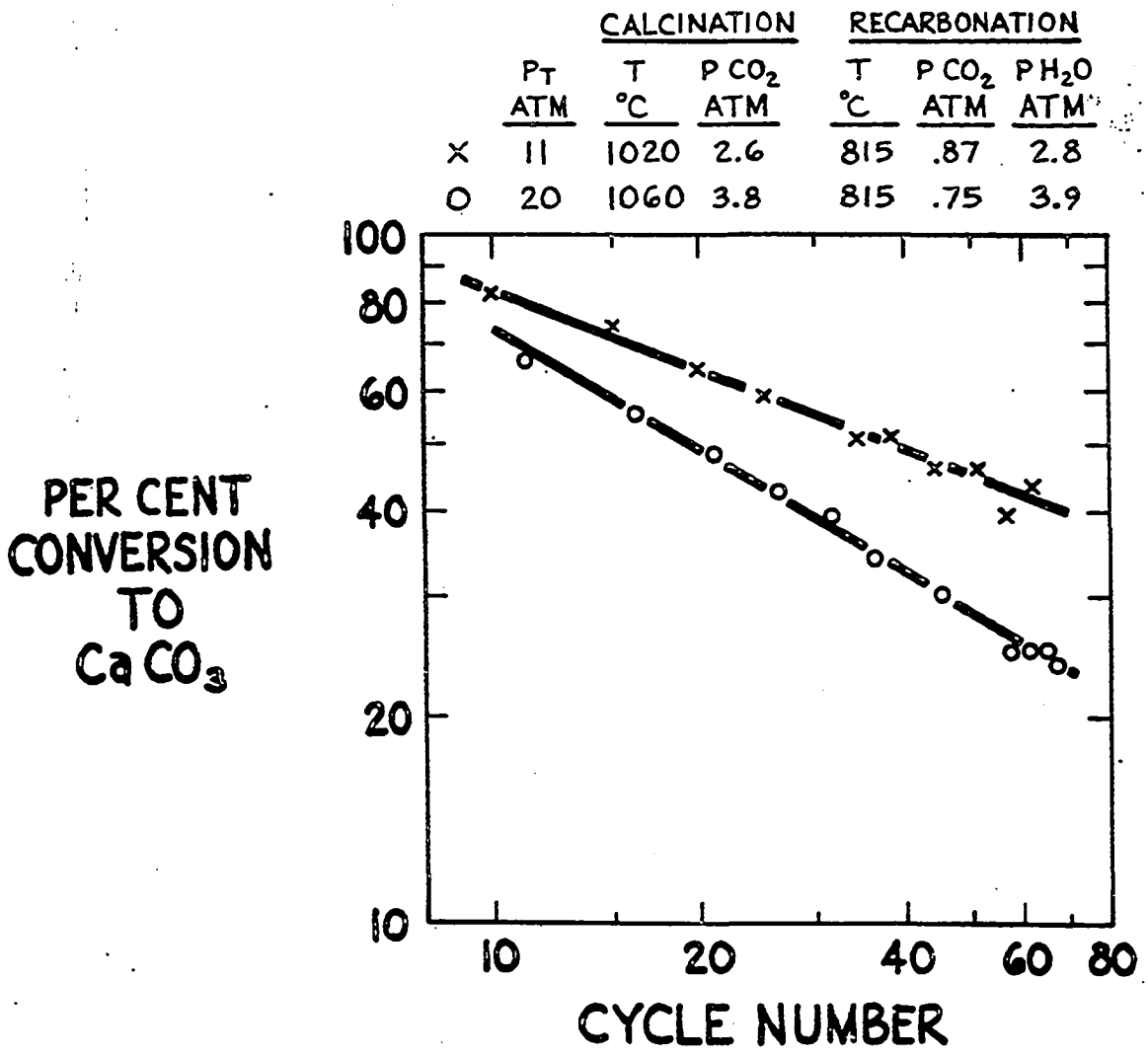

Figure 31. Cyclic Recarbonation of Calcined Dolomite in Consol's Continuous Bench Scale Unit (21,40)

Table 7: Deactivation Rate Constant in Cyclic Recarbonation of Calcined Dolomite

$$\alpha_t = aN^{-b}$$

Reference	Calcination Conditions				Recarbonation Conditions			b
	P_T atm.	P_{CO_2} atm.	P_{H_2O} atm.	T °C	P_{CO_2} atm.	P_{H_2O} atm.	T °C	
(21)*	20	3.6	--	1060	0.75	3.9	815	0.592
(40)	11	2.6	--	1020	0.87	2.8	815	0.305
this work	21	4	--	1030	4	--	700	0.350
L. Sterns	1	0.5	0.5	870	0.5	0.5	700	0.296
L. Sterns	1	0.5	0.5	870	0.5	0.5	550	0.255

*char combustion in calciner

for reaction with the gas atmosphere; i.e. $SO_2 > CO_2 > H_2O > O_2$, air $> N_2$ (65). On the basis of this criteria, an oxide with superior reactivity will be obtained if the calcination is carried out in nitrogen. Low has shown, on the basis of infrared studies, that SO_2, H_2S and H_2O are strongly chemisorbed by the CaO surface (57,66,67). Activated sintering in reactive gas atmospheres may be related to sorption of these species on the crystallite surface. Carbon dioxide, in particular, was found to activate the sintering of $CaCO_3$ (59,68,69), MgO (41,70) and CaO (27-29,59,62,70-73) (in descending order of activation). Peterson and Cutler present data for activated sintering of CaO by steam at 920 to 1123°C (74).

Surface migration in calcium carbonate can occur as low as 264°C; bulk migration takes place at 533°C (38). Above 700°C annealing of calcium carbonate is quite rapid (50). As a result, soaking of calcium carbonate at temperatures below decomposition will reduce its subsequent decomposition rate (50).

Magnesium oxide crystallites formed from both magnesite and dolomite are reported to sinter and grow in carbon dioxide atmospheres above their decomposition temperatures (800°C) (41,70). Sintering of magnesium oxide in CO_2-free atmospheres becomes important at temperatures above 975°C (75).

Surface migration of ions in calcium oxide becomes significant above 675°(59); bulk migration and crystallite growth take place rather suddenly at 900°C (59,61,75-77).

This accounts for the drastic reduction in capacity reported by Curran et al. for isothermal cyclic recarbonation of calcined dolomite at 954°C in comparison to runs made below 887°C (40).

The equilibrium size of product crystallites in both calcination and recarbonation is governed by the interaction of the nucleation and growth rate, both of which may be functions of the gas atmosphere. In carbon dioxide atmospheres above the sintering temperature, the growth of product crystallites is favored over nucleation of new crystallites (70). The effect of high rates of reaction, in general, results in much smaller crystallite sizes, and is consistent with the fact that annealing processes usually lag behind interfacial reaction rates (38,62,72). As a result, smaller calcium oxide crystallites are obtained for calcination in vacuo and for calcination under rapid heating conditions.

The importance of calcination rate on reactivity may help to interpret the observed effect of calcination pressure on the recarbonation rate. The recarbonation rate (700°C, 300 psig, P_{CO_2} = 1 atm) for a solid calcined at 300 psig in 1 atmosphere CO_2 is shown in Figure 32 to be much slower than for a solid calcined at atmospheric pressure in CO_2. The effect of calcination pressure is twofold. At high pressure the calcination reaction may be diffusion controlled, and as a result its rate will be lower than at atmospheric pressure. This has, in fact,

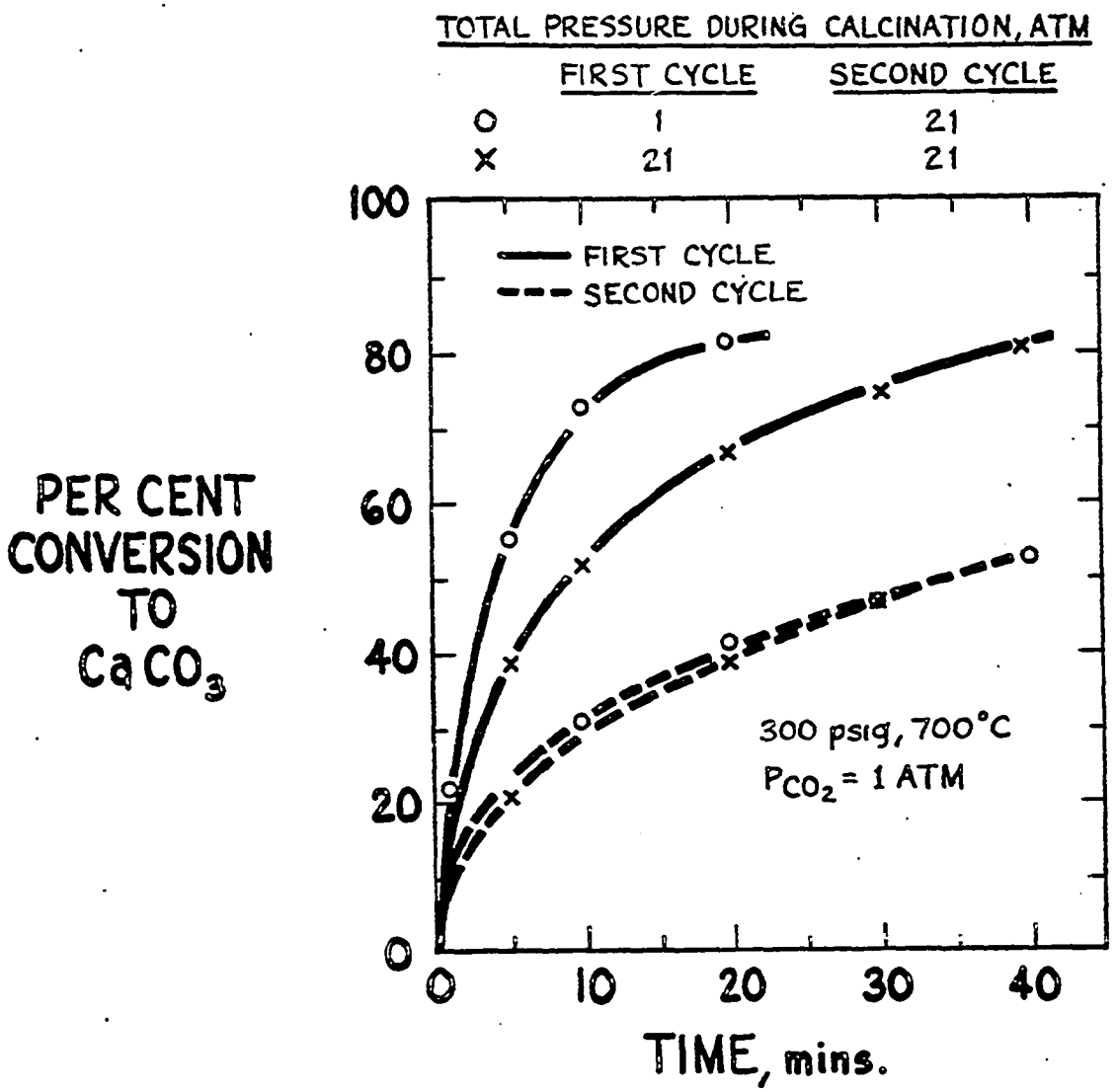

Figure 32. Recarbonation of Calcined Dolomite at 700°C, 300 psig, in 1 atm. CO_2, for Calcination in 1 atm. CO_2 Partial Pressure at Atmospheric and at 300 psig Total Pressure

been observed in our high pressure studies. In addition, the effect of diffusion control will be to raise the carbon dioxide partial pressure at the reaction interface. Both these factors, i.e. lower calcination rates and higher interfacial carbon dioxide partial pressures, will result in the formation of larger and more annealed calcium oxide crystallites, thus lowering the solid's reactivity towards recarbonation. In a subsequent cycle, where both solids were calcined at the same conditions at pressure, the recarbonation rate for the two solids is shown in Figure 32 to be substantially identical.

The above sintering phenomena help to explain the observed reduction in recarbonation activity with increasing calcination temperatures from 800 to 1030°C, as well as the similar reduction in activity obtained with soaking of the calcinate in carbon dioxide at 925°C. In our high pressure cycling experiments sintering was confirmed by caking of the powdered samples to a sponge-like mass for all runs having calcinations at 1030°C (4 atmospheres CO_2). No caking was observed in any of the calcinations at lower temperatures. Gluud and Klempt (22) considered 1050°C as an absolute upper limit for the calcining temperature in their CO-shift process. Significant deactivation in the CO_2-Acceptor process is likely the result of the high calcination temperatures employed (1060°C) (21).

In the recarbonation of calcium oxide the factors which govern the initial reaction rate are: the initial crystallite size, the concentration of potential nucleation

sites, the nucleation rate, the rate of interfacial reaction with carbon dioxide, and the porosity of the material (50-53).

Subsequent reaction will be governed by the nature of the product calcium carbonate layer. Unlike the calcination reaction, recarbonation requires the transport of carbon dioxide through the solid to the reaction interface. Due to the much larger specific molar volume of calcium carbonate (36.9 cm^3/g-mole) relative to calcium oxide (16.9 cm^3/g-mole), the oxide will become covered by a layer of carbonate of much lower porosity. As a result, the carbon dioxide may not have free access to the reaction interface, but has to diffuse through pores and cracks in the product layer to reach the interface. As the reaction proceeds its rate will become progressively slower due to the increasing thickness of the product layer.

In cases where the effective diffusivity of the product layer is low, the reaction may cease altogether. This phenomenon is referred to in the literature as retention (51) or impedance (50) and is responsible for the low capacities of limes in reactions with carbon dioxide and sulfur dioxide (78). In the recarbonation of lime the reaction ceases after about 70 to 80 percent conversion. Inspection of the resulting solid revealed an almost complete loss of porosity and surface area as a result of product layer impedance (29,34). The magnitude of this effect is governed by the crystallinity of the product layer formed. Conditions which promote fissurization or recrystallization will lessen the degree of impedance (50).

The ability of calcined dolomite (first cycle) to achieve complete recarbonation is related to the ultrafine dispersion of magnesium oxide crystallites in the solid which helps to maintain good porosity during the entire course of reaction (27).

Deactivation of acceptors with repeated cycling can take two forms, one of which affects the reaction rate and another which determines the extent of final conversion. In the cyclic recarbonation of calcined dolomite we observe both effects. Loss of reactivity with repeated cycling is illustrated by the results shown in Figures 13, 14 and 20, while loss of capacity is illustrated in Figures 16 and 17. The former effect is governed by the change in size and lattice strain of the calcium oxide crystals with cycling. Since calcination is carried to completion, the nature of the product layer should not change with cycling except as a result of changes in the size of the calcium oxide crystallites. Loss of capacity is related to two distinct phenomena. If recarbonation is not carried to completion there will be some calcium oxide crystallites which will anneal during calcination to the extent that they will remain inert towards recarbonation. These crystallites will simply sinter and grow with each cycle, thus increasing the proportion of calcium oxide unavailable for reaction. This process is similar to the high temperature process (1200^{o}C) of "deadburning". In addition, as the average crystallite size of the calcium oxide increases with cycling due to sintering in the

calcination step, the level of conversion will decrease for a given penetration depth of carbon dioxide through the carbonate layer. This will result in increasing retention and hence a loss of capacity with cycling.

Kriek et al. have shown that the admixing of CaO to MgO prevents the sintering and deadburning of the magnesium oxide by reducing the probability for particle-to-particle contact (79). This suggests that fully-calcined dolomite should be able to resist sintering and hence chemical deactivation better than calcium oxide or magnesium oxide individually. A key factor for the durability of dolomite is, therefore, the fine scale of segregation of the calcium and magnesium species in the solid.

Curran et al. (40) describes the change in crystallite sizes taking place during the cyclic recarbonation of dolomite. After calcination, both the calcium and magnesium oxide crystallites are about 400Å in size. After only a few cycles at process conditions the calcium and magnesium oxide crystals have grown to greater than 2000Å; the calcium carbonate crystallites remaining at 400Å. Samples taken from their continuous reactor showed that after several cycles the calcium and magnesium species had segregated completely, the crystallites having reached the enormous dimensions of 10 to 20 microns. Note, calcination was carried out at 1060°C.

The deactivation of calcined dolomite in cyclic recarbonation may therefore be attributed to sintering in

the calcination step. Growth of the calcium oxide crystallites reduces both the reactivity towards recarbonation as well as its ability to withstand loss of capacity due to product layer impedance. In the limit, complete segregation of the calcium and magnesium species in dolomite will yield a solid having chemical properties no different than that produced from limestone.

In line with the above picture for deactivation of calcined dolomite, a reduction in the size of the calcium oxide crystallites should be able to reactivate the solid. A test of this hypothesis was made by Sterns and is shown in Figure 33. After three cycles of recarbonation at 550°C, in which calcination was carried out in 1 atmosphere carbon dioxide to 925°C, a calcination in nitrogen to 800°C was made. The subsequent recarbonation proceeds extremely fast, even relative to the first recarbonation. By calcining in nitrogen the average crystallite size is reduced, thus producing a solid of much higher reactivity. However, complete conversion was not attained due to the presence of "deadburnt" calcium oxide formed during the earlier cycles which cannot be reactivated by simple calcination in nitrogen.

7.07 Tentative Conclusions from Exploratory Studies of Cyclic Recarbonation of Calcined Dolomite

(a) The recarbonation reaction is approximately first order in partial pressure of carbon dioxide in the range of 0.5 to 4 atmospheres CO_2.

(b) The activation energy for the recarbonation

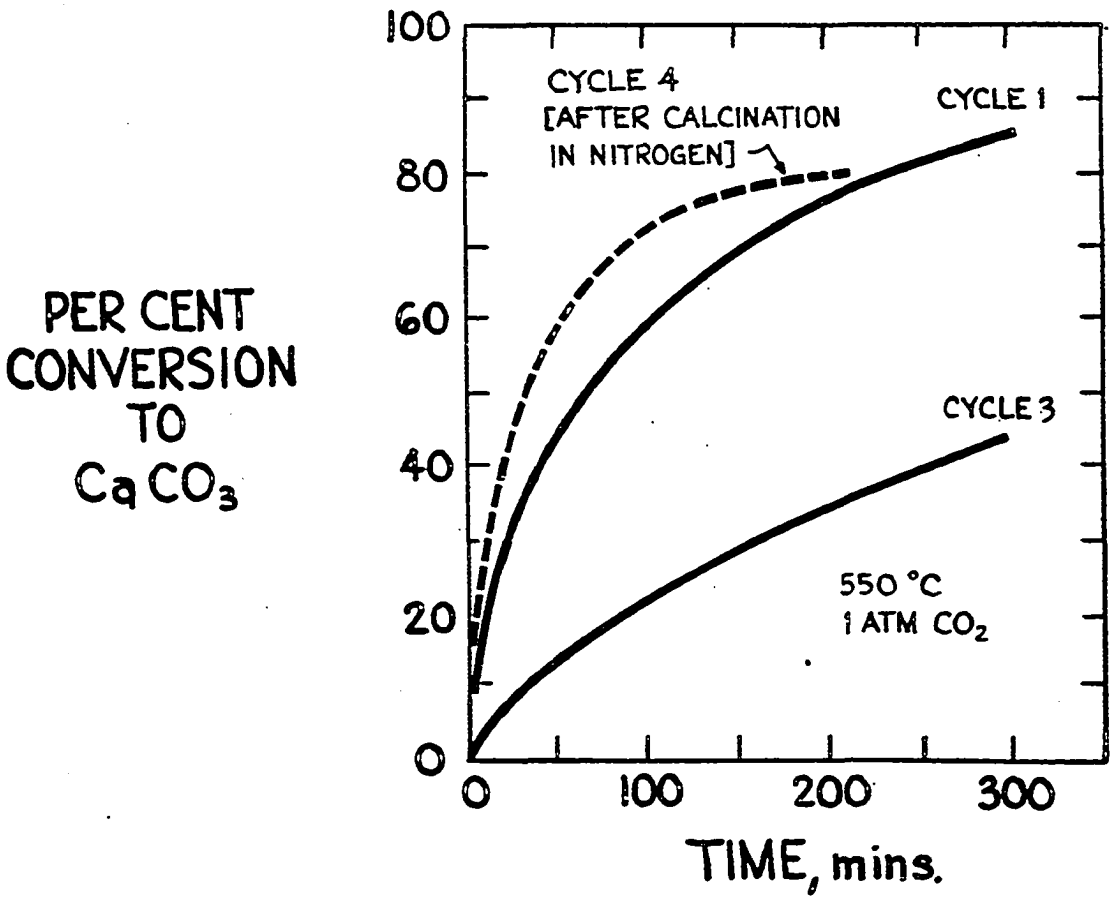

Figure 33. Cyclic Recarbonation of Calcined Dolomite at 700°C and Atmospheric Pressure in CO_2; First 3 Cycles Calcined in CO_2 Followed by 4th Cycle Calcined in N_2 (L. Sterns)

reaction is estimated to be about 20 kcal/g-mole.

(c) Addition of steam to the recarbonation atmosphere increases the recarbonation rate by two orders of magnitude. The catalytic effect of steam has no "memory" and is proposed to catalyze the interfacial reaction rate directly.

(d) Increasing calcination temperatures and hence partial pressures of carbon dioxide result in a less reactive material for recarbonation. Active calcined dolomite, prepared at lower temperatures (800°C) in nitrogen, will quickly lose reactivity if allowed to soak at higher temperatures (925°C) in carbon dioxide. Visible sintering of a powdered sample is obtained at a calcination temperature of 1030°C (in 4 atmospheres of CO_2).

(e) Deactivation of calcined dolomite during cyclic calcination and recarbonation results in both a loss of reactivity and capacity. This has been attributed to growth and eventual segregation of the calcium and magnesium oxide crystallites during repeated calcinations. Reactivation of a portion of the solid was achieved by calcining at a lower temperature (800°C) in nitrogen, thereby reducing the size of the calcium oxide crystallites.

7.08 Suggestions for Further Work on Cyclic Recarbonation

It has to be reemphasized that the investigation of the cyclic recarbonation of calcined dolomite was principally undertaken in order to demonstrate the utility of the

high pressure thermobalance for high pressure process studies, in particular, for cyclic acceptor processes.

Many of the effects noted for this reaction sequence may have important consequences to other reaction cycles with this solid; e.g., cyclic sulfur absorption and regeneration of half- or fully-calcined dolomite. It is therefore recommended that further study of these effects be carried out. Kinetic investigations using the thermobalance should be paralleled by an equivalent effort of microscopic observation and physical inspection of the solids produced at various stages in a cyclic experiment under various selected experimental conditions. The combination of the two approaches may yield fundamental information on the important processes taking place in the solid during cyclic reaction.

8.0 Closing Remarks and Recommendations

The goal of this research was to develop a high pressure thermobalance capable of process studies. This goal has been successfully achieved by modification and pressurization of a duPont 950 TGA for operation to 30 atmospheres, temperatures to 1100°C, corrosive gas atmospheres, and steam partial pressures to 15 atmospheres.

The utility of this instrument for process studies was demonstrated by an exploratory investigation of the cyclic calcination and recarbonation of calcined dolomite at high pressures. The results indicate effects that may be expected for acceptor solids, in particular, dolomitic acceptors.

The instrument is ready to proceed to the study of other cyclic acceptor reactions. In particular, the instrument will be used to study the cyclic sulfur absorption and regeneration of half-calcined dolomite.

We foresee a need for an instrument of this type in other research laboratories doing process development work on noncatalytic gas-solid reactions. It is therefore recommended that thought should be given for further modification of the existing setup to make it more suitable for commercialization and thereby to broaden its application base.

9.0 Appendix - Flow Dynamics in High Pressure Thermobalance and Flow System

9.01 The Interactions of Steam Generation and Flow Dynamics

As mentioned earlier in Section 4.06 difficulties were initially experienced when trying to feed high pressure steam to the thermobalance. Condensation of steam always occurred inside the balance housing and no amount of purge flow or auxiliary heating of the ceramic block was able to prevent its occurrance.

Upon closer examination, it was determined that steam penetration into the balance housing could not be attributed to any steady state effects, but must be the result of some flow disturbance in the system. This was confirmed by sharp periodic pulses in the recorded weight when operating with high pressure steam. Ultimately, of course, condensation became severe enough to completely disrupt weight measurements. The flow disturbances were traced to the unsteady nature of the vaporization process taking place in the steam generator. Steam is formed explosively as each droplet of water leaving the injector (see Figure 8) comes into contact with hot metal surfaces.

These pulses of steam are propagated through the entire system unhindered. Due to the relatively large free volume of the balance housing and bell jar, the steam can penetrate the balance housing even against the large flow of purge gas in the ceramic block.

The following dynamic analysis will confirm that pulses of steam can penetrate into the balance housing and will also suggest a solution.

9.02 Formulation of the Problem

The flow system and the thermobalance may be schematically represented by

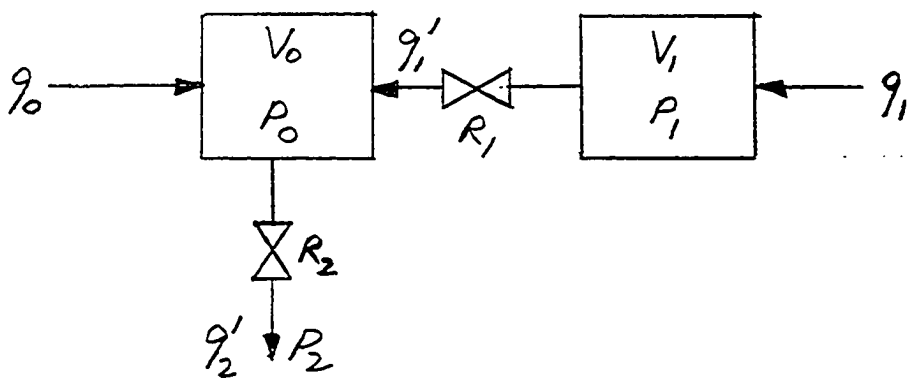

(9.1)

where V_o represents all the volume in the reaction gas line leading to the thermobalance, the free volume in the furnace tube, and the volume downstream of the thermobalance, including the sulfur knockout vessel and the condenser. V_1 represents the free volume in the balance housing and bell jar and the volume in the purge gas line leading to the thermobalance. q_o is the reaction gas flow and q_1 is the purge gas flow. R_1 is the flow

resistance through the passage in the ceramic block, and R_2 is the linearized flow resistance through the back pressure regulator.

The governing equations for a general flow element, shown below,

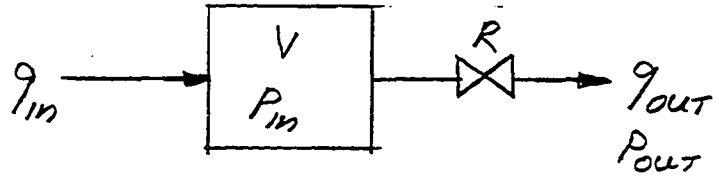

(9.2)

are given by (80):

$$q_{in} - q_{out} = \frac{V}{P_{in,s}} \frac{dP_{in}}{dt} \tag{9.3}$$

where the subscript s indicates the steady state value

$$q_{out} = \frac{1}{R}(P_{in} - P_{out}) \tag{9.4}$$

where R is the linearized flow resistance given by

$$R = \frac{1}{n}\left(\frac{P_{in,s} - P_{out,s}}{q_{out,s}}\right) \tag{9.5}$$

n = 1 for a laminar flow element

and n = 0.5 for an orifice element

For the system shown earlier in (9.01) we may write

$$q_0 - q_1' - q_2' = \frac{V_0}{P_{0s}} \frac{dP_0}{dt} \tag{9.6}$$

$$q_1 - q_1' = \frac{V_1}{P_{1s}} \frac{dP_1}{dt} \tag{9.7}$$

$$q_1' = \frac{1}{R_1}(P_1 - P_0) \tag{9.8}$$

$$q_2' = \frac{1}{R_2}(P_0 - P_2) \tag{9.9}$$

Transforming the variables and parameters,

$$\left.\begin{aligned} &\tilde{Q} = (q - q_s)/q_s \qquad \tilde{P} = (P - P_s)/P_s \\ &\tilde{R} = R\frac{q_{in,s}}{P_{in,s}} = \frac{1}{n}\left(\frac{P_{in,s} - P_{out,s}}{P_{in,s}}\right) \\ &\theta = \frac{V}{q_{out}} \\ &\alpha = \frac{q_{os}}{q_{2s}} \qquad \beta = \frac{P_{2s}}{P_{os}} \end{aligned}\right\} \tag{9.10}$$

Equations (9.6) through (9.9) become

$$\alpha\tilde{Q}_0 + (1-\alpha)\tilde{Q}_1' - \tilde{Q}_2' = \theta_0\frac{d\tilde{P}_0}{dt} \tag{9.6a}$$

$$\tilde{Q}_1 - \tilde{Q}_1' = \theta_1\frac{d\tilde{P}_1}{dt} \tag{9.7a}$$

$$\tilde{Q}_1' = \frac{1}{R_1}(\tilde{P}_1 - \tilde{P}_0) \qquad [\text{Note: } P_{1s} \simeq P_{os}] \tag{9.8a}$$

$$\tilde{Q}_2' = \frac{1}{R_2}(\tilde{P}_0 - \beta\tilde{P}_2) \tag{9.9a}$$

where both $\tilde{Q}_1$ and $\tilde{P}_2$ are set equal to zero.
Taking Laplace transforms of Equations (9.6a) through (9.9a) using the boundary conditions:

(i) $P_2(s) = 0$

(ii) $Q_1(s) = 0$

(iii) $Q_0(s)$ is given

gives

(9.11)

$$\frac{Q_1'(s)}{Q_0(s)} = \frac{-\alpha \tilde{R}_2 \theta_1 s}{1+[(1-\alpha)(\tilde{R}_2\theta_1)+(\tilde{R}_1\theta_1)+(\tilde{R}_2\theta_0)]s+(\tilde{R}_2\theta_0)(R_1\theta_1)s^2}$$

The frequency response for purge flow out of the balance is given by (9.12)

$$G_1'(\omega) = \frac{\alpha \tilde{R}_2 \theta_1 \omega}{\sqrt{[1-(\tilde{R}_2\theta_0)(\tilde{R}_1\theta_1)\omega^2]^2+[(1-\alpha)(\tilde{R}_2\theta_1)+(\tilde{R}_1\theta_1)+(\tilde{R}_2\theta_0)]^2\omega^2}}$$

From Section 9.05 for operation at about 300 psig

$\alpha = 0.33$

$\theta_0 = 6\,min$ $\qquad \tilde{R}_1 = 2.5\times10^{-8}$

$\theta_1 = 2\,min$ $\qquad \tilde{R}_2 = 2$

$$40\ min^{-1} < \omega < 2000\ min^{-1}$$

A Bode diagram for the dynamic response of the purge flow will show that we are operating in a frequency domain of maximum instability, with $G_1'(\omega)$ given by

$$G_1'(\omega) = \frac{\alpha \tilde{R}_2 \theta_1}{(1-\alpha)\tilde{R}_2\theta_1+\tilde{R}_2\theta_0} = \frac{\alpha\theta_1}{(1-\alpha)\theta_1+\theta_0} = \left(\frac{q_{0s}}{q_{1s}}\right)\left(\frac{V_1}{V_1+V_0}\right)$$

(9.13)

9.03 Steam Penetration

The unsteady vaporization of liquid water may be dynamically represented by a periodic impulse given by

$$Q_o(s) = A \frac{1}{1 - e^{-sT}} \tag{9.14}$$

where $A = m/q_{os}$

m - pulse volume $= q^*T$

q^* - time averaged flow of steam

T - time between pulses $= 2\pi/\omega$

Therefore $A = (q^*/q_{os})T$ (9.15)

Equation (9.15) into (9.11) gives

$$Q_1'(s) = -\alpha \tilde{R}_2 \Theta_1 A \left[\frac{s}{(1-e^{-sT})(1-\tau_1 s)(1-\tau_2 s)} \right]$$

where

$$\left.\begin{aligned} \tau_1 &= [(1-\alpha)(\tilde{R}_2\Theta_1) + (\tilde{R}_2\Theta_0)] \\ \tau_2 &= (\tilde{R}_2\Theta_0)(\tilde{R}_1\Theta_1)/\tau_1 \end{aligned}\right\} \tag{9.16}$$

Taking the inverse Laplace transform of (9.16); for steady state ($t > 10T$) we obtain

$$\tilde{Q}_1' = \frac{-\alpha R_2 \Theta_1 A}{\tau_1} \left[\frac{1}{\tau_2} \frac{e^{-t'/\tau_2}}{1 - e^{-T/\tau_2}} - \frac{1}{\tau_1} \frac{e^{-t'/\tau_1}}{1 - e^{-T/\tau_1}} \right] \tag{9.17}$$

where t' is measured relative to the start of a pulse (cf. figure on following page).

The periodic impulse response, $\tilde{Q}_1'$, is schematically shown by

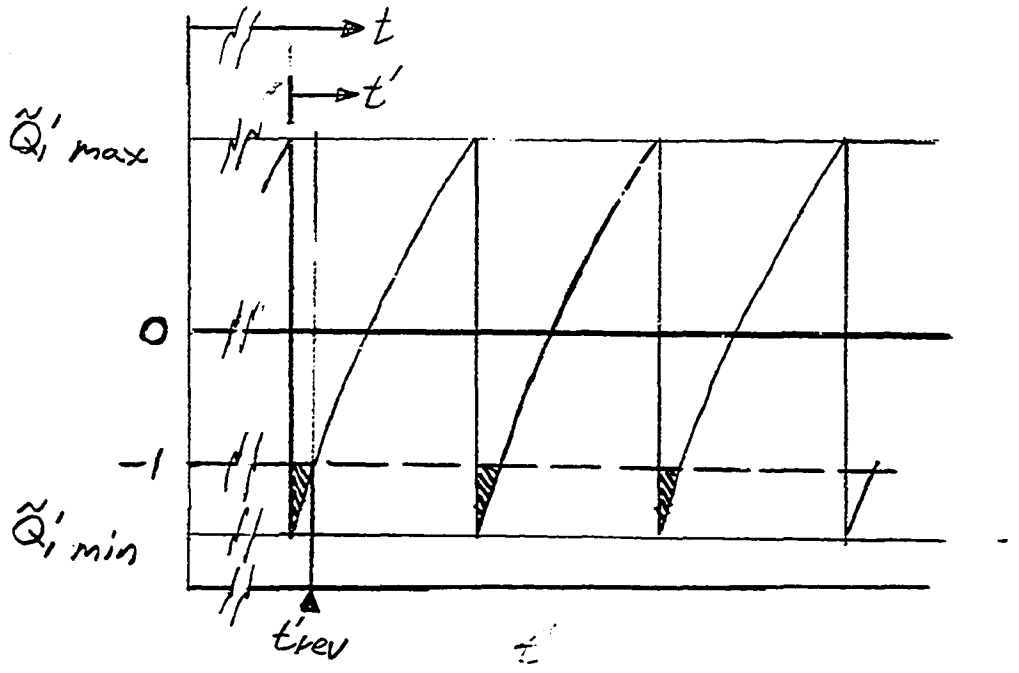

Penetration is seen to occur only if $\tilde{Q}'_{1min} < -1$; i.e. if

$$\frac{\alpha A}{\tilde{R}_1 \theta_0} > 1$$

For values of the parameters given earlier we predict that penetration will take place at all steam flows at 300 psig.

The extent of penetration may be determined by integrating Equation (9.17) from 0 to t'_{rev} to yield

$$\delta Q'_{1,rev} = \frac{\alpha \tilde{R}_1 \theta_1 A}{T \gamma_1} \left[\frac{1 - e^{-t'_{rev}/\gamma_2}}{1 - e^{-T/\gamma_2}} - \frac{1 - e^{-t'_{rev}/\gamma_1}}{1 - e^{-T/\gamma_1}} \right] \qquad (9.18)$$

where $\delta Q'_{1rev}$ is the time averaged fraction of the purge gas being reversed. t'_{rev} may be obtained by solving equation (9.17) for $\tilde{Q}'_1 = -1$. Over the entire range of T we obtain $t'_{rev}/\tau_2 > 5$. Equation (9.18) therefore simplifies to

$$\delta Q'_{rev} = \frac{A}{T}\frac{\tilde{R}_2 Q_1}{\gamma_1} = \left(\frac{q^*}{q_{os}}\right)\left(\frac{q_{os}}{q_{is}}\right)\left(\frac{V_1}{V_0+V_1}\right) = \left(\frac{q^*}{q_{is}}\right)\left(\frac{V_1}{V_0+V_1}\right) \qquad (9.19)$$

The fraction of the steam feed that penetrates into the balance housing, δq^*, is given by the simple relation

$$\delta q^* = \left(\frac{q_{os}}{q_{is}}\right)\left(\frac{V_1}{V_o+V_1}\right) \qquad (9.20)$$

This relation implies that the steam pulse penetrates the balance totally unhindered. Volume V_1 simply behaves as an extension of volume V_o. Apparently, resistance R_1 is insufficient to damp out the violent pulses of steam. The only way to prevent steam penetration into the balance housing is to damp the pulses at its source - the steam generator.

9.04 Damping of Steam Generation Disturbances

Since the inherent flow resistances in the system are unable to mitigate the steam pulsing, additional damping must be provided downstream of the steam generator. A dynamic analysis follows for sizing surge volume, V_2, and flow resistance, R_3, in order to prevent unsteady state penetration of steam into the balance housing.

The flow system is now represented by

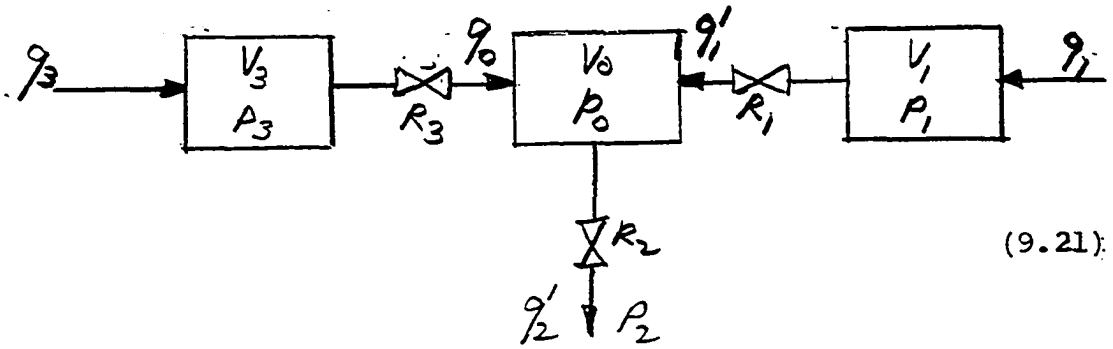

(9.21)

Transforming the variables and parameters as in (9.10) we obtain

$$\alpha\tilde{Q}_o + (1-\alpha)\tilde{Q}_1' = \theta_o \frac{d\tilde{P}_o}{dt} \tag{9.22}$$

$$\tilde{Q}_1 - \tilde{Q}_1' = \theta_1 \frac{d\tilde{P}_1}{dt} \tag{9.23}$$

$$\tilde{Q}_3 - \tilde{Q}_o = \theta_2 \frac{d\tilde{P}_3}{dt} \tag{9.24}$$

$$\tilde{Q}_1' = \frac{1}{\tilde{R}_1}(\tilde{P}_1 - \tilde{P}_o) \quad [\text{Note: } P_{1s} \simeq P_{os}] \tag{9.25}$$

$$\tilde{Q}_o = \frac{1}{\tilde{R}_3}(\tilde{P}_3 - \tilde{P}_o) \quad [\text{Note: } P_{3s} \simeq P_{os}] \tag{9.26}$$

$$\tilde{Q}_2' = \frac{1}{\tilde{R}_2}(\tilde{P}_o - \beta\tilde{P}_2) \tag{9.27}$$

Again, taking the Laplace transform of the above equations with the boundary conditions:

(i) $P_2(s) = 0$

(ii) $Q_1(s) = 0$

(iii) $Q_3(s) =$ given

gives:

$$\frac{Q_1'(s)}{Q_3(s)} = \frac{-\alpha \tilde{R}_2 \theta_1 s}{\left\{ \begin{array}{l} 1 + [\alpha(\tilde{R}_2 Q_2) + (1-\alpha)(\tilde{R}_2\theta_1) + (\tilde{R}_2\theta_0) + (\tilde{R}_1\theta_1) + (R_3 Q_2)]s \\ + [\alpha(\tilde{R}_2\theta_2)(\tilde{R}_1\theta_1) + (1-\alpha)(\tilde{R}_2\theta_1)(\tilde{R}_3 Q_2) + (\tilde{R}_2\theta_0)(\tilde{R}_1\theta_1) \\ \qquad + (\tilde{R}_2\theta_0)(\tilde{R}_3 Q_2) + (\tilde{R}_1\theta_1)(\tilde{R}_3 Q_2)]s^2 \\ + (\tilde{R}_2\theta_0)(\tilde{R}_1\theta_1)(\tilde{R}_3\theta_2)s^3 \end{array} \right\}} \qquad (9.28)$$

For $R_3 \simeq 10^{-2}$ and $\theta_2 > 1$, the frequency response is approximated by:

$$G_1'(\omega) = \frac{\alpha R_2 \theta_1 \omega}{\left(\begin{array}{l} [1 - \{(1-\alpha)(\tilde{R}_2\theta_1)(\tilde{R}_3\theta_2) + (\tilde{R}_2\theta_0)(\tilde{R}_3\theta_2)\}\omega^2]^2 \\ + [\{\alpha(\tilde{R}_2\theta_2) + (1-\alpha)(\tilde{R}_2\theta_1) + (\tilde{R}_2\theta_0)\} \\ \qquad - (\tilde{R}_2\theta_0)(\tilde{R}_1\theta_1)(\tilde{R}_3 Q_2)\omega^2]^2 \omega^2 \end{array} \right)^{1/2}} \qquad (9.29)$$

A Bode diagram showing the dynamic response for the damped system is illustrated in Figure 34. It can be seen that in contrast to the earlier undamped system we are no longer operating in a frequency domain of high instability. This, however, does not guarantee that steam penetration will not occur; dynamic analysis to a periodic impulse disturbance is required.

Along the lines of Section 9.04, we obtain for the steady state response

$$\tilde{Q}_1' = \frac{-\alpha \tilde{R}_2 \Theta_1 A}{\phi}\left[(\gamma_3-\gamma_2)\frac{e^{-t/\gamma_1}}{1-e^{-\tau/\gamma_1}} + (\gamma_1-\gamma_3)\frac{e^{-t/\gamma_2}}{1-e^{-\tau/\gamma_1}} + (\gamma_2-\gamma_1)\frac{e^{-t/\gamma_3}}{1-e^{-\tau/\gamma_3}}\right] \tag{9.30}$$

where

$$\left.\begin{aligned} \phi &= (\gamma_1-\gamma_2)\gamma_1\gamma_2 + (\gamma_2-\gamma_3)\gamma_2\gamma_3 + (\gamma_3-\gamma_1)\gamma_3\gamma_1 \\ \gamma_1 &= \alpha(\tilde{R}_2\Theta_1) + (1-\alpha)(\tilde{R}_2\Theta_1) + (\tilde{R}_2\Theta_0) \\ \gamma_2 &= \{(1-\alpha)(\tilde{R}_2\Theta_1)(\tilde{R}_3\Theta_2) + (\tilde{R}_2\Theta_0)(\tilde{R}_3\Theta_2)\}/\gamma_1 \\ \gamma_3 &= \{(\tilde{R}_2\Theta_0)(\tilde{R}_1\Theta_1)(\tilde{R}_3\Theta_2)\}/\gamma_1\gamma_2 \end{aligned}\right\} \tag{9.31}$$

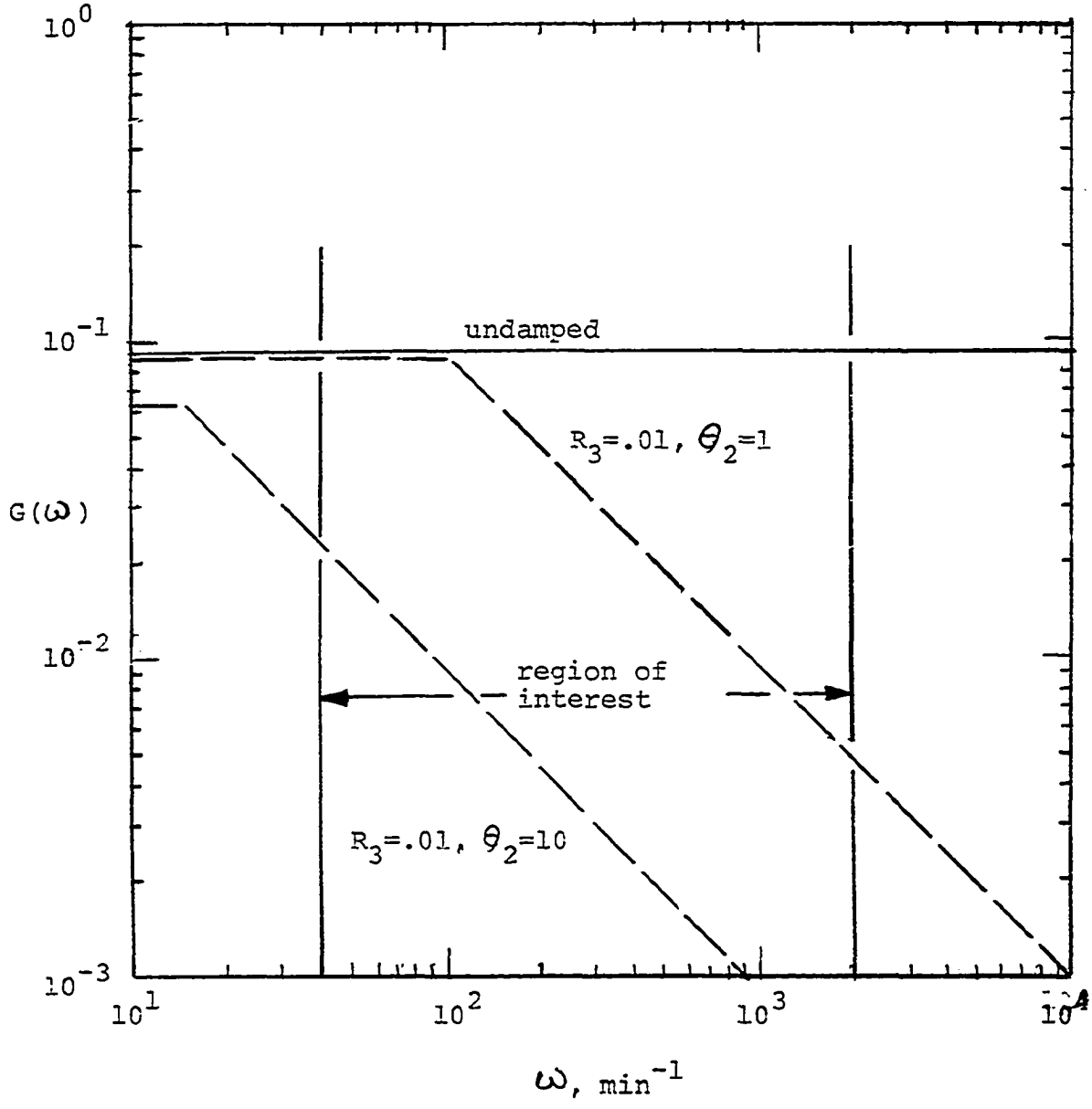

Figure 34. Bode Diagram for Dynamics of Flow System of High Pressure Thermobalance at 300 psig

For values of the system parameters given earlier, Equation (9.30) will reduce to the much simpler relation (9.17), with the time constants τ_1, τ_2 defined by (9.31). For $\tilde{R}_3 = 10^{-2}$ and $\theta_2 > 1$, we find that $Q'_{1min} > -1$, at all values of $10^{-3} \leq T \leq 10^{0}$, so that no steam penetration will occur for the damped system.

For a safe measure, we should design for $\tilde{R}_3 = 0.02$ and $\theta_2 = 20$, which physically corresponds to a 2 liter surge volume followed by an orifice having a C_v factor of 0.002.

9.05 System Parameters at 300 psig

(a) purge flow = 200 cm^3/min (actual)

volume of balance housing and purge lines = 400 cm^3

Therefore, $\theta_1 = 2$ min

(b) reaction gas flow = 100 cm^3/min (actual)

volume of flow system outside balance housing = 600 cm^3

Therefore, $\theta_o = 6$ min

(c) for back pressure regulator

$$\tilde{R}_2 = \frac{1}{n}\,\frac{(P_o - P_2)}{P_o} \simeq \frac{1}{n} = 2$$

(d) for passage in ceramic block

$D_{eq} = 0.6$ cm

$L = 5$ cm

$Q = 200$ cm^3/min (actual)

$\mu = 0.02$ cp (N_2 @ 200°F)

Using laminar flow relation

$R_1 = 0.5 \times 10^{-8}$

(e) From measurements of diameter for largest drop of water issuing from vaporizer injector we find that $V_{liquid} = 0.025\ cm^3$. Assuming that the actual size is reduced in the vaporizer by a factor of ten as a result of thermal shock, we obtain a value of 3 cm^3 (STP) for the size of the steam pulse. At steam flows of 1 to 50% of the reaction gas flow we obtain the following characteristics of the steam pulse disturbance

frequency, ω = 40-2000/min

period, T = 0.003 to 0.15 min

10.0 References

1. Rabatin, J.G., Card, C.S., Analytical Chem., 31, 1689 (1959)

2. Baker, E.N., J. Chem. Soc., 1962, 464

3. Biermann, W.J., Heinrichs, M., Can. J. Chem., 40, 1361 (1962)

4. McKewan, W.M., Trans. AIME, 224, 387 (1962)

5. Boehlen, B., Hausmann, W., Guyer, A., Helv. Chim Acta, 47, 1815 (1964)

6. Feldkirchner, H.L., Johnson, J.L., Rev. Sci. Instr., 39, 1227 (1968)

7. Sasaki, M., Homma, T., Yamada, T., Makino, K., Bunseki Kagaku, 18, 1179 (1969)

8. Brown, Jr., H.R., Penski, E.C., Callahan, J.L., Thermochimica Acta, 3(4), 271 (1972)

9. Ho Bae, J.. Rev. Sci. Instr., 43, 983 (1972)

10. Williams, J.R., Simmons, E.L., Wendlandt, W.W., Thermochimica Acta, 5(2), 101 (1972)

11. Williams, J.R., Wendlandt, W.W., Thermochimica Acta, 7(4), 253 (1973)

12. O'Neill, E.P., Keairns, D.L., Kittle, W.F., Proc. 3rd Intl. Conf. Fluidized Bed Combustion, Oct. 29 - Nov. 1, 1972, Houston Woods, Ohio, Vol. I, p. 167

13. Keairns, D.L., Archer, D.H., et al. Evaluation of the Fluidized-Bed Combustion Process Vol. I-Pressurized Fluidized-Bed Combustion. Process Development and Evaluation. Report EPA-650/2-73-048a from Westinghouse Research Laboratories, December 1973, pp. 103-340.

14. Gardner, N., Samuels, E., Wilks, K., Adv. in Chem. Series, 131, 217 (1974)

15. Chauhan, S.P., Feldmann, H.F., Stambaugh, L.E.P., Oxley, J.N., ACS Div. of Fuel Chem. Preprints, 20(4), 207 (1975)

16. Tomita, A., Mahajan, O.P., Walker, Jr. P.L., ACS Div. of Fuel Chem. Preprints, 20(3), 99 (1975)

17. Ruth, L.A., Squires, A.M., Graff, R.A., Env. Sci. Tech., 6, 1009 (1972)

18. Ruth, L.A., Ph.D. Dissertation, City University of New York, (Ch.E.), 1972

19. Pell, M., Ph.D. Dissertation, City University of New York (Ch.E.), 1971

20. Squires, A.M., Graff, R.A., Pell, M., CEP Symposium Series, 67(115), 23 (1971)

21. Curran, G.P., Fink, C.E., Gorin, E., Advances in Chemistry Series, 69, 141 (1967)

22. Gluud, W., Keller, K., Klempt, W., Bestehorn, R., Ber. der. Ges. für Kohlentechnik, 3, 211 (1930)

23. Zawadski, J., Bretsnajder, S., Zeit. Phys. Chem., B22, 60,79 (1933); ibid, B40, 158 (1935)

24. Schwob, Y., Rev. materiaux construction trav. publ., Ed C, 411, 409 (1949); ibid, 413, 33,85 (1950)

25. Bischoff, F., Monatshefte, 81, 606 (1950)

26. Britton, H.T.S., Gregg, S.J., Winsor, G.W., Trans. Faraday Soc., 48, 70 (1952)

27. Richer, A., Compt. rend., 238, 339 (1954)

28. Ohno, Y., Sekko to Sekkai, 1, 1366 (1957)

29. Ohno, Y., Fujiyama, S., Sekko to Sekkai, 1, 1469 (1957)

30. Hyatt, E.P., Cutler, I.B., Wadsworth, M.E., J. Am. Ceram. Soc., 41, 70 (1958)

31. Siske, V., Proks I., Chem. zvesti, 12, 201,275 (1958)

32. Cremer, E., Nitsch, W., Tonind.-Ztg. u. Keram. Rundschau, 83, 579 (1959)

33. Shushinov, V.A., Fedyakova, K.G., Uchenye Zapiski Gor'Kovst. Gosudarst. Univ. im. N.I. Lobachevskogo, Ser. Khim., 1958, No. 32, 13

34. Glasson, D.R., J. Appl. Chem., 10, 42 (1960)

35. Richer, A., Vallet, P., Compt. rend., 252, 1780 (1961)

36. Davtyan, O.K., Ovchinnikova, E.N., Soboleva, N.M., Nauch. Ezhegodnik, Odessk. Gosudarst. Univ., Khim. Fak., 1961, No. 2, 128

37. Nitsch, W., Z. Elektrochem., 66, 703 (1962)

38. Dedman, A.J., Owen, A.J., Trans. Faraday Soc., 58, 2027 (1962)

39. Ketov, A.M., Pechkovskii, V.V., Larikov, V.V., Obsch. Prikl. Khim, 1970, No. 3, 48 (1970)

40. Curran, G.P., Fink, C.E., Gorin, E., OCR R&D Report No. 16, Interim Report No. 3 "Phase III - Bench-Scale Research on CSG Process, Book 3: Operation of the Bench-Scale Continuous Gasification Unit"

41. Noll, W., Ang. Chemie, 62, 567 (1950)

42. Asboth, K., Austria Pat. 172,931 (1952)

43. Curran, G.P., Rice, C.H., Gorin, E., ACS Div. of Fuel Chem. Preprints, 8(1), 128 (1964)

44. Squires, A.M., Adv. in Chem. Series, 69, 205 (1967)

45. Fink, C., Curran, G., Sudbury, J., "CO_2 Acceptor Process Pilot Plant - 1974", paper presented at Sixth Synthetic Pipeline Gas Symposium, Oct. 28, 1974, Chicago

46. Pell, M., Graff, R.A., Squires, A.M., Sulfur & SO_2 Developments a CEP Technical Manual, 1971, p. 151

47. Cremer, E., Nitsch, W., Zeit. Elektrochem., 66, 697 (1962)

48. Frank-Kamenetskii, D.A., Diffusion and Heat Transfer in Chemical Kinetics, Plenum Press, New York, 1969, ch. 2

49. Sestak, J., Satava, V., Wendlandt, W.W., Thermochimica Acta, 7(5), 447 (1973)

50. Garner, W.E., Chemistry of the Solid State, Academic Press, New York, 1955, ch. 8

51. Young, D.A., Decomposition of Solids, Pergamon Press, New York, 1966

52. Galwey, A.K., Chemistry of Solids, Chapman and Hall, London, 1967, ch. 5

53. Pannetier, G., Souchay, P., Chemical Kinetics, Elsevier, Amsterdam, 1967, pp. 393-416

54. Schwab, G.M., Taylor, J.S., Spence, R., Catalysis from the Standpoint of Chemical Kinetics, D. Van Nostrand, New York, 1937, p. 16

55. MacIntire, W.H., Stansel, T.B., Ind. and Eng. Chem., 45, 1548 (1953)

56. Bischoff, F., Zeit. anorg. Chem., 262, 288 (1950)

57. Jacobs, H., Low, M.J.D., J. Colloid and Interface Sci., 46(1), 165 (1974)

58. Haul, R.A.W., Schoning, F.R.L., Zeit. anorg. Chem., 269, 120 (1952)

59. Glasson, D.R., J. Appl. Chem., 11, 201 (1961)

60. Bischoff, F., Claus, D., Lehmann, H., Tonind.-Ztg. u. Keram. Rundschau, 83, 293 (1959)

61. Glasson, D.R., J. Appl. Chem., 8, 793 (1958)

62. Hedin, R., Svenska Forskningsinst. Cement Betong Vid Kgl. Tek. Hogskol. Stockholm Sartryck, 16, 661 (1961)

63. Kovalenko, E.N., Mater. Sci. Res., 3, 485 (1966)

64. Yanev, I.P., Angelov, B.D., Radenkova, M.Z., Dokl. Bolg. Akad. Nauk., 23(10), 1219 (1970)

65. Clark, L.M., Rec. trav. Chim., 68, 969 (1949)

66. Low, M.J.D., Goodsel, A.J., Takezawa, N., Environ. Sci. Technol., 5, 1191 (1971)

67. Lee, P.L., Low, M.J.D., Water, Air, Soil Pollut., 2(1), 75 (1973)

68. Proks, I., Jaskova, V., Silikaty, 11(3), 201 (1967)

69. Proks, I., Siska, V., Silikaty, 12(1), 13 (1968)

70. Bachmann, L., Cremer, E., Zeit. anorg. u. allgem. 309, 65 (1961)

71. Hashimoto, H., Kogyo Kagaku Zasshi, 64, 250 (1961)

72. Hedin, R., Tek. Trdskr., 92, 101 (1961)

73. Cremer, E., Nitsch, W., Sci. Ceram., 1, 295 (1962)

74. Peterson, R.O., Cutler, I.B., J. Amer. Ceram. Soc., 51(1), 21 (1968)

75. Pampuch, R., Silicates Industriele, 23, 119 (1958)

76. Fischer, H.C., J. Amer. Cer. Soc., 38, 284 (1955)

77. Tagawa, H., Sudo, F., Kogyo Kagaku Zasshi, 61, 949 (1959)

78. Kruel, M., Juntgen, H., Chem. Ing. Tech., 39, 607 (1967)

79. Kriek, H.J.S., Ford, W.F., White, J., Trans. Br. Ceram. Soc., 58, 1 (1959)

80. Buckley, P.S., Techniques of Process Control, Wiley, New York, 1964

81. Norem, S.D., O'Neill, M.J., Gray, A.P., Thermochimica Acta, 1, 29 (1970)

11.0 Addendum-Modification of Equipment Subsequent to Completion of Research

Several modifications and improvements to the equipment were introduced by George Kan following completion of this research and are described below.

11.01 Modifications to Thermobalance

Several failures of the balance movement, at first thought to be the result of intermittent H_2S penetration, were soon more accurately traced to damage caused by overheating from the adjacent beaded heating elements surrounding the furnace tube. An 1/8" pancake cooling coil on the face of the aluminum balance housing has been installed, and no breakdowns have since been experienced (see Figure 34).

11.02 Modifications of Flow System

The flow system was modified as shown in Figure 35. Balancing of pressures inside the TGA with its surrounding atmosphere is now achieved by providing continuity of the bomb atmosphere with the exhaust gas line following the zinc oxide bed. A separate gas line now carries purge nitrogen directly to the rear of the thermobalance, thus insuring positive flow of purge at all times. Pressurization and depressurization is achieved via the pressure balancing line directly.

Some difficulties were encountered with the back pressure regulator as discussed in Section 4.05. At 300 psig the pressure cycled ± 5 psig every five minutes or so.

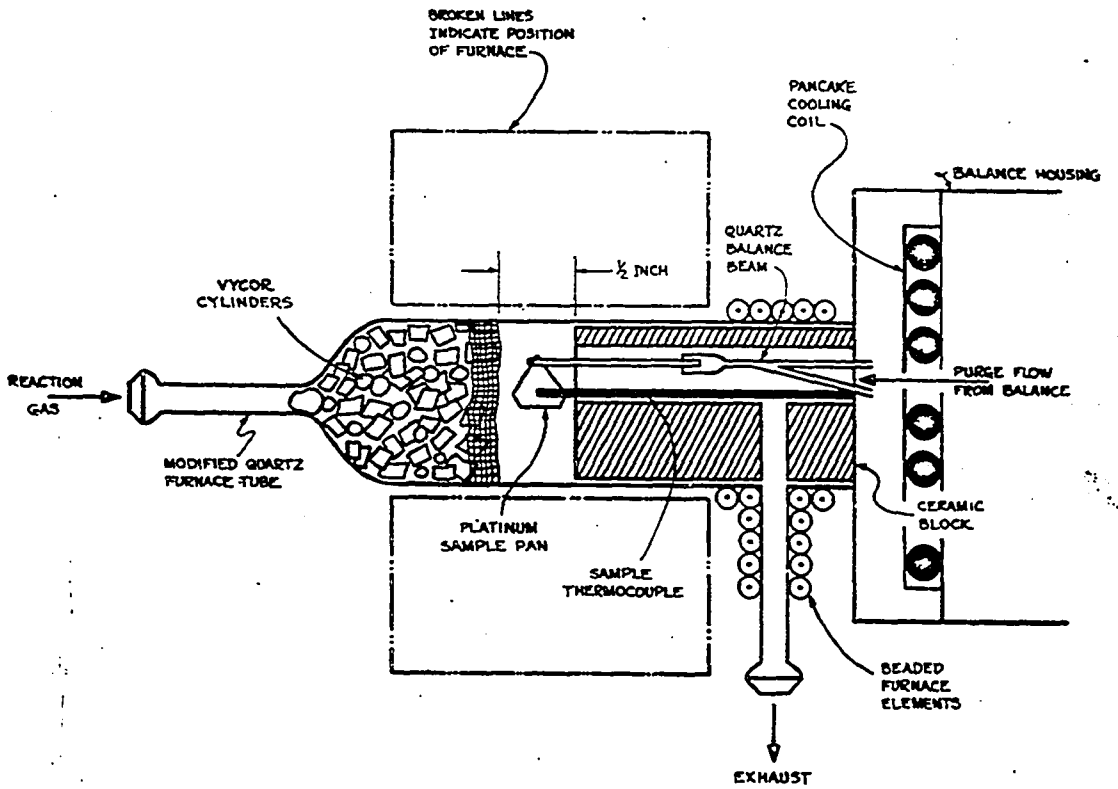

Figure 35. Modifications to High Pressure TGA (G. Kan)

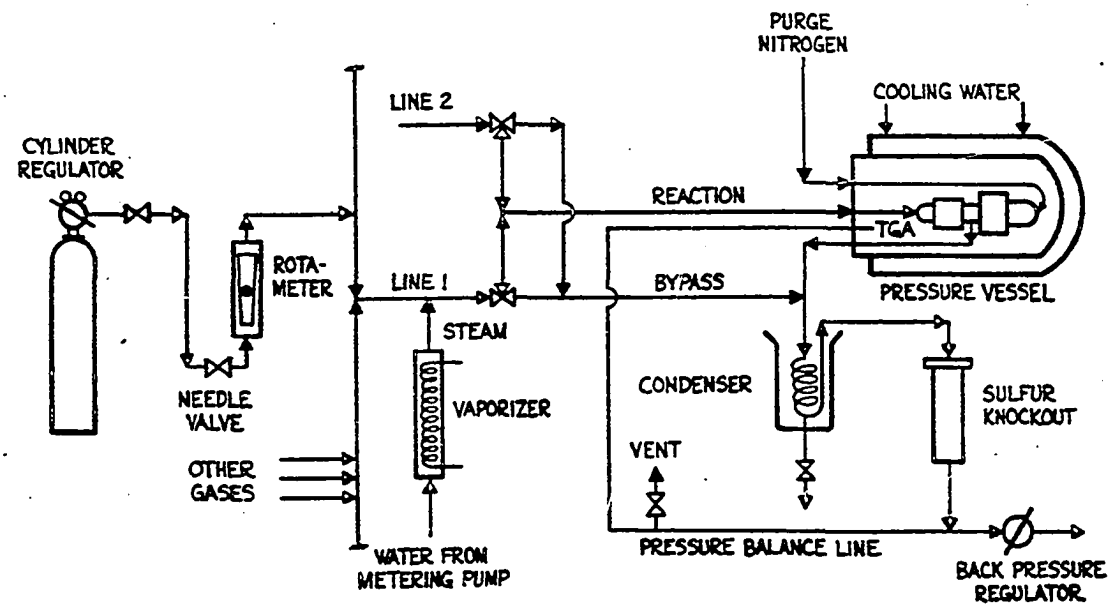

Figure 36. Modifications to Flow System for High Pressure Thermobalance (G. Kan)

Since gas flows to the thermobalance were small in comparison to the gas volume of the pressure vessel, this cycling caused "breathing" inside the thermobalance. This condition was remedied by lining out the back pressure regulator with a large bypass flow of nitrogen.

11.03 Modifications to Steam Generating System

More difficulties were experienced with the Harvard 975 syringe pump. This pump is now replaced by an ISCO LC pump capable of pressures of 2000 psig, flows to 3 ml/min (liquid) and has a capacity of 375 ml.

11.04 Temperature Calibration of Sample Thermocouple

A routine procedure, based on the more accurate Perkin-Elmer magnetic standards, has been adopted for calibrating temperatures (81). This procedure is executed every time a different set of gas compositions or pressure is planned. Figure 36 shows the results of a series of calibrations made at low and high pressures. A maximum difference between readings at low and high pressures of 25°C occurs at about 500°C. This should be compared with a maximum difference of 100°C obtained without the present modifications to the TGA. In general, the indicated temperature was found to be accurate to within 15°C, except for temperatures beyond 800°C where indicated temperatures begin to lag behind "true" temperatures. At 1000°C the indicated temperature for low and high pressure alike lags

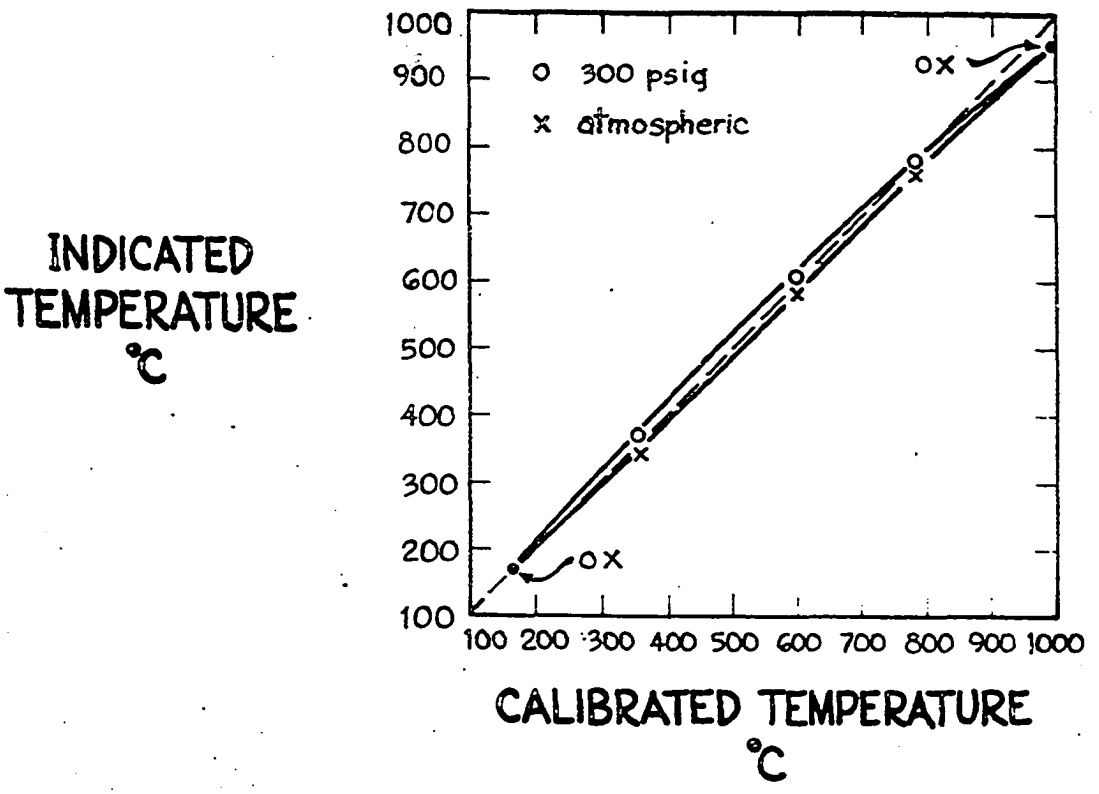

Figure 37. Temperature Calibration of Sample Thermocouple Using Magnetic Standards (G. Kan)

by 35°C. While the accuracy of the indicated temperature leaves something to be desired, with calibration the sample temperature can be reproducibly determined to within 5°C.